Multiscale Infectious Disease Dynamics: Linking Epidemiology and Testing for Outbreak Neutralization

by

Casey Middleton

B.S., Rhodes College, 2018

A thesis submitted to the

Faculty of the Graduate School of the

University of Colorado in partial fulfillment

of the requirements for the degree of

Doctor of Philosophy

Department of Computer Science

2025

Committee Members:

Daniel Larremore, Chair

Sarah Cobey

Stephen Kissler

Orit Peleg

Sara Sawyer

Middleton, Casey (Ph.D., Computer Science)

Multiscale Infectious Disease Dynamics: Linking Epidemiology and Testing for Outbreak Neutralization

Thesis directed by Prof. Daniel Larremore

Infectious disease dynamics are shaped by interactions across multiple scales. Within a host, pathogens interact with cellular and immune processes, driving fluctuations in pathogen concentrations and immune responses. Between hosts, infectious contacts facilitate pathogen transmission, driving fluctuations in case counts and population immunity levels. However, traditional mathematical models often focus on only one of these scales. This dissertation addresses this gap by leveraging multi-scale modeling to examine how within-host dynamics influence population-level transmission. By integrating models of within-host viral and immune dynamics with between-host epidemiological transmission models, this work provides insights into infectious disease spread and intervention strategies.

First, a multi-scale model is developed to estimate testing effectiveness, the reduction in transmission due to testing and subsequent isolation, using a probabilistic framework which incorporates viral kinetics, test attributes, and testing behaviors. This model provides a general framework for comparing testing strategies for any virus. Second, these results are incorporated into a compartmental modeling framework to analyze the effectiveness of vaccinate-or-test policies for COVID-19. Lastly, a framework is developed to evaluate our ability to learn about correlates of protection by linking immunological marker concentrations with observed infection events in test-negative design studies. This research highlights the importance of incorporating both within-host and between-host processes to understand infectious disease dynamics and evaluate intervention strategies.

Dedication

To my parents. For moving mountains so I could walk a smoother path. Thank you.

Acknowledgements

I would first like to thank the mentors who have invested in me throughout my educational journey. Dr. Erin Bodine was the first to show me the beauty of mathematical modeling, and I would not be where I am today without her investment in my life. My thesis committee members, Drs. Daniel Larremore, Sarah Cobey, Stephen Kissler, Orit Peleg, and Sara Sawyer, have provided invaluable guidance during my thesis preparation. I would specifically like to thank Dan for teaching me more than I have room to elaborate on here. I am a better scientist, communicator, and mentor thanks to your support.

To my friends: thank you for giving me a soft place to land. I would particularly like to thank my Memphis friends, Emily, Sydney, Courtney, Cheryl, and Wylde + Siushan, for supporting me despite the miles between us, as well as my Colorado friends, Kate, Katie, Hannah, Kristyna, Claire, and Greta, for all the love, support, and fun you have given me over the last five years. You all bring my life so much color.

Next, I want to thank my Colorado family. Beans and Asha, thanks for the most loving pals a girl could ask for. Bruening family, thank you for celebrating me like I am one of your own. And Garrick, thank you for so many things, but mostly for just always being there. I cherish this life with you.

Lastly, I could not have done this without my family. My siblings have always inspired me by demonstrating what perseverance truly means. My grandparents have always been at the other end of the phone when I need to talk. And my parents have always modeled what it means to work hard and love deeply. Their support has allowed me to take risks that they were not afforded. Thank you for your tireless love and sacrifice, and for always being there when I need you. I love you guys.

Contents

Chapter

1 Introduction **1**

1.1 Between-host modeling 2

1.2 Within-host modeling 3

1.3 Multi-scale modeling 4

1.4 Outline 4

2 Modeling the Transmission Mitigation Impact of Testing for Infectious Diseases **6**

2.1 Introduction 6

2.2 Results 8

2.2.1 A model for testing effectiveness (TE) 8

2.2.2 Testing effectiveness varies by strategy and pathogen 11

2.2.3 Impacts of timing and availability of elective post-symptom testing 14

2.2.4 Reevaluation of the sensitivity/turnaround tradeoff for SARS-CoV-2 17

2.2.5 Estimating costs: isolation days and test consumption 21

2.3 Discussion 22

2.4 Materials and Methods 25

2.4.1 Mathematical Model for Testing 25

2.4.2 Model Estimates 30

2.4.3 Parameterization of the Model 33

3 SARS-CoV-2 Transmission and Impacts of Unvaccinated-Only Screening in Populations of Mixed Vaccination Status **36**

3.1 Introduction . . . 36

3.2 Results . . . 38

3.2.1 High vaccination rates drive total infections and hospitalizations down, increase the proportions of vaccine breakthroughs, and shift the drivers of transmission . . . 38

3.2.2 The impacts of unvaccinated-only screening depend on population immunity, compliance, and VE . . . 47

3.2.3 Unvaccinated-only screening shifts the balance of unvaccinated vs breakthrough transmission but not infection or hospitalization . . . 52

3.3 Discussion . . . 54

3.4 Materials and Methods . . . 58

3.4.1 SEIR model . . . 58

3.4.2 Incorporation of community testing . . . 60

3.4.3 Transmission modes and forces of infection . . . 61

3.4.4 Reproductive number . . . 61

4 Statistical Methods for Estimating the Protective Effects of Immune Markers Using Test-Negative Designs **63**

4.1 Introduction . . . 63

4.2 Results . . . 64

4.2.1 Standard logistic regression recovers only exponential protection from TND data . . . 64

4.2.2 Logistic regression is poorly suited to recover a general protection function . . . 66

4.2.3 The scaled logit model can recover many functional relationships between antibody titers and risk reduction from TND data . . . 67

4.2.4 Scaled logit model accuracy depends on sample size . . . 70

4.2.5 The scaled logit model has poor accuracy if antibodies do not provide perfect protection . . . 71
4.3 Discussion . . . 73
4.4 Materials and Methods . . . 75
4.4.1 Simulating test-negative design (TND) data . . . 76
4.4.2 Estimating protection function . . . 77

5 Conclusion **80**
5.1 Significance . . . 80
5.2 Limitations . . . 81
5.3 Future research . . . 82
5.3.1 Estimating individual infectiousness profiles . . . 82
5.3.2 Incorporating serology data into epidemiology models . . . 84
5.4 Concluding remarks . . . 85

Bibliography **86**

6 Appendix **111**
6.1 Chapter 2 supplementary materials . . . S1
6.1.1 Imperfect isolation behaviors . . . S10
6.1.2 Test to exit strategies . . . S10
6.2 Chapter 3 supplementary materials . . . S12
6.2.1 Derivation of effective reproductive number . . . S21
6.3 Chapter 4 supplementary materials . . . S22
6.3.1 Fitting the scaled logit model to TND data . . . S26

Tables

Table

S1 Summary of viral load, infectiousness, and testing parameters S9

S2 Summary of population, infection and testing parameters used in test-or-vaccinate modeling and simulation S12

S3 Summary of immunity parameters used in test-or-vaccinate modeling and simulation S13

Figures

Figure

2.1 Testing Effectiveness model diagram 9

2.2 Testing effectiveness varies considerably by strategy and pathogen 12

2.3 Relative timing of symptom onset, infectiousness, and detectability vary by pathogen and individual 13

2.4 Optimal use of tests depends on the number of tests available and when they are used 16

2.5 RT-qPCR vs RDT tradeoffs for the SARS-CoV-2 omicron era 19

2.6 Fixed isolation recommendations may lead to unnecessary isolation when symptomatic testing ascertainment is high 20

3.1 Vaccination affects which population drives transmission and dominates infections and hospitalizations 40

3.2 Vaccination and prior infection rates affect epidemic potential, vaccine breakthroughs, and drivers of transmission 42

3.3 Transition points for breakthrough infections, hospitalizations, and transmission 45

3.4 The impact of unvaccinated-only screening corresponds to three distinct parameter regions . 47

3.5 The impacts of unvaccinated-only screening depend on population immunity, compliance, and vaccine effectiveness 49

3.6 Unvaccinated-only screening during omicron transmission cannot achieve $R_{\text{eff}} < 1$ except in low-vaccination and high-frequency regimes 51

3.7 Screening and vaccine effectiveness affect transition points to majority-breakthrough regimes 53

4.1 Logistic regression provides an accurate estimate of antibody protection for an exponential protection function 66

4.2 Logistic regression does not provide an accurate estimate for a sigmoidal protection function 67

4.3 The scaled logit model can recover complicated antibody protection functions 69

4.4 The scaled logit model is better specified to recover sigmoidal protection from TND data than logistic regression 71

4.5 Scaled logit model has reduced accuracy if antibodies do not provide perfect protection . . . 72

5.1 Within-host modeling can help differentiate infectious virus from non-infectious virus 84

S1 Ascertainment rates vary considerably by strategy and pathogen S1

S2 Population-level infectiousness curves for all Figure 2.2 scenarios S2

S3 Sensitivity analysis of testing effectiveness patterns observed in Figure 2.2 . . . . . S3

S4 Testing effectiveness after symptom onset depends on the pathogen, the number and type of tests available, and when they are used S4

S5 Ascertainment of testing after symptom onset depends on the pathogen, the number and type of tests available, and when they are used S5

S6 Sensitivity analysis of optimal timing of RDT usage after symptom onset S6

S7 Optimal timing of testing after known exposure depends on the number of tests available . . S7

S8 Examples of modeled viral kinetics S8

S9 Vaccination's impact on the total number of infections depends on vaccine effectiveness and R_0^{NPI} S14

S10 Vaccination and past infection affect epidemic potential, vaccine breakthroughs, and drivers of transmission S15

S11 The impacts of unvaccinated-only screening on total infections depend on population immunity, compliance, and vaccine effectiveness S16

S12 Unvaccinated-only screening during omicron transmission cannot achieve $R_{\text{eff}} < 1$ except in low-vaccination and high-frequency regimes S17

S13 Universal testing during omicron transmission can achieve $R_{\text{eff}} < 1$ in high-compliance and high-frequency regimes S17

S14 The impacts of screening on total infections and hospitalizations depend on population immunity, compliance, and vaccine effectiveness S18

S15 Screening via testing and vaccine effectiveness affect transition points to majority-breakthrough regimes S19

S16 SEIR Model Flow Diagram S20

S17 The scaled logit model can recover complicated antibody protection functions, while logistic regression is limited in its scope S23

S18 The scaled logit model can recover complicated antibody protection functions, even under different titer distributions S23

S19 Scaled logit model fit with low sample sizes S24

S20 The scaled logit model has low accuracy at small sample sizes S24

S21 Protection functions used for data simulation S25

Chapter 1

Introduction

Public health practitioners are tasked with improving health outcomes, and one piece of this puzzle is the prevention of infectious diseases. These diseases, and the pathogens that cause them, range widely in characteristics, such as mode of transmission, pathogenicity, virulence, latency, seasonality, symptom timing, and more. The potential landscape of interventions is equally vast, from non-pharmaceutical interventions such as testing, masking, and quarantining to medical interventions like vaccination and anti-viral treatment. In the face of these many variables, public health practitioners are tasked with a daunting question: which intervention, or combination of interventions, will prevent the most sickness and death with minimal interruptions to daily life?

Mathematical modeling provides a strong foundation to help make these choices, comparing the costs and benefits of potential interventions in a "mock population" before choosing one to implement in the real world. In 2019-2020, severe acute respiratory syndrome coronavirus 2 (SARS-CoV-2) ripped through the population, causing an estimated 83.7 million confirmed COVID-19 infections and 1.8 million deaths in 2020 alone [183]. In the face of uncertainty about how to minimize sickness and death for such a transmissible virus, modeling was used to make recommendations for many public health decisions. Before vaccines were developed, college campuses [70, 112] and skilled nursing facilities [103, 155] used modeling to implement testing programs that protected students and residents. More broadly, modeling was also used to make testing [136] and masking [47, 61] recommendations for the general population. As vaccines were being developed, the World Health Organization (WHO) also relied on modeling studies to inform who

should be prioritized for initial doses when supplies were limited [30, 169].

1.1 Between-host modeling

Early work in the field of infectious disease modeling focused on "between-host" dynamics – i.e. who is infected, who is susceptible, and how does disease spread between them? The earliest example of this comes from 1760, when Daniel Bernoulli used differential equations and life tables to show that smallpox vaccination is associated with increased life expectancy, despite the small risk associated with being vaccinated [17, 54]. A few hundred years later, the idea of the basic reproduction number (R_0) was introduced by Ronald Ross in 1911 to define the average number of expected secondary infections in a fully susceptible population [206]. This work was soon followed by the introduction of the susceptible-infectious-exposed (SIR) compartmental model by Kermack and McKendrick in 1927 [118] and the Reed-Frost model which incorporates individual heterogeneity in 1928 [37].

These foundational models laid the groundwork for modern day infectious disease modeling. The SIR model is arguably the single most commonly employed tool in an epidemiological modeler's toolkit. Some simple SIR model variations introduce more complexity to the transmission process by adding an exposed (E) compartment for individuals who have been infected but cannot yet transmit to others, or adding vector species which facilitate transmission [24, 151]. Simple model variations to explore intervention strategies may include vaccination [27, 30, 169] or isolation after a positive test result [70, 103].

While powerful for studying transmission, the standard SIR model and its many variations share a few key assumptions which may not accurately reflect the real world. First, populations are assumed to exhibit "homogeneous mixing" where everyone is equally likely to come into contact, which we know poorly represents highly assortative real-world contact networks [170, 192, 227]. Second, everyone within a given compartment is treated identically. This masks the heterogeneity in individual attributes such as susceptibility and infectious potential [21, 255], assuming instead that everyone experiences the average of these values. Lastly, these models exhibit exponential wait time distributions. This means that even if the average infectious period is 6 days, some individuals will spend much longer in this compartment, impacting

epidemic timing and probability of epidemic extinction. To understand if these assumptions reflect reality, we must zoom in and focus on infected *individuals* instead of infected populations.

1.2 Within-host modeling

Within-host modeling seeks to understand how a pathogen interacts with a host's cellular and immune systems. Studies on viral kinetics quantify the amount of virus in an infected individual throughout the course of their infection [93, 94, 121, 124, 126, 141]. These studies have been used to identify that children have a longer duration of pre-symptomatic influenza viral shedding than adults [178], that individual SARS-CoV-2 infectiousness varies over time [116] and across infected individuals [255], and inform Human Immunodeficiency Virus (HIV) anti-retroviral treatment strategies [68, 180, 189].

Beyond viral kinetics, within-host modeling can also be used to understand the host immune response to vaccination or infection. Measuring key components of the adaptive immune system, such as antibodies or T cells, may provide information about one's level of protection from subsequent infection or development of severe disease. Immunological studies have been used to predict lower immunity to the omicron variant than previously circulating variants during the COVID-19 pandemic [73, 163], predict vaccine effectiveness for the Mpox vaccine [19], and estimate how immunity wanes over time for multiple pathogens [51, 242, 254].

One consistent observation in within-host dynamics is the existence of variation across individuals. The time-course of infection looks different for each infected individual, meaning individuals may not contribute equally to transmission dynamics [116]. Similarly, immune response to vaccination varies across individuals, meaning everyone may not experience the same level of protection when given the same vaccine [51]. This variation highlights the limitations of typical between-host modeling approaches, which assume average infectiousness and protection levels for all, and points us toward a need for more complex models.

1.3 Multi-scale modeling

Multi-scale modeling recognizes the importance of both within-host and between-host modeling, and attempts to combine the strengths of both to make better predictions [77,152]. There are multiple approaches to combining models across scales, as outlined by Garira [77]. "Multi-domain integration frameworks" run two models in parallel, the within-host sub-model informing the between-host model dynamics [77]. Early multi-scale models fell into this framework, embedding individual viral-immune models into population-level network transmission models to simulate disease dynamics [98,128,234]. A similar approach has been used to compare testing strategies for COVID-19, considering the importance of viral load when comparing tests with varying sensitivities [103, 133, 134, 136]. These multi-scale models provide more insight than either of the two components individually, but they are burdened by high parameter and computational costs and low tractability for mathematical analysis [152].

Alternatively, "simultaneous integration frameworks" use the within-host sub-model to describe the entire infectious disease system, often through some statistical analysis of the sub-model results, omitting the need for a between-host model altogether [77]. One example of this framework is the use of viral kinetics curves to directly infer individual transmission risk, using the area under the curve as a proxy for infectious potential without incorporation of a between-host transmission model [29, 69]. Comparing expected viral kinetics with and without an intervention has been used to provide insight into the effectiveness of interventions like symptomatic isolation and contact tracing [69] and traveler screening programs [29].

1.4 Outline

This thesis will utilize multi-scale modeling to address three key questions in the field of infectious diseases. Broadly, this work focuses on multi-scale modeling for testing, from the impact of viral kinetics on diagnostic testing practices, to the impact of serological tests on inferred immunity levels.

Chapter 2 considers the question of how effective different testing decisions may be to control respiratory virus transmission, when paired with isolation after a positive test. For example, how does the use of

at-home rapid tests compare to the use of clinical diagnostic tests, and when is the optimal time to use a test after symptoms start? To answer these questions, we define testing effectiveness (TE) to be the reduction in transmission due to testing and subsequent isolation for a particular testing strategy. We then develop a simultaneous integration framework, which uses within-host viral kinetics to probabilistically estimate individual transmission potential with and without testing. We evaluate post-symptom testing recommendations for SARS-CoV-2, influenza A, and respiratory syncytial virus (RSV) using this framework.

Aside from general population-wide testing recommendations, we may be interested in testing only select groups. During the COVID-19 pandemic, the development of vaccines led to questions about re-prioritizing testing resources toward unvaccinated populations. Chapter 3 incorporates the results of Chapter 2 into a traditional SIR modeling framework to look at targeted testing for SARS-CoV-2. This chapter provides an example of a serial integration framework, where the within-host model is solved prior to running the between-host model. This work clarified the scenarios in which COVID-19 test-or-vaccinate policies could be used to control transmission, and when they couldn't.

While the previous two chapters focused on using viral kinetics to inform transmission potential, we may also use the abundance of immune markers, such as antibodies, to inform protection levels. In order to use within-host immunological models to inform susceptibility levels in between-host transmission models, we must understand the relationship between a given immune marker and the relative protection it provides. Chapter 4 shows that current inference methods used to estimate this relationship are limited in their ability to infer realistic protection functions. An alternative model is proposed and tested, which provides a strong foundation to learn how within-host immune markers are associated with reductions in susceptibility. This chapter lays the groundwork for future multi-scale modeling efforts to incorporate serology data into between-host transmission models.

Chapter 5 concludes this work with a synopsis of results from each chapter. This chapter discusses the implications of the findings in this thesis, limitations to the body of work, and open questions which may inform future research prospects.

Chapter 2

Modeling the Transmission Mitigation Impact of Testing for Infectious Diseases

Portions of this chapter are adapted from:

Casey E. Middleton, Daniel B. Larremore, *Modeling the transmission mitigation impact of testing for infectious diseases.* Sci. Adv. 10:eadk5108, 2024. DOI: 10.1126/sciadv.adk5108.

2.1 Introduction

Throughout the SARS-CoV-2 pandemic, the status quo for diagnostic test usage evolved. Despite documented successes of routine screening for SARS-CoV-2 in nursing homes [155], college campuses [200], and even nations [186], regular screening via RT-qPCR or rapid diagnostic tests (RDTs) gave way to elective testing after known exposures or symptom onset, typically with RDTs alone. At the same time, the variety and targets of available diagnostics continues to grow, with numerous available RDTs for respiratory syncytial virus (RSV; [18]) and influenza A [159], new RDTS for SARS-CoV-2 utilizing exhaled aerosols [79], and simultaneous testing for all three viruses via both multiplex RT-qPCR [44] and rapid antigen lateral flow "triple tests" [67]. Rapid diagnostics have proved valuable for a broader set of pathogens too, including HIV [92] and measles [60], as well as *P. falciparum*, with sufficient impact that rapid diagnosis and treatment have even selected for RDT-escape mutations among *P. falciparum* parasites [66].

Direct empirical estimation of the population-scale impact of testing is difficult, and only possible retrospectively, elevating the value of mathematical modeling that can predict it from first principles. Mathematical models estimating the impacts of testing on transmission [16, 82, 103, 124, 129, 136, 185, 200, 222] and treatment [158, 258] proved useful in guiding policy and recommendations for SARS-CoV-2, building

in many ways on a broad set of earlier efforts to estimate transmission reduction, clinical impact, and cost effectiveness for routine HIV screening (e.g., [107, 256]). However, these successes have been restricted to a limited number of pathogens and either routine screening or risk-group based testing, highlighting the need for more flexible modeling to accommodate an increasing array of diagnostic tests for a growing set of pathogens, used electively after known exposures or symptom onset. Moreover, because testing guidelines are only as effective as human behaviors allow them to be, it would be valuable for models to incorporate key behaviors such as imperfect participation [92] and compliance [21] and imperfect adherence to post-diagnosis isolation [221].

Here, we fill this gap by introducing a more general mathematical model for testing without restricting analysis to a single pathogen, test, testing pattern, or set of behaviors. Our focus is to estimate (i) the extent to which testing reduces the risk of transmission for infected individuals, (ii) the distribution of diagnosis times and the probability that individuals are diagnosed at all, and (iii) the costs of test consumption and isolation days corresponding to these diagnosis and transmission mitigation benefits. Taken together, this model places various intuitions about disease mitigation via testing on firm quantitative ground, and exposes important testing-associated variables and behaviors to *in silico* experimentation and optimization.

To demonstrate how one might use our model, we apply it to the study of the respiratory pathogens RSV, influenza A, and SARS-CoV-2. We first analyze differences between pathogens and between testing strategies by asking whether a single testing strategy might be optimal for all three focal pathogens. Second, we ask when one should test after respiratory symptoms appear, acknowledging that supplies may be limited and infection may not yet be detectable at symptom onset. Third, we reevaluate the tradeoffs between test sensitivity and turnaround time for SARS-CoV-2 in light of shifts in viral kinetics and symptom onset time caused by immune experience and new variants. Finally, we compare the costs and benefits of fixed-duration and test-to-exit isolation guidelines using the model's cost estimates for test consumption and days spent in isolation. In this way, this chapter has twin goals: to first introduce a flexible mathematical model for testing, and then demonstrate its value in the service of relevant scientific and policy questions.

2.2 Results

2.2.1 A model for testing effectiveness (TE)

To examine the impact of testing on community transmission, we developed a probabilistic model which integrates four key elements: (i) the properties of a particular diagnostic test, (ii) a strategy for its administration, (iii) the time-varying profiles of infectiousness, symptoms, and detectability over the course of an infection, and (iv) the key behaviors of participation (whether or not one refuses to test), compliance (whether or not one takes a recommended test), and isolation length. Given these elements, the model generates a distribution of probable diagnosis times, and uses them to compute the expected reduction in the risk of transmission due to testing. By then incorporating heterogeneity between individuals, the model estimates *testing effectiveness*, the proportion by which a testing program reduces population-level transmission, in expectation, given by the relationship between reproductive numbers R with and without testing,

$$TE = 1 - \frac{R_{\text{testing}}}{R_{\text{no testing}}} \quad \leftrightarrow \quad R_{\text{testing}} = (1 - TE)\, R_{\text{no testing}} \,. \tag{2.1}$$

This definition intentionally mirrors the language of vaccine effectiveness (VE) against onward transmission, that is, the expected reduction in post-infection transmission risk for vaccinated vs unvaccinated individuals [25, 64]. However, we name the present quantity *testing effectiveness* instead of *test effectiveness* due to the simple observation that the same test, used differently, may have a markedly different impact.

We built our analyses around a simple, common, and computationally efficient model of within-host pathogen kinetics: after some post-exposure latent period, the pathogen load grows exponentially at some proliferation rate until reaching a peak, and then declines exponentially at some clearance rate. This leads to a piecewise linear model of log pathogen load which requires only the four parameters of latent, proliferation, and clearance periods, and a peak load, which we draw from distributions estimated from studies of RSV [210, 213], influenza A [34, 108, 220], and SARS-CoV-2 measured for both the founder strain in naive hosts during the pre-vaccination era [121, 124, 136] and omicron variants in experienced hosts during the post-vaccination era [94, 121] (see Table S1). While the results presented here utilize this simplistic model

of viral kinetics, the modeling framework is highly flexible to incorporate more sophisticated alternatives.

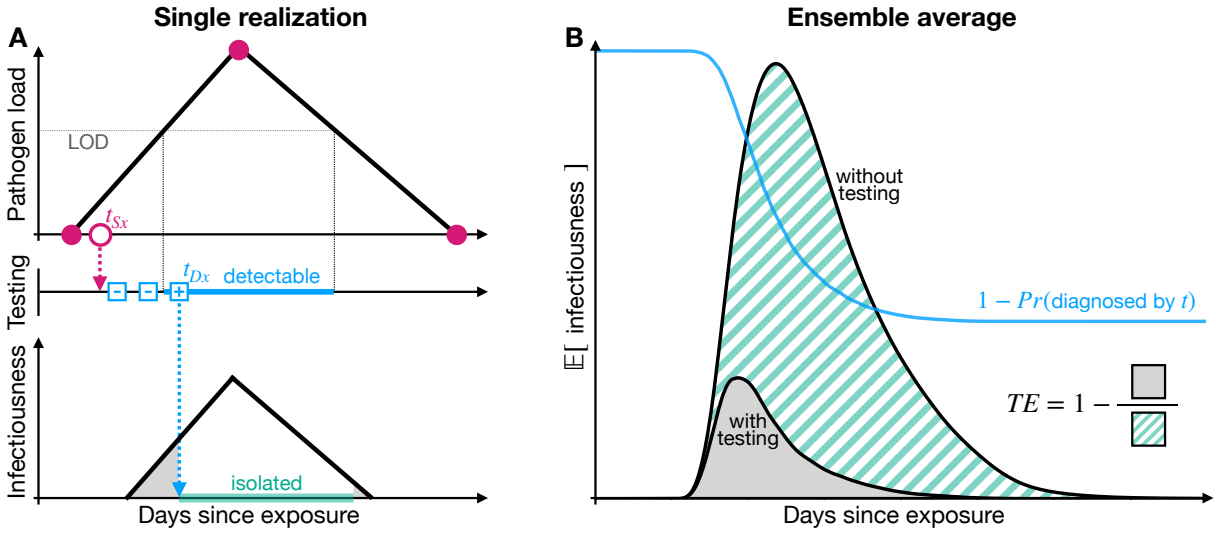

Figure 2.1: **Model diagram.** (A) Each realization of the stochastic testing model first draws four control points to specify a piecewise linear model of pathogen load on a logarithmic scale (filled pink circles) and a symptom onset time (t_{Sx}, open pink circle). The realization then draws a set of testing times (open blue squares), which may be triggered by symptoms (pink arrow), triggered by a known exposure (not shown), or ongoing at a particular cadence (not shown). A test taken during the detectable window (blue bar) when pathogen load exceeds the test's limit of detection (LOD, gray line) will return a positive diagnosis with a fixed probability after a specified turnaround time (not shown). However, not all tests are necessarily taken, due to imperfect compliance (not shown). Diagnosis at time t_{Dx} leads to isolation and thus reduced infectiousness (grey). (B) The ensemble mean, whether computed through integrals or estimated via Monte Carlo, produces expected infectiousness curves with and without testing. The areas under these curves are proportional to their respective reproductive numbers, enabling estimation of testing effectiveness TE (see Eq. (2.1)). The model also computes the proportion of individuals who remain undiagnosed at time t (blue curve), a curve which approaches zero as ascertainment approaches 100%.

We used stochastic realizations from this simple pathogen load model in three ways. First, we assumed that a test taken at time t would return a negative diagnosis if the pathogen load was below the test's

limit of detection (LOD), and would return a positive diagnosis with some probability when pathogen load was above the LOD. Due to the importance of test turnaround time [136], we modeled sample-to-answer delays by returning results after a specified turn-around time (TAT). Second, we took infectiousness to be proportional to the logarithm of pathogen load in excess of an empirically estimated threshold [116, 117], consistent with observations that higher viral loads are associated with more efficient transmission for pathogens including SARS [187], SARS-CoV-2 [21], influenza [138], and RSV [173]. Alternative relationships between pathogen load and infectiousness are possible [116, 136]. Third, we drew symptom onset times relative to the times of peak pathogen load, reflective of the typical manner of reporting in the literature [138, 141]. In this way, our model is similar in spirit to the CEPAC model (Cost-Effectiveness of Preventing AIDS Complications), which provides stochastic individual-level realizations of post-HIV-infection dynamics, costs, and outcomes [1].

Our model generates its estimates by integrating over the timing of possible symptoms and tests, to calculate a distribution of diagnosis times, including the possibility of no diagnosis at all. If receiving a diagnosis, each individual is assumed to isolate thereafter for a specified number of days, or until released by a negative test (via a so-called test-to-exit plan), with mitigated infectiousness during isolation (Fig. 2.1A). By averaging outcomes over the ensemble defined by its random variables, whether by integration or via Monte Carlo, the model produces estimates of the expected infectiousness curves over time, with and without testing (Fig. 2.1B). The areas under these two curves are proportional to the total transmission potential with and without testing, and thus, their respective reproductive numbers. The model also provides a curve representing the cumulative probability that a randomly chosen infected individual has not yet been diagnosed by some time (Fig. 2.1B). The long-time limit of this curve is particularly useful because it represents the proportion of the infected population who escape diagnosis entirely. Its complement, the proportion of the infected population to receive a diagnosis at any point, is therefore the ascertainment of the testing scenario, a quantity also called protocol sensitivity in the literature [222]. A complete mathematical description and details of parameterizations can be found in Materials and Methods.

2.2.2 Testing effectiveness varies by strategy and pathogen

Despite the 2023 end to the World Health Organization's COVID-19 public health emergency [253], the burden of COVID-19 and respiratory viruses more broadly remains substantial. In the U.S. alone, an estimated 9 million cases of influenza A caused 100,000 hospitalizations (2021-2022 season; [239]), and a global estimate of 33 million RSV infections in children under 5y led to 3.6 million associated hospitalizations and 101,400 associated deaths, the vast majority of which were in low- and middle-income countries (2019; [145]). With the broad expansion of diagnostic testing globally, including at-home rapid diagnostic tests (RDTs) for influenza A, RSV, and SARS-CoV-2, we sought to determine whether a single testing strategy might be optimal for all three common respiratory pathogens.

To examine the potential impacts of testing, we considered three distinct testing behaviors, meant to capture both institutional testing strategies and elective testing in response to exposure or symptoms. First, we considered routine weekly RDT screening (turnaround time TAT $= 0$, LODs Table S1). Given the markedly different sensitivities of different RDT kits and RT-qPCR protocols [14, 15], a representative limit of detection (LOD) was chosen for each respiratory virus to investigate general principles of testing (see Materials and Methods). To incorporate the fact that not all policy-prescribed tests are actually taken in practice [21], this scenario included compliance of only 50%, such that each test was taken or not taken independently with probability $\frac{1}{2}$. Second, we considered an elective testing scenario in which individuals experiencing symptoms used one RDT per day for 2 consecutive days following the onset of symptoms (TAT $= 0$; see Table S1 for stochastic timing and prevalence of symptoms). Finally, we considered an elective testing scenario in which 75% of individuals sought out a single RT-qPCR test (TAT $= 2$, see Table S1 for LODs) between 2d and 7d after exposure; the other 25% did not participate. For each scenario, and each of the three circulating respiratory viruses (RSV, influenza A, and SARS-CoV-2), we calculated TE, the timing of diagnoses, and ascertainment—the total fraction of individuals receiving a positive diagnosis—based on 10^5 stochastic realizations of viral load, symptom onset, testing, diagnosis, and isolation. For SARS-CoV-2 we specifically considered within-host dynamics and RDTs associated with omicron variants in immune-experienced hosts.

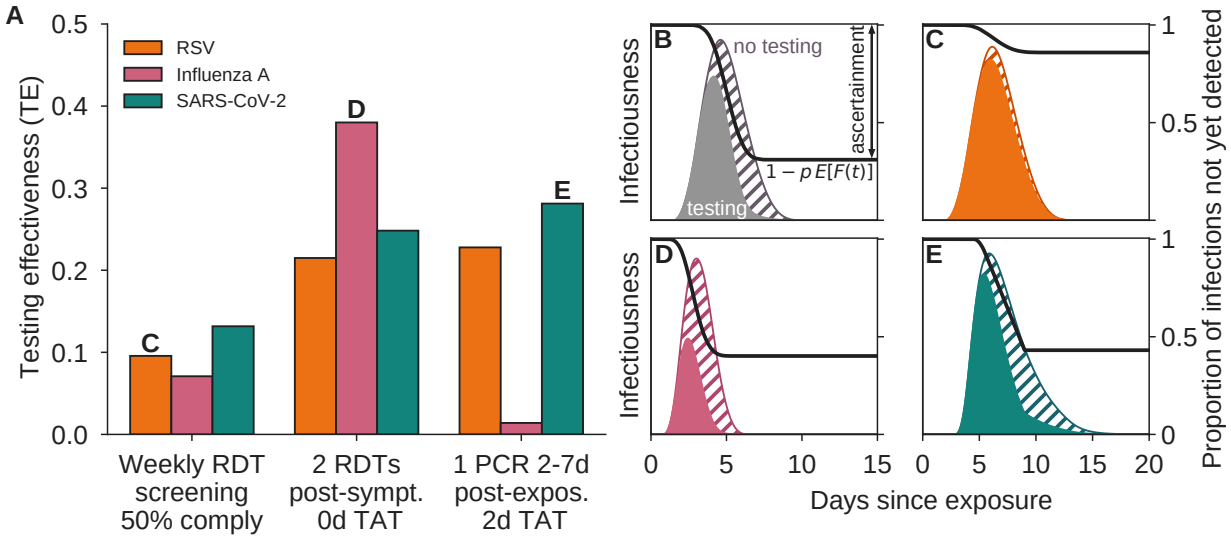

Figure 2.2: **Testing effectiveness varies considerably by strategy and pathogen.** (A) Testing effectiveness is shown for RSV (orange), influenza A (pink), and SARS-CoV-2 omicron in experienced hosts (green) under three testing programs: (1) weekly rapid diagnostic test (RDT) screening with 50% compliance, (2) testing with one RDT per day for two days starting at symptom onset, and (3) one RT-qPCR test administered 2-7d after exposure, with 75% participation and 2d test turnaround time (TAT). Panels C-E depict population-level infectiousness curves without (hatched) and with (filled) testing and isolation for the labeled pathogen and testing program, and panel B provides annotations for an example simulation. Black curves represent the proportion of infections not yet detected by time t. See Fig. S1 for scenario ascertainment rates and Fig. S2 for population-level infectiousness curves for all testing scenarios.

This analysis demonstrated that a test, how it is used, and the pathogen it targets, can interact in potentially complicated ways. For instance, we found that weekly RDT screening with 50% compliance exhibited low TE for all three pathogens, ranging from 13% for omicron-era SARS-CoV-2 down to just 7% for influenza A (Fig. 2.2A). These low values are driven by the fact that the time windows during which the pathogens are detectable via RDT are almost always shorter than 7d, meaning that weekly testing missed a considerable number of infections (Fig. 2.3). These short detection windows are compounded by the assumed 50% compliance, leading to low ascertainment across pathogens (11-14%).

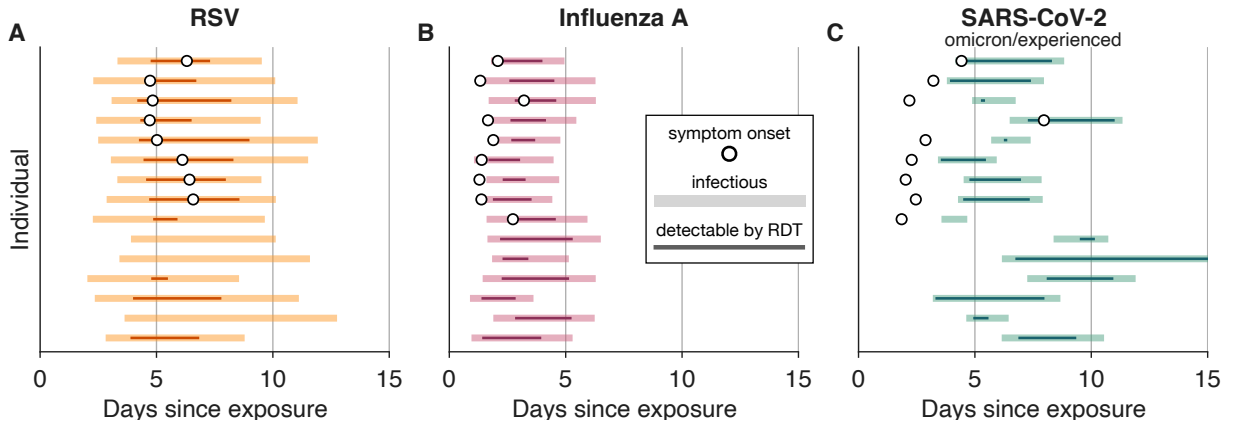

Figure 2.3: **Relative timing of symptom onset, infectiousness, and detectability vary by pathogen and individual.** Symptom onset time (open circles), infectious period (shaded rectangles), and window of detectability by a rapid diagnostic test (RDT, colored lines) are shown for 15 stochastic realizations of RSV (A, orange), influenza A (B, pink), and SARS-CoV-2 omicron/experienced (C, green) infections. The absence of an open circle indicates an asymptomatic infection. See Supplementary Table S1 for parameters and references.

In contrast to regular screening, elective testing with the same RDT at symptom onset achieved 38% TE for influenza A, but only 21% for RSV (Fig. 2.2A). This difference in effectiveness primarily reflects differences in the relative timing of symptoms, infectiousness, and detectability: both influenza A and RSV typically become detectable by RDT within one day of symptom onset, but RSV infections are characterized by higher rates of asymptomatic and pre-symptomatic infectiousness (Fig. 2.3A,B). In contrast, TE for elective testing at SARS-CoV-2 symptom onset was middling at 25%, balancing early detection for those who test positive with lower ascertainment as a result of testing too early to be detected (Fig. 2.3C). Due to their highly overlapping symptom sets, our results indicate that testing immediately after symptom onset with a single three-pathogen RDT [67] is therefore likely to mitigate transmission most for influenza A, followed by SARS-CoV-2 omicron and RSV.

This ordering of differential TE was inverted for a single elective RT-qPCR between 2d and 7d post-exposure, which was least effective for influenza A (Fig. 2.2A). This ordering reflects a substantially faster

onset of infectiousness after exposure for influenza A (Fig. 2.3B), meaning that a post-exposure test that is timed effectively for SARS-CoV-2 and RSV is administered far too late to effectively control influenza A. Thus, in a scenario where an individual seeks a highly sensitive multiplex diagnostic test within one week after a known exposure to an unknown respiratory pathogen, our results indicate an impact on transmission of 28% for SARS-CoV-2, 22% for RSV, and just 2% for influenza.

Our results highlight the fact that variation in viral kinetics, symptom onset time, tests' analytical sensitivities, and interactions thereof, lead to markedly different impacts on transmission, even under the same testing guidance. Given these complexities, we explored whether varying either the pathogen load above which individuals are considered infectious or the RDT limit of detection would substantially alter our findings. These sensitivity analyses showed that, while the magnitude of TE varies slightly, the primary trends documented above remain consistent (Fig. S3).

Throughout these experiments, we observed that ascertainment—the proportion of infections diagnosed via testing—was only weakly related to TE, showing that a testing program's information value and mitigation impact are distinct quantities. For instance, elective RDT testing post-symptoms for influenza A showed TE and ascertainment of 38% and 60%, respectively; for elective RT-qPCR testing post-exposure, TE decreased by 36 percentage points to just 2% but ascertainment decreased by only 10 percentage points to 50% (Fig. S1). To illustrate the reason for this difference, we plotted the infectiousness curves $\beta(t)$ with and without testing, averaged over all 10^5 simulated individuals, as well as the curves showing the fraction of individuals remaining undiagnosed $1 - p\,\mathbb{E}\left[F(t)\right]$ (Fig. 2.2C,D,E). In instances where diagnoses typically arrive earlier, the average $\beta(t)$ (and thus the area beneath it, R_{testing}) is more substantially reduced, while the same number of diagnoses, arriving later, leave more area under the $\beta(t)$ curve. Thus, TE incorporates not just whether one is diagnosed, but also when.

2.2.3 Impacts of timing and availability of elective post-symptom testing

In an era of increasing elective and self-administered rapid diagnostic test (RDT) usage, two key questions are when to test and how many tests to use. We sought to answer these questions by modeling the

impact of changes in timing and supply of RDTs on TE for RSV, influenza A, and SARS-CoV-2 omicron in experienced hosts. In these experiments, we considered that individuals would wait 0d-5d after symptom onset and then begin using one RDT per day, with 1-6 RDTs available. For comparison, we also computed TE for a single RT-qPCR with a two-day turnaround. For each fixed supply of tests, we then identified the optimal number of days post-symptoms that one should wait to maximize TE, separately for each pathogen (Fig. 2.4, white stars).

This experiment showed three common patterns for RSV and influenza A. First, the most effective timing of post-symptom testing was zero days, with TE decreasing monotonically for each additional day of delay (Fig. 2.4A,B). Second, although using two tests was superior to using one, using more than two tests was roughly equivalent to two. And third, using just one RDT provided superior TE to a single RT-qPCR with a two-day turnaround time, highlighting the importance of RDT availability and rapid results for transmission control.

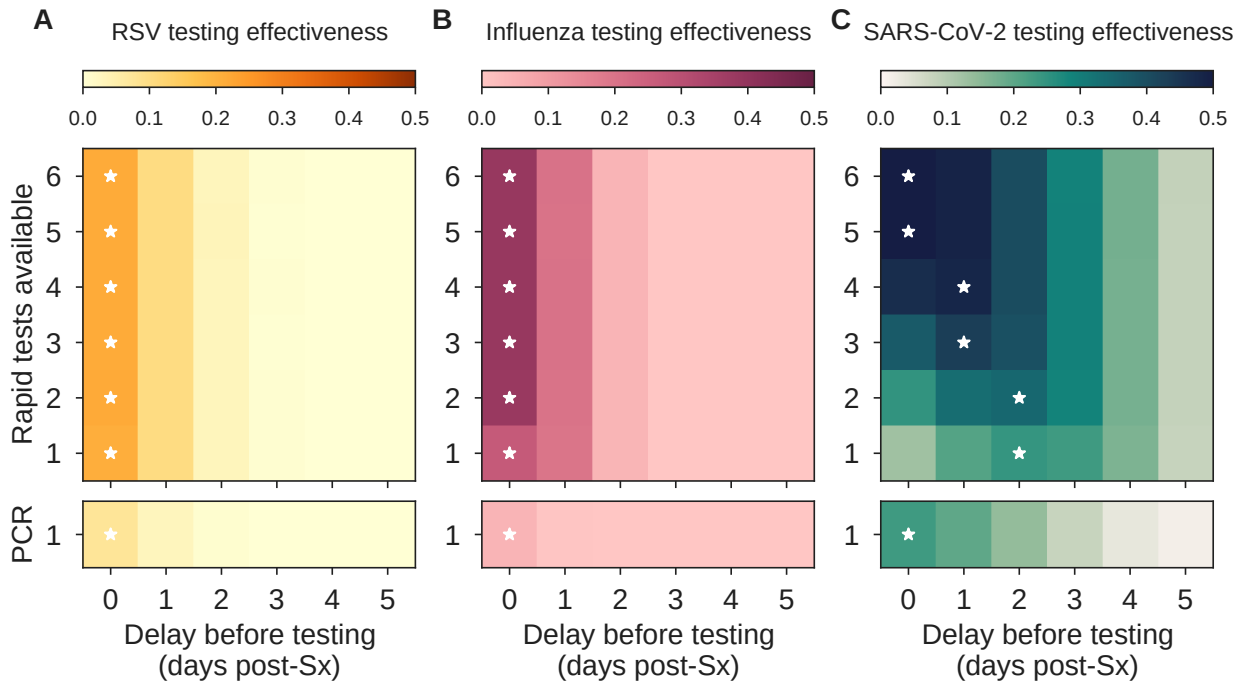

Figure 2.4: **Optimal use of tests depends on the number of tests available and when they are used.** Testing effectiveness (TE) of rapid test (RDT) and RT-qPCR with 2 day turnaround time, used x days after symptom (Sx) onset using y tests once per day is shown for RSV (A, orange), influenza A (B, pink), and SARS-CoV-2 omicron in experienced hosts (C, green). Darker colors represent higher TE as indicated. In each row, the testing strategy with highest TE is annotated with a white star. Turnaround times: rapid tests, TAT $= 0$; RT-qPCR TAT $= 2$. See Supplementary Table S1 for LODs and Fig. S4 and Fig. S5 for monochromatic TE and ascertainment visualizations, respectively.

In contrast, for SARS-CoV-2 omicron in experienced hosts, the number of available tests markedly shifted the optimal time at which one should begin testing, such that when only 1-2 RDTs were available, daily testing was most effective beginning 2d post-symptoms; with 3-4 RDTs, 1d; and with 5-6 RDTs, testing should begin immediately upon symptom onset (Fig. 2.4C). These results reflect a tradeoff arising from the variable gap between symptom onset and first detectability by RDTs (Fig. 2.3C): using tests later improves the probability of diagnosis but decreases the impact per diagnosis. A large test supply alleviates this tradeoff by enabling one to test early, with the potential for high impact, while also testing later to avoid

missing a diagnosis entirely. Furthermore, for a fixed delay before testing, using more SARS-CoV-2 RDTs was always superior, yet a single RT-qPCR on the first day of symptoms provided approximately equivalent TE to using one RDT starting on day two.

Together, these results suggest a unified recommendation for the timing of post-symptom testing via RT-qPCR for all three pathogens and post-symptom RDTs for RSV and influenza A: one should test immediately, regardless of the number of available tests. In contrast, the timing of optimal SARS-CoV-2 RDT use in supply-limited scenarios depends on the number of available tests. In sensitivity analyses varying the RDT limits of detection and changing the pathogen load threshold for infectiousness, these general findings were unchanged (Fig. S6), though the precise recommended post-symptom wait time for SARS-CoV-2 RDTs shifted in some sensitivity analyses by up to 1d.

One common point surfaced by our investigations of elective post-symptom testing was that the existence of any asymptomatic and presymptomatic transmission implies that $TE < 1$ for symptom-driven testing, regardless of the quality of the diagnostic test itself. This implies that even groundbreaking advances in diagnostic LODs, cost, or turnaround times must be paired with appropriate recommendations for usage.

Finally, we briefly note that identical questions of when to test and how many tests to use also arise after known exposure to a pathogen. An otherwise identical analysis recommends wait times of 3-5d after RSV or SARS-CoV-2 exposure, and 0-2d after influenza A exposure, depending on the number and type of available tests (Fig. S7).

2.2.4 Reevaluation of the sensitivity/turnaround tradeoff for SARS-CoV-2

Modeling studies in 2020 and 2021 argued that test sensitivity was secondary to frequency and turnaround time for SARS-CoV-2 screening [16, 26, 136, 162], using within-host dynamics and rapid diagnostic test (RDT) sensitivities for the founder strain in naive hosts. However, three important observations regarding the omicron variants circulating in 2023 led us to revisit these findings. First, studies of viral load trajectories, estimated via prospective longitudinal sampling, show lower peak viral loads, shorter clear-

ance times, and slightly longer proliferation times for omicron infections in experienced hosts compared to founder-strain infections in naive hosts [94, 124], leading to shorter windows of detectability (Fig. 2.5A). Second, symptom onset is typically 3-5d earlier for omicron/experienced vs founder/naive, relative to peak viral load, an observation argued to be due to the immune experience of hosts in particular [86, 94, 232]. Third, the analytical sensitivity of RDTs is estimated to have worsened for omicron variants vs founder strain, with limits of detection (LODs) increasing by $0.5 - 1.0$ orders of magnitude depending on the test [14, 15]. Together, these factors led us to hypothesize that the previously established superiority of RDTs over RT-qPCR for mitigation of founder-strain SARS-CoV-2 in a naive population could be equalized or reversed for omicron-variant SARS-CoV-2 in an immune experienced population.

To test our hypothesis, we estimated TE for RDT testing (0d turnaround time, TAT) and RT-qPCR testing (2d TAT) programs, in twice-weekly, weekly, and elective post-symptom testing scenarios, and compared our findings for founder/naive vs omicron/experienced parameters. We found that in each of the three founder/naive testing scenarios, RDTs provided higher TE than RT-qPCR (Fig. 2.5B), replicating the claims of the literature [16, 26, 136, 162]. However, each of the three omicron/experienced scenarios saw a reversal, with RT-qPCR providing higher TE than RDTs, despite the modeled 2d RT-qPCR turnaround time (Fig. 2.5C). In general, we also observed that TE decreased for RDTs from the founder-strain era to the omicron era (Fig. 2.5B vs C), while staying approximately the same (twice weekly, weekly) or even increasing (post-symptom) for RT-qPCR. Together, these results suggest that, setting aside any differences in cost or regulatory complexity, RT-qPCR-based SARS-CoV-2 testing would be superior to otherwise identical RDT-based testing in the omicron and immune-experienced era.

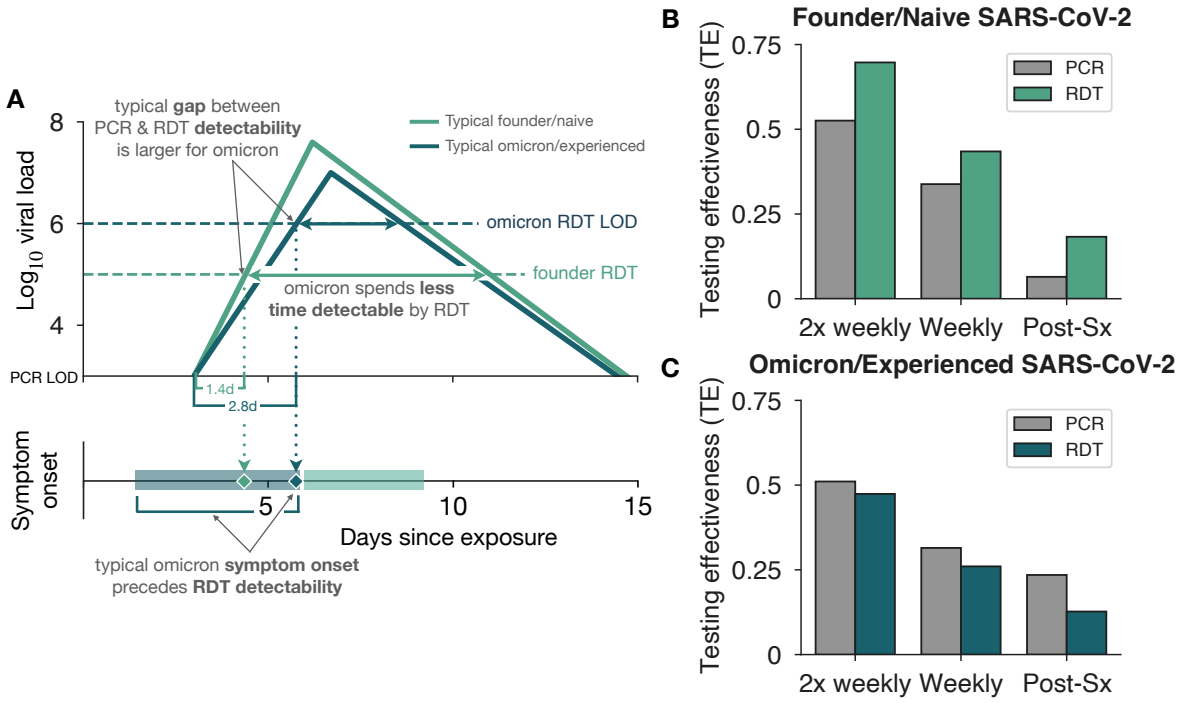

Figure 2.5: **RT-qPCR vs RDT tradeoffs for the SARS-CoV-2 omicron era.** (A) Typical viral kinetics for founder SARS-CoV-2 strains in naive hosts and SARS-CoV-2 omicron variants in experienced hosts ($\log_{10}$ cp mRNA / mL). Trajectories are characterized above the RT-qPCR limit of detection (LOD = 10^3) with their respective rapid diagnostic test (RDT) LODs indicated by horizontal dashed lines (10^5 and 10^6 for founder strain and omicron variant, respectively). Individuals are considered infectious when the viral load exceeds $10^{5.5}$ cp mRNA / mL. Potential symptom onset times for each trajectory are shaded on the lower axis. (B,C) Testing effectiveness using RT-qPCR with 2 day turnaround time (gray) or RDT with immediate delivery of results (green) for twice weekly and weekly screening, or testing immediately upon symptom (Sx) onset using one test.

To what can we attribute this apparent reversal in the prioritization of speed vs sensitivity, and how might such principles generalize? First, we note that during viral proliferation, there exists a gap between the time of first detectability via RT-qPCR and the time of first detectability via RDT. This gap represents a potential diagnostic advantage for the RT-qPCR test, but it can be realized only if (i) a test is actually taken during the gap, and (ii) the turnaround time for the RT-qPCR is smaller than the gap. For founder-

strain SARS-CoV-2 in the naive host, the typical gap is just 1.4d, vs 2.8d for SARS-CoV-2 omicron variants in experienced hosts (Fig. 2.5A). Thus, changes in viral proliferation and RDT limits of detection lead to a longer "head start" for RT-qPCR in the era of omicron variants. Second, we note that shortening the window of analytical detectability reduces the chance of diagnosis. For founder-strain SARS-CoV-2 in the naive host, the typical RDT detection window lasts 6.6d, vs 2.2d for SARS-CoV-2 omicron variants in experienced hosts. Thus, RDTs in the omicron variant era have fewer opportunities to contribute to testing effectiveness than those in the founder strain era. We expect both the head start and detection window intuitions to generalize, yet caution that direct estimation of TE is superior to intuition, as not all infections contribute equally to transmission so an apparent advantage for one test over another in the average case may disappear or reverse in the most consequential cases.

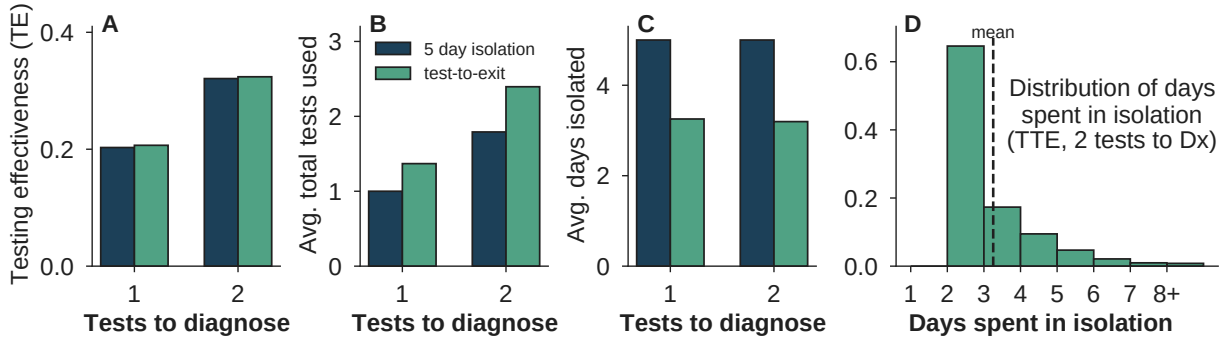

Figure 2.6: **Fixed isolation recommendations may lead to unnecessary isolation when symptomatic testing ascertainment is high.** (A) Testing effectiveness, (B) total test consumption over diagnosis and test-to-exit (TTE) usage, and (C) average isolation duration for detected individuals are shown for a fixed 5d isolation period (dark blue) and a test-to-exit isolation program requiring one negative rapid diagnostic test to exit isolation (light green) when 1 or 2 tests were available to diagnose (Dx), used daily beginning one day after symptom onset for SARS-CoV-2 omicron variants in experienced hosts. (D) The distribution of individual days spent in isolation for a test-to-exit scheme using 2 tests to diagnose, with the average isolation time indicated by the vertical dashed line. TTE scenarios assumed individuals waited 2 days after diagnosis before beginning exit-testing.

2.2.5 Estimating costs: isolation days and test consumption

Diagnosis-driven isolation provides a mitigation benefit of TE, but at the cost of testing resources and days spent in isolation. Therefore, in addition to quantifying the benefits of TE and ascertainment, we estimated the costs of test consumption and isolation days (Materials and Methods). When calculating these costs, we also recognized that diagnostic tests may be used to determine when one should exit isolation, via so-called test-to-exit (TTE) guidelines [238], potentially increasing test consumption in order to decrease isolation days, with the additional risk of early release from isolation due to a non-analytical test failure. Based on these modeling needs, we modified our estimates of all model outputs to incorporate TTE strategies (see Appendix).

To explore the ways in which our model could assist in evaluating complex cost-benefit tradeoffs across scenarios, we considered elective post-symptom testing for SARS-CoV-2 omicron variants in experienced hosts, using either one or two RDTs daily after symptom onset to attempt diagnosis. Diagnosis was followed by either a fixed-duration isolation of 5d, the minimum time recommended by CDC at time of writing [238], or a TTE policy of daily testing using the same RDT, beginning after a minimum of 2d spent in isolation. In each of the 2×2 scenarios, we computed TE, the average number of tests consumed per infected individual, and the average number of isolation days per diagnosed individual.

At a high level, using two tests to diagnose led to substantially higher TE than using just one (Fig. 2.6A), mirrored by an increase in per-infection testing cost from 1 to 1.8 tests for the fixed-isolation scenario, and from 1.4 to 2.4 for the TTE scenario (Fig. 2.6B). Average isolation days per diagnosis were identically 5d for the two-fixed isolation scenarios by definition, and reduced to 3.2-3.3d for TTE (Fig. 2.6C). Thus, as intended, TTE programs decreased average isolation days without a large impact on TE, driven by the fact that the most common outcome of TTE was release after just 48-72h, while nevertheless maintaining long isolations for those remaining detectable for longer periods (Fig. 2.6D).

2.3 Discussion

This chapter quantifies the impact of testing as a non-pharmaceutical intervention by defining testing effectiveness (TE) as the expected reduction in the risk of transmission for a particular testing behavior, test, and infecting pathogen. While TE varies considerably across the scenarios we explored, three general principles emerge. First, no single elective testing strategy provides superior control across respiratory viruses, due to important differences in their dynamics within host. This highlights the importance of models linking within-host kinetics to between-host transmission when establishing testing guidelines, and the risks of blanket recommendations for respiratory virus transmission control. Second, elective post-symptom or post-exposure testing can have a substantial impact on transmission, but timing is important and depends on the pathogen, test, and available supply. While greater availability of tests leads to strictly larger TE, in supply-limited scenarios, a strategic delay may lead to greater TE by diagnosing more infections, even if they are not detected as early. Last, by modeling tests and testing through different parameters, our analyses show the importance of key behaviors, including compliance, post-diagnosis isolation, and the manner in which to test. These present opportunities to markedly increase the mitigation impact of testing through not only test technology and availability, but through usage guidance and policy as well, based on quantitative guidance from the model.

By exploring TE under various testing scenarios for three common respiratory viruses, this chapter demonstrated that an effective strategy for one pathogen may be ineffective for another, and vice versa. This is driven by the complex tradeoffs between a test's timing, probability of diagnosis, and number of potentially avoided future transmissions should the test come back positive. Intuitively, early testing leads to fewer diagnoses with higher impact per diagnosis, while delayed testing leads to more diagnoses but lower impact per diagnosis. Mathematical models integrating over these contingent factors, stochasticity, and heterogeneity between individual infections, are critical to putting this intuition on a quantitative foundation.

Exemplifying this value, our analysis showed that the use of rapid diagnostic tests upon symptom onset may be an effective strategy for transmission control of RSV and influenza A, but strategic delays in

testing may provide higher effectiveness when test availability is limited for SARS-CoV-2. Our analysis also showed that testing with a slower but more sensitive RT-qPCR exhibited a higher TE than otherwise identical rapid antigen testing for SARS-CoV-2 omicron variants in experienced hosts (but not founder SARS-CoV-2 strains in naive hosts), updating a previously published finding that emphasized turnaround time over sensitivity for founder-strain SARS-CoV-2 [136]. Importantly, this analysis focused only on TE under an assumption of identical participation and compliance. However, self-administered rapid diagnostics may have greater availability, lower cost, and higher tolerability than RT-qPCR tests, factors which may lead to differences in participation and compliance which in turn could be incorporated into updated TE estimates. These examples show how TE and its modeling framework may empower researchers or public health strategists to prospectively evaluate diverse testing strategies and behaviors.

The model introduced in this chapter was necessary because empirical evaluation of the impact of a testing program or behavior is difficult, with compelling analyses nevertheless lacking formal controls [186, 200] or requiring enormous scale [155]. In contrast with various methods to empirically estimate vaccine effectiveness VE, we know of no direct identification strategies for testing effectiveness (or similar quantities) in real-world settings. Complicating matters, our calculations suggest that any effective testing program will also shorten the generation interval and increase ascertainment, two quantities that impact the data and models underyling common estimators of the reproductive number R [246]. This suggests that an R-based empirical TE estimator would present challenges. Methodological development in this direction would be valuable.

Our modeling provides four potentially useful outputs beyond TE. First, we have attempted to quantify the twin costs of test consumption and isolation days, enabling the Pareto frontier between cost and benefit to be explored under a variety of assumptions. When weighted by dollar costs, these estimates may be useful for individuals and policymakers alike. Second, our calculations estimate ascertainment, which may be useful for surveillance and situational awareness. Third, the distribution of $t_{\text{Dx}} - \text{TAT}$, the post-exposure time at which the diagnosing test was taken, could be a valuable inclusion in "nowcasting" models, while the implied distribution of pathogen loads in diagnosing samples may be useful in estimating

population-scale epidemiologic dynamics [93]. Finally, in smaller populations, actual testing effectiveness may differ from TE estimates due to finite size effects, variation which could be estimated from sets of Monte Carlo approximations, enabling the incorporation of uncertainty into testing strategy evaluation.

Our work is subject to a number of important limitations associated with the structure of our model. First, we assumed that symptoms may trigger testing, but do not trigger isolation in and of themselves. Relaxation of this assumption would require empirical estimates of self-isolation behavior or simply the additional assumption that a proportion of individuals isolate at symptom onset without testing [136]. Second, we modeled participation/refusal, compliance, and isolation behaviors as statistically independent between individuals, but health-related behaviors are known to be clustered [104, 126, 147], a type of heterogeneity not included in our TE calculations. In principle, estimates of TE for a set of behaviorally homogeneous groups could be computed and integrated into appropriately structured transmission models [27]. Finally, our model includes no treatment of specificity, an important factor for certain classes of diagnostic tests. The inclusion of imperfect specificity in our model would not affect TE estimates, but could substantially affect cost estimates, particularly if a low positive predictive value led to markedly more isolation days. For such scenarios, our model could be easily extended to include a second confirmatory test to derive a new distribution for t_{Dx}.

Our work is also subject to limitations associated with parameterization. For instance, we relied on estimates of pathogen load dynamics and symptom onset time, including variation thereof across a population. These are relatively well characterized for variants of SARS-CoV-2 in moderate to large population cohorts [116, 117, 121, 124, 208], but are sparse for RSV [210, 213] and influenza A [34, 108, 220] where they come typically from small numbers of healthy volunteers in human challenge studies and are typically presented through population means and confidence intervals, which, at best, indirectly inform between-host variation [257]. Even weakly characterized distributions are effectively unknown for many other pathogens, particularly prior to symptom onset. Joint estimates of viral kinetics and symptom prevalence and timing for many communicable diseases would be powerful for our modeling, and useful in many other applications as well, including studies of the value of early diagnosis as a path to timely treatment [158, 258]. Another im-

portant limitation is the assumption that infectiousness can be parameterized as a function of the logarithm of viral load. While viral load and infectiousness are empirically linked in some studies [21, 113, 116], their precise relationship is more complicated. For instance, studies of SARS-COV-2 have shown fewer plaque-forming units per copy of viral RNA during an infection's clearance phase than during its proliferation phase [86].

Finally, as with any public health intervention, there are important ethical considerations related to this work. This chapter focused on using resources (tests and isolation days) to provide a benefit (decreased transmission), yet not all individuals, communities, or settings may be equally well positioned to afford tests or isolation time. Similarly, our modeling focuses on population-scale transmission, but ignores heterogeneity in vulnerability among those to whom a disease may be transmitted. Finally, stigma around infection status could lead to low participation, particularly if that otherwise private status will be disclosed [132]. Application of this work should consider affordability, incentives, vulnerability, and privacy in local contexts.

2.4 Materials and Methods

2.4.1 Mathematical Model for Testing

We introduce testing effectiveness TE as the proportion by which a testing program decreases the risk of transmission, given infection, for an infectious disease [Eq. (2.1)] and define a mathematical model to prospectively estimate it. This model combines known or assumed properties of (i) a particular diagnostic test, (ii) a strategy for its administration, (iii) behavior/isolation after diagnosis, and (iv) the time-varying profiles of infectiousness and detectability over the course of an infection. Due to its integration of these elements, the model can also estimate a testing program's ascertainment (the proportion of infections detected), the impact of testing on the generation interval and selection coefficients, the distribution of diagnosis times, and the expected number of tests and isolation days required per diagnosis.

2.4.1.1 Infectiousness

In the absence of testing, the individual reproductive number ν_0 quantifies the expected number of secondary infections from that person [149], under typical behavior. It is given by the area under that individual's infectiousness curve $\beta(t)$ over time,

$$\nu_0 = \int_0^\infty \beta(t)\, dt\ . \tag{2.2}$$

The mean across all individual reproductive numbers is R by definition, and therefore

$$R_{\text{no testing}} = \mathbb{E}\left[\nu_0\right] = \int_0^\infty \mathbb{E}\left[\beta(t)\right]\ dt\ . \tag{2.3}$$

By prompting a post-diagnosis behavior change, participation in testing may isolate or attenuate part of that individual's infectiousness, decreasing its total from ν_0 to $\bar{\nu}_{\text{testing}}$. Provided that one's ν_0 and one's testing behaviors are statistically independent, then the mean across all individuals' $\bar{\nu}_{\text{testing}}$ is related to the effective reproductive number as

$$R_{\text{testing}} = p\mathbb{E}\left[\bar{\nu}_{\text{testing}}\right] + (1-p)\mathbb{E}\left[\nu_0\right]\ , \tag{2.4}$$

where p represents the proportion of the population participating in testing. The participation rate incorporates both the proportion of the population that "opts in" to testing, as well as the fact that even among those opting in, not all will experience symptoms (for elective post-symptom testing) or be alerted to their having been exposed (for elective post-exposure testing). Our focus in the derivation that follows is to estimate $\bar{\nu}_{\text{testing}}$ for each person, after which we may average to get R_{testing} and thus TE.

2.4.1.2 Isolation after diagnosis

Suppose that at time t_{Dx}, an individual receives a diagnosis that causes them to attenuate their infectiousness via a change in behavior, such as isolation, masking, or increased ventilation. Here, we develop the mathematics corresponding to perfect isolation post-diagnosis, but provide equations for partial and/or time-varying impacts of behavior on transmission in Appendix. Post-diagnosis isolation leads to

$$\nu_{\text{testing}}(t_{\text{Dx}}, t_{\text{exit}}) = \int_0^{t_{\text{Dx}}} \beta(t)\, dt\ + \int_{t_{\text{exit}}}^\infty \beta(t)\, dt\ , \tag{2.5}$$

which has the simple interpretation that one's infectiousness is simply that which occurred prior to diagnosis at t_{Dx} and that which occurred after exiting isolation at t_{exit}. While more complicated test-to-exit equations are developed in the Appendix, here we consider only fixed isolation periods of duration ℓ, such that $t_{\text{exit}} = t_{\text{Dx}} + \ell$.

2.4.1.3 Time of diagnosis as a random variable.

In practice, the time of diagnosis t_{Dx} depends on numerous factors including test availability or schedule or the timing of symptoms. We model t_{Dx} as a random variable with probability density function $f(t_{\text{Dx}})$. This leads to an effective infectiousness, calculated in expectation over the probable times of diagnosis, of

$$\bar{\nu}_{\text{testing}} = \int_0^\infty \nu_{\text{testing}}(t_{\text{Dx}})\, f(t_{\text{Dx}})\, dt_{\text{Dx}} \ . \tag{2.6}$$

Substituting in the definition of $\nu_{\text{testing}}(t_{\text{Dx}})$ from Eq. (S1), rearranging, and making use of the cumulative probability of a diagnosis $F(t)$,

$$\bar{\nu}_{\text{testing}} = \nu_0 - \int_0^\infty \beta(t)\, [F(t) - F(t-\ell)]\ dt \ . \tag{2.7}$$

We note that if one reinterprets $F(t)$ as the cumulative probability of symptom onset (as if symptoms were the diagnostic test itself), with an exhaustive isolation thereafter (large ℓ), then Eq. (2.7) recovers the core notion of symptom-based controllability of Fraser et al. [69]. However, unlike symptom onset, the time of diagnosis via testing t_{Dx} depends on within-host kinetics, test administration, and of course the test itself, as we calculate next.

2.4.1.4 Calculating t_{Dx}: testing, compliance, failure rates, detectability, and turnaround time

To calculate the distribution of diagnosis times $f(t_{\text{Dx}})$, we combine test administration—the probability that a test is administered at a particular time—and detection—the conditional probability that said test would return a positive diagnosis. This approach naturally separates a test administration strategy from the properties and performance of the particular diagnostic to be modeled.

Let $A(t)$ be the prescribed rate of test administration in tests per day, such that for sufficiently small

δ,

$$\Pr(\text{test administered between } t \text{ and } t+\delta) = \int_t^{t+\delta} A(t')\,dt' \,. \tag{2.8}$$

For instance, setting $A(t) = \frac{1}{7}$ would model a weekly screening regimen, while $A(t) = 2$ for $4 \leq t \leq 6$ would represent twice-daily testing starting 4 days post-exposure and ending on day 6.

Let $D(t)$ be an indicator function representing the analytical detectability of the infection at time t for a given diagnostic, such that $D(t) = 1$ when an infection is, in principle, detectable by that diagnostic, and $D(t) = 0$ otherwise. For example, to model qPCR, $D(t) = 1$ when concentrations of RNA or DNA from a biospecimen exceed the assay's limit of detection; below the limit of detection, $D(t) = 0$.

Combining administration with detectability, the cumulative number of scheduled tests with the potential to return a positive result by time t is

$$m(t) = \int_0^{t-\text{TAT}} A(t')\,D(t')\,dt' \,. \tag{2.9}$$

Note that the integral's upper limit is shifted by TAT, the test turnaround time, i.e., the amount of time between a test's administration and the return of actionable results. Although any particular person may have taken only an integer number of tests, $m(t)$ computes a real-valued expectation over all testing schedules or phases that match the specified rate $A(t)$.

The function $A(t)$ represents an *intended* test administration strategy (e.g., a policy or guideline), yet in many circumstances, imperfect compliance may result in missed tests. To account for compliance, we let c be the independent Bernoulli probability that each test is actually taken as intended.

Similarly, a test may fail for reasons unrelated to the analytical limit of detection or presence of a symptom. For example, poor biospecimen collection technique (e.g. poor nasal swab technique) could result in test failure irrespective of an assay's limit of detection [14]. To account for test failure of this type, we let ϕ be the independent Bernoulli probability that a test fails for non-analytical reasons.

Combining the number of possible positive tests taken $m(t)$ with compliance c and test failure ϕ,

allows us to compute the cumulative probability that one has received a positive test by time t,

$$F(t) = 1 - (1 - \bar{m}(t))[1 - c(1 - \phi)]^{m(t)-\bar{m}(t)} - \bar{m}(t)[1 - c(1 - \phi)]^{m(t)-\bar{m}(t)+1} \tag{2.10}$$

where $\bar{m}(t) = m(t) \bmod 1$. This function reflects the cumulative probability that for a monotonically increasing number of possible positive tests $m(t)$, there are two possibilities: one may have taken either $m(t) - \bar{m}(t)$ tests with probability $(1 - \bar{m}(t))$, or $m(t) - \bar{m}(t) + 1$ tests with probability $\bar{m}(t)$. In turn, each of these integer number possible positive tests tests may fail (with probability ϕ) or be missed due to non-compliance (with probability $1 - c$). We note that this is an improper CDF which need not reach 1 in the limit of large t, as not all individuals will necessarily receive a diagnosis.

In the case where the product $A(t)D(t)$ is a constant $\bar{A}$ between t_1 and t_2, and 0 otherwise, the associated improper PDF is

$$f(t) = \bar{A}c(1 - \phi)\left(1 - c(1 - \phi)\right)^{m(t)-\bar{m}(t)} \tag{2.11}$$

for $t_1 + \text{TAT} \leq t \leq t_2 + \text{TAT}$ and 0 otherwise.

In the specific case of elective testing at symptom onset, the functions above require slight modification to include the symptom onset time t_{Sx}. We modeled t_{Sx} as a random offset from the time of peak viral load, drawn from a specified uniform distribution (see Supplementary Table **??**), a choice that reflects the way symptom onset is typically reported in the literature. For the cases considered in this chapter, individuals wait x days after symptoms and test for y days at rate $\bar{A}$ per day, leading to a test administration function,

$$A(t, t_{\text{Sx}}) = \bar{A}\left[u(t - t_{\text{Sx}} - x) - u(t - t_{\text{Sx}} - x - y)\right] , \tag{2.12}$$

where $u(t)$ is the unit step function defined as 0 prior to t and 1 thereafter. This equation means that Eq. (2.9) depends on t_{Sx}, and thus so does the cumulative probability of detection,

$$F(t, t_{\text{Sx}}) = 1 - (1 - \bar{m}(t, t_{\text{Sx}}))[1 - c(1 - \phi)]^{m(t,t_{\text{Sx}})-\bar{m}(t,t_{\text{Sx}})} - \bar{m}(t, t_{\text{Sx}})[1 - c(1 - \phi)]^{m(t,t_{\text{Sx}})-\bar{m}(t,t_{\text{Sx}})+1} . \tag{2.13}$$

The cumulative probability of detection can then be computed by integrating Eq. (2.13) against the t_{Sx} distribution.

2.4.2 Model Estimates

2.4.2.1 Testing effectiveness

Testing effectiveness TE can now be computed by substituting Eq. (2.7) ($\bar{\nu}_{\text{testing}}$) into Eq. (2.4) ($R_{\text{testing}}$) into Eq. (2.1), to get

$$TE = p \int_0^\infty \mathbb{E}\left[\beta(t)\left[F(t) - F(t-\ell)\right]\right] dt \Big/ \int_0^\infty \mathbb{E}\left[\beta(t)\right]\, dt\,, \tag{2.14}$$

where Eq. (2.10) can be used to compute the CDF $F(t)$ of diagnosis times t_{Dx}. If isolation is of sufficient duration to prevent all post-diagnosis transmission, TE simplifies to

$$TE = p \int_0^\infty \mathbb{E}\left[\beta(t)F(t)\right] dt \Big/ \int_0^\infty \mathbb{E}\left[\beta(t)\right]\, dt\,. \tag{2.15}$$

Note also that the integrands enclosed in expectations above have useful interpretations: they represent the expected infectiousness trajectories with (numerator) and without (denominator) participation in testing.

2.4.2.2 Ascertainment, and diagnosis and swab time distributions

For a single individual, the distribution of diagnosis times is given by its improper $f(t_{\text{Dx}})$ or CDF $F(t)$. The related improper distribution of "diagnosing swab" times is given by shifting the CDF by the turnaround time TAT.

The long-time limit of $F(t)$ is the probability that that individual will be diagnosed at all. Ascertainment, the proportion of infections diagnosed by a particular strategy at the population scale, can therefore be estimated by taking the expectation of the long-time limits over individuals, and scaling by the participation rate,

$$\alpha = p \lim_{t\to\infty} \mathbb{E}\left[F(t)\right]\,. \tag{2.16}$$

Here, the expectation is taken over individual heterogeneity in within-host dynamics across the population (just as in Eqs. (2.3) and (2.4)).

2.4.2.3 Mean generation interval and selection coefficient

The mean generation interval, defined as the typical time between infection and subsequent transmission, can be computed from the centers of mass of the expected infectiousness curves that appear in the numerator and denominator of Eq. (2.14). Such estimates may be important for post-hoc estimation of TE from empirical data, given that methods of estimating R_t from empirical case counts often rely on the mean generation interval.

If a single test is capable of diagnosing two strains of the same pathogen, then there is the potential for testing to alter the selection coefficient. Here, TE calculations can estimate this impact, such that the selection coefficient is predicted to shift from $s = \frac{R_A}{R_B}$ to $s_{\text{testing}} = s\frac{(1-TE_A)}{(1-TE_B)}$.

2.4.2.4 Test Consumption

How many tests are consumed during the course of a testing regimen? We break this calculation into two cases, depending on whether the individual receives a diagnosis or not.

First, suppose an individual never tests positive. This implies that any tests that were meant to be taken when the infection was detectable, i.e. when $D(t) = 1$, were either (i) not taken, due to a failure of compliance (probability $1 - c$), or (ii) taken yet failed to provide the correct positive diagnosis (probability $c\phi$). Because only the latter case consumes a test, this means that a key quantity is $c\phi/(1 - c + c\phi)$, the relative probability that a planned test consumed a test, given the absence of diagnosis. On the other hand, any tests meant to be taken when the infection was undetectable, i.e. when $D(t) = 0$, were taken with probability c. Summing these two provides an estimate of average test consumption for those who are not diagnosed.

$$\bar{q}_{\text{no-Dx}} = \frac{c\phi}{1 - c + c\phi} \int_0^\infty A(t)D(t)\, dt + c \int_0^\infty A(t)\left[1 - D(t)\right]\, dt\ . \tag{2.17}$$

The reason that we call this an estimate and not an exact calculation is that testing and diagnosis are causally linked, and therefore conditioning on a no-diagnosis outcome means that the prescribed test administration may no longer be $A(t)$ exactly.

In contrast, if an individual receives a diagnosis at t_{Dx}, we assume that no additional tests were consumed thereafter, and that at least one test was consumed—if not, no diagnosis could have been produced. For a fixed time of diagnosis,

$$q_{\text{Dx}}(t_{\text{Dx}}) = 1 + c\left[\left\lfloor \int_0^{t_{\text{Dx}}-\text{TAT}} A(t)\,dt \right\rfloor + \left\lfloor \int_{t_{\text{Dx}}-\text{TAT}}^{t_{\text{Dx}}} A(t)\,dt \right\rfloor\right]. \tag{2.18}$$

Above, the first integral accounts for non-diagnostic test consumption up until the diagnosing test, while the second integral accounts for additional tests consumed while waiting for the diagnosing test. The separate floor functions are a necessary consequence of conditioning on the separate counting of the diagnosing test. Taking an expectation over t_{Dx} yields

$$\bar{q}_{\text{Dx}} = 1 + \frac{pc}{\alpha}\left[\int_0^{\infty}\left\lfloor \int_0^{t_{\text{Dx}}-\text{TAT}} A(t)\,dt \right\rfloor f(t_{\text{Dx}})\,dt_{\text{Dx}} + \int_0^{\infty}\left\lfloor \int_{t_{\text{Dx}}-\text{TAT}}^{t_{\text{Dx}}} A(t)\,dt \right\rfloor f(t_{\text{Dx}})\,dt_{\text{Dx}}\right]. \tag{2.19}$$

Combining our calculations for $\bar{q}_{\text{no-Dx}}$ and $\bar{q}_{\text{Dx}}$, weighting the latter by ascertainment and the former by its complement, we get a general expression for the expected test consumption among infected individuals,

$$\bar{q}_{\text{infected}} = (1-\alpha)\,\bar{q}_{\text{no-Dx}} + \alpha\,\bar{q}_{\text{Dx}}\,. \tag{2.20}$$

Of course, the whole point of testing is that one does not know *a priori* who is infected and who is not. Consequently, we can estimate consumption by those who are not infected as

$$\bar{q}_{\text{not infected}} = c\int_0^{\infty} A(t)dt\,. \tag{2.21}$$

Finally, combining Eqs. (2.20) and (2.21), we get

$$Q = p\big[\,(\theta\,\text{se}_{\text{ref.}})\;\bar{q}_{\text{infected}} + (1-\theta)(1-\text{sp}_{\text{ref.}})\,\bar{q}_{\text{not infected}}\big]\,, \tag{2.22}$$

where p is the population participation rate, θ is the prevalence of the pathogen, and $\text{se}_{\text{ref.}}$ and $\text{sp}_{\text{ref.}}$ are the sensitivity and specificity of the scheme used to refer people to testing, respectively. Such referral schemes include contact tracing, the appearance of symptoms, membership in a group with known high risk of infection, or even universal testing (in which case the referral "program" would have $\text{se} = 1$ and $\text{sp} = 0$).

2.4.2.5 Days spent in isolation

For fixed-duration perfect isolation of length ℓ, the average number of isolation days per infected person is given by the product of ℓ and ascertainment $d = \ell\,\alpha$. A similar calculation for test-to-exit policies is found in Supplementary Equation S10.

2.4.3 Parameterization of the Model

2.4.3.1 Viral kinetics, symptoms onset, and infectiousness

We parameterized the time-varying profiles of viral load and infectiousness using a simplified model which captures four features common to RSV [213], influenza A [34], and multiple variants of SARS-CoV-2 [124]: (i) a post-exposure period where virus is undetectable by any known test, (ii) a proliferation period of exponential growth, (iii) a peak viral load (VL), followed by (iv) a clearance period of exponential decline. We capture these features using a piecewise linear function describing the logarithm of viral load, specified by three points: (t_0,LLOQ), the first time at which VL exceeds the lower limit of quantification (LLOQ); (t_{peak},V_{peak}), peak VL timing and concentration; and (t_f,LLOQ), the last detectable time [124, 136], where t represents the time since exposure in days (Fig. S8). For the pathogens considered here, the LLOQ is equal to the RT-qPCR LOD. Because within-host kinetics vary from one infection to another, each trajectory is parameterized using independent draws from random variables for each control point.

While summarized in Table S1, we briefly review the studies and sources of evidence used to parameterize our simple viral load models. Influenza A latent period parameters were drawn from a review of challenge studies by Carrat et al. supporting a 0.5–2d delay between inoculation and first detectable instance using a gold standard test [34], noting that this range is slightly wider than in other studies [220]. Data from a household study from Ip et al. characterized peak VL between 1–3d after symptom onset, and noted that symptom onset and first detectability were indistinguishable. Their data also showed peak VL between 6–8.5 $\log_{10}$ cp RNA/mL, followed by 2–3d clearance times [108]. We note that these clearance times were shorter than those observed in challenge studies [34, 220]. Symptom onset time was specified as taking place between 2d and 0d prior to peak VL from observations of naturally acquired infection [138].

RSV viral kinetics were characterized using vaccine efficacy challenge studies, which reported only geometric means of viral load, measured in days since challenge inoculation [210, 213]. Placebo group data from both studies support a 2–4d latent period and 3-6d between peak VL and clearance [210, 213]. Schmoele-Thoma et al. present individual data points for longitudinal sampling of infected participants supporting a proliferation phase of 2–4d and peak VL between 4.5–8 $\log_{10}$ cp RNA/mL [213]. Sadoff et al. indicate slightly later and lower peaks, but we weight these less heavily in model parameterization because only mean and confidence intervals are presented, but not individual data points [210]. Symptom onset time was specified as taking place between 1d prior to and 1d after peak VL from an additional human challenge study [141].

We briefly note that our characterization of influenza A and RSV viral kinetics relies primarily on studies meant to capture vaccine [210, 213] and drug [220] efficacy, or to report symptom dynamics [108]. In all four studies, viral kinetics data are reported as a secondary finding, and typically as a geometric mean since time of onset—including, in two instances, all the individuals for whom inoculation failed [210, 213]. Due to the lack of viral load data linked at the level of individuals to inform distributional choices of kinetics parameters across a population, we assumed uniform distributions over supported parameter ranges for both viruses.

In contrast, our estimates of SARS-CoV-2 viral kinetics parameters were drawn from studies performed specifically to characterize within-host viral dynamics. Kissler et al. and Hay et al. provide mean and 95% credible interval estimates for peak VL and the durations of the proliferation and clearance phases for founder-strain/naive and omicron-strain/experienced SARS-CoV-2, respectively [94, 124]. Parameter distributions were assumed to be Lognormal with parameters μ and σ, whose values were adapted from published means, 95% credible intervals, and sample sizes. Specifically, we selected values such that an equal number of draws from Lognormal(μ, σ) would lead to a frequentist confidence interval matching the published mean and credible interval to the closest approximation. See Table S1 for these parameter values. Given the possibility of the occasional non-biologically large draw from the Lognormal distributions, we rejected proliferation phases shorter than 0.5d and longer than 10d, and rejected clearance phases shorter

than 0.5d and longer than 25d for both SARS-CoV-2 models. A challenge study provides support for a 2.5-3.5d latent period after inoculation [121]. Symptom onset time was specified as taking place between 0-3d after peak VL for founder-strain/naive infections [86, 94, 232], and between 1-5d before peak VL for omicron-variant/experienced infections [121, 130, 181].

Given a stochastic realization of viral kinetics from the model above, we calculated infectiousness $\beta(t)$ as proportional to the logarithm of viral load in excess of some minimum threshold, specified by the typical viral load (concentration of RNA cpRNA/ml) at which plaque forming units are consistently found (> 1 PFU/ml). While this type of log-viral-load infectiousness assumption is common for studies of influenza A [34, 55], SARS-CoV-2 [133], and RSV [247], alternative relationships between viral load (or other quantities) and infectiousness are possible [115, 136].

2.4.3.2 Analytical sensitivity and failure rate of diagnostic tests

Analytical sensitivities (limits of detection; LODs) were drawn from the literature for RT-qPCR and RDT tests for influenza A, RSV, founder-strain SARS-CoV-2, and SARS-CoV-2 omicron variants. Due to the variability in LODs between assays of the same type for the same pathogen, we chose a single value (Table **??** to represent each pathogen and test type. Above a test's estimated LOD, false negative rates ϕ were available only for SARS-CoV-2 [14] at approximately 5%, a rate we assumed for RSV and influenza A, collectively modeling factors such as sample contamination, poor biospecimen collection, or manufacturing error. In general, parameters were more widely available and better characterized for SARS-CoV-2 tests than for RSV or influenza A. See Table S1 for LODs, failure rates, and relevant sources.

Chapter 3

SARS-CoV-2 Transmission and Impacts of Unvaccinated-Only Screening in Populations of Mixed Vaccination Status

Portions of this chapter are adapted from:

Kate M. Bubar*, **Casey E. Middleton***, Kristen K. Bjorkman, Roy Parker, and Daniel B. Larremore.

SARS-CoV-2 Transmission and Impacts of Unvaccinated-Only Screening in Populations of Mixed Vaccination Status. Nature Communications 13(1):2777, 2022. DOI: 10.1038/s41467-022-30144-7.

* authors contributed equally

3.1 Introduction

SARS-CoV-2 created a pandemic in which morbidity and mortality were partially mitigated in many areas by widespread vaccination. COVID-19 vaccines are extremely effective at preventing severe disease (vaccine efficacy, VE $> 90\%$, [62]), while also reducing susceptibility to infection (VE_S) and risk of onward transmission (VE_I). In spite of these reductions, so-called vaccine breakthrough infections and subsequent transmission have been widely documented [214], and increased dramatically with the emergence of the omicron variant in late 2021 [10, 57]. These developments raise the question of how to best mitigate transmission in partially vaccinated populations.

Prior to the approval of COVID-19 vaccines, transmission mitigation via regular and repeated screening was shown to be an effective approach to break chains of transmission and decrease the burden of COVID-19 using both RT-PCR [21, 136, 199] and rapid antigen testing [136, 186]. Specifically, screening via testing, which we hereafter refer to simply as screening in most cases, is effective at the community

level because it decreases transmission from individuals who are already infected [136, 156]. However, policy proposals in 2021 and early 2022 shifted to focus routine testing requirements on only the unvaccinated population, including an requirement announced by the Italian government in October, 2021 [105] and a U.S. requirement for healthcare workers beginning February, 2022 [204]. By reducing rates of transmission from only the unvaccinated population, such policies may be limited by the extent to which transmission is, in fact, driven by the unvaccinated. This raises critical questions about projected policy impacts relative to other non-pharmaceutical interventions [91, 215]—particularly in areas where the unvaccinated population is small.

The role of vaccines in reducing transmission is complex and changing. First, VE_S and VE_I vary depending on which vaccine was administered [25]. Second, both VE_S and VE_I wane with time since vaccination [11, 40, 80], but can be boosted to higher levels for those receiving an additional dose [74]. Third, those who have experienced a SARS-CoV-2 infection also show decreased risks of reinfection and subsequent transmission [25], providing partial protection to those who are previously infected and remain unvaccinated, but also augmenting protection for those who are both vaccinated and previously infected [74, 163]. Finally, preliminary estimates of VE_S and VE_I, and their prior-infection equivalents, are markedly lower for the omicron variant [10, 89]. Thus, the relative estimates of risk reductions due to vaccination, prior infection, or both, as well as the sizes of the populations falling into each category of immunity, will affect transmission dynamics—with or without testing.

In this chapter, we model the spread of SARS-CoV-2 in populations of mixed vaccination status, focusing on three critical questions. First, how do vaccinated and unvaccinated populations each contribute to community spread and hospitalizations, and how do those contributions vary with rates of vaccination and prior infection? Second, how do testing-based screening programs focused on unvaccinated individuals alone affect community spread and hospitalizations? Third, how effective are delta-era screening strategies likely to be against variants with higher breakthrough and reinfection rates? This chapter's goals are not to make perfectly calibrated predictions but instead to elucidate more general principles of transmission and unvaccinated-only testing in partially vaccinated populations. As such, our analyses consider a wide range

of parameters and scenarios.

3.2 Results

Unvaccinated-only testing-based screening programs have been discussed and implemented during transmission of both the delta and omicron variants, yet these variants differ in their transmission and disease parameters, particularly among vaccinated or previously infected individuals—the focus of the present chapter. As such, the analyses that follow incorporate a range of empirically estimated parameters for the delta variant and plausible parameters associated with the omicron variant.

3.2.1 High vaccination rates drive total infections and hospitalizations down, increase the proportions of vaccine breakthroughs, and shift the drivers of transmission

To examine the dynamics of transmission in a population with mixed vaccination status, we first modeled transmission within and between communities of vaccinated (V) and unvaccinated (U) individuals in the absence of a screening program. Based on a standard Susceptible Exposed Infected Recovered (SEIR) model, we tracked the four transmission modes by which an infection might spread: $U \to U$, $U \to V$, $V \to U$, and $V \to V$ (Fig. 3.1a). A constant and equivalent fraction of both populations was assumed to have experienced prior SARS-CoV-2 infection, resulting in four categories of imperfect immunity: unprotected (unvaccinated with no prior infection), infection-acquired, vaccine-acquired, and both vaccine- and infection-acquired (so-called "hybrid" immunity). To account for introductions of infection from outside the population, all susceptible individuals were subject to a small, constant rate of exposure, with infection-acquired and vaccine-acquired immunity providing partial protection against subsequent infection.

Traditionally, the basic reproductive number R_0 is defined as the number of secondary infections generated by a typical infector in an entirely susceptible population, i.e., a population without any non-pharmaceutical interventions (NPIs). At the time of writing, NPIs such as masking, ventilation and physical distancing are commonplace in many areas, so we hereafter define R_0^{NPI} to be the expected number of secondary infections generated by a typical infector in a population with possible NPIs, but prior to any

impacts of population immunity. Furthermore, because precise estimates of R_0^{NPI} vary by context, variant, and over time, we consider a range of R_0^{NPI} values from 4 to 6. In our baseline modeling scenario, vaccines were assumed to reduce susceptibility to infection by $\text{VE}_S = 65\%$, the likelihood of transmission to others by $\text{VE}_I = 35\%$, and the likelihood of disease progression to hospitalization conditioned on infection by $\text{VE}_P = 86\%$, values which land within plausible literature estimates for the effectiveness of two doses of mRNA vaccine against the delta variant in the absence of dramatic waning and without boosting [25, 64, 73, 74]. Though less often studied in the literature, we assumed that prior SARS-CoV-2 infection would lead to 63% and 13% decreases in risk of infection and transmission based on a statistical model relating immunity to neutralization [74], and that hybrid immunity would be superior to either vaccination or prior SARS-CoV-2 infection alone. We further assumed an additional 54% decrease in risk of hospitalization conditioned on infection for individuals with prior SARS-CoV-2 infection [8], and that individuals with hybrid immunity receive the greater of vaccinated or prior immunity's protection against hospitalization. See Materials and Methods and Supplementary Tables S2 and S3 for a complete description of the model and parameters.

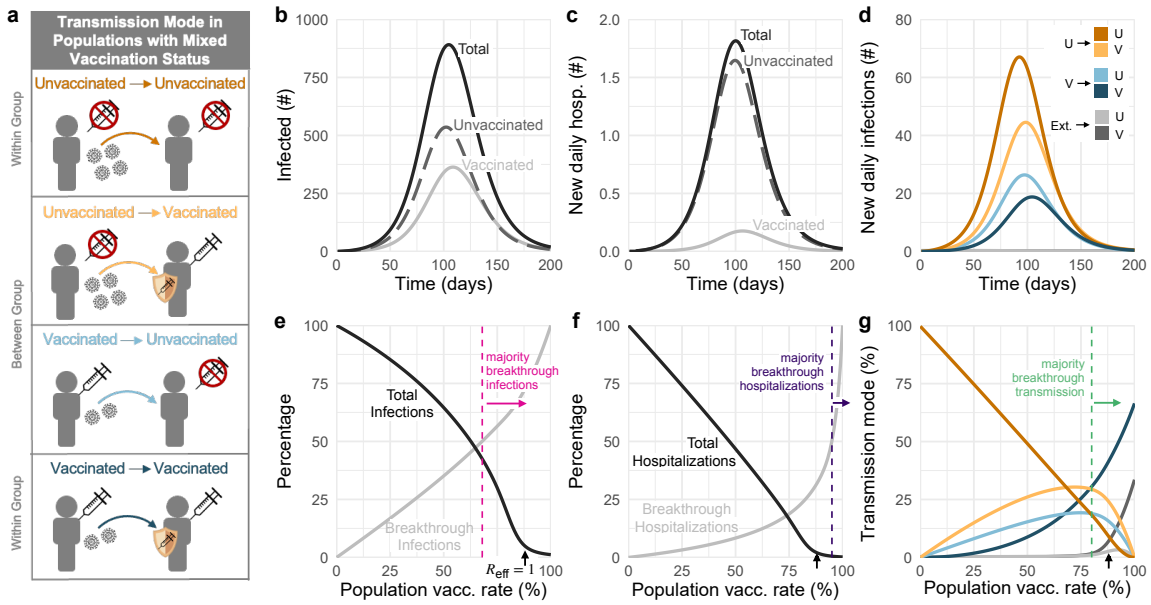

Figure 3.1: **Vaccination affects which population drives transmission and dominates infections and hospitalizations.** (a) Diagram of four transmission modes within and between vaccinated and unvaccinated communities, where vaccines and prior infection decrease risks of infection, transmission, and hospitalization. (b) Number of infected individuals and (c) new daily hospitalizations over time (solid black), stratified by unvaccinated (dashed gray) and vaccinated (solid gray) populations. (d) Daily transmission events separated and colored by transmission mode (see legend). (e) Cumulative infections and (f) hospitalizations as a percentage of total infections/hospitalizations without vaccination (black), and the percent of each accounted for by vaccine breakthroughs (gray) for varying vaccination rates. (g) Transmission mode (see legend) as a percentage of cumulative infections for varying vaccination rates. Black arrows in panels e, f, and g indicate vaccination rate at which $R_{\text{eff}} = 1$; vertical dashed lines indicate the lowest vaccination rates for which vaccinated individuals account for the majority of infections, hospitalizations, and transmission as annotated. $R_0^{\text{NPI}} = 4$ for all plots, with baseline VE and immunity parameters vs the delta variant (Materials and Methods, Supplementary Tables S2 and S3); no screening. Panels b, c, and d: 58% vaccination rate and 35% rate of prior infection.

In a modeled population of $N = 20,000$ with 58% vaccination rate (corresponding to U.S. estimates

as of Nov. 4, 2021 [236]) and 35% past infection rate, outbreaks still occurred, despite assuming a partially mitigated delta variant ($R_0^{\text{NPI}} = 4$). During the ensuing outbreak, 59% of total infections and 89% of hospitalizations occurred in unvaccinated individuals (Fig. 3.1b,c), despite making up only 42% of the population. Furthermore, the peak burden of disease occurred first in the unvaccinated community and then one week later in the vaccinated community (Fig. 3.1b), a known consequence of disease dynamics in populations with heterogeneous susceptibility and transmissibility [205, 251]. By categorizing transmission events into four distinct modes (Fig. 3.1a), we observe that infections during a delta outbreak in both communities were driven predominantly and consistently by the unvaccinated community ($U \to U$, $U \to V$; Fig. 3.1d), but that there was nevertheless some transmission from the vaccinated community (breakthrough transmission). These differences occurred despite a "well mixed" modeling assumption—namely, that an individual with a given vaccination status is no more or less likely to associate with a member of their own group vs the other group.

Vaccination and past infection rates vary widely across the U.S. [236] and the world [202] due to impacts of both vaccine availability [202] and refusal [56], as well as the success or failure of transmission mitigation policies. We therefore asked how a population's vaccination and past infection rates would affect our observations about infections, hospitalizations, and the relative impacts of the four modes of transmission. This analysis revealed three important points.

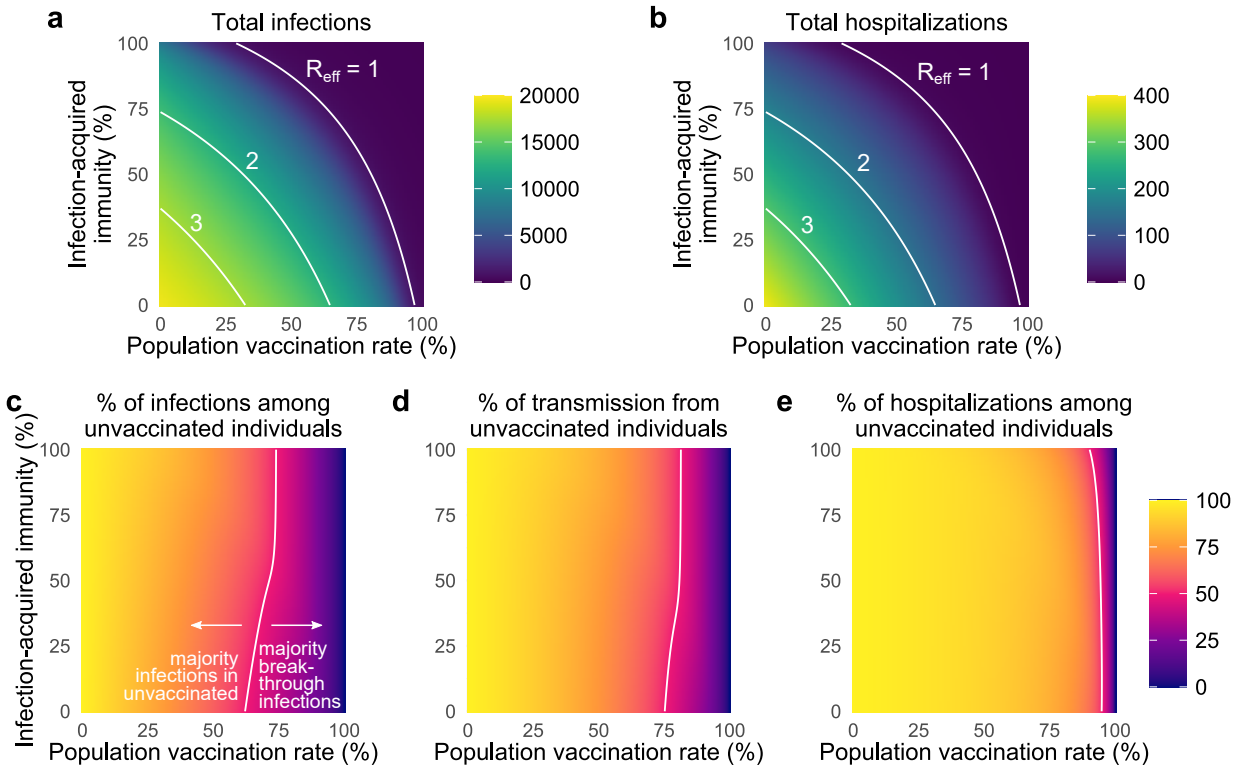

Figure 3.2: **Vaccination and prior infection rates affect epidemic potential, vaccine breakthroughs, and drivers of transmission**. Heatmaps show (a) the total number of infections, (b) the total number of hospitalizations, (c) the percentage of total infections occurring in the unvaccinated population (d) the percentage of total infections caused by the unvaccinated population, and (e) the percentage of total hospitalizations occurring in the unvaccinated population for simulated epidemics (see text). White annotation curves show (a, b) isoclines of the effective reproductive number R_{eff} calculated at $t = 0$, and the line of parameters along which (c) 50% of infections were breakthroughs, (d) 50% of transmission was due to breakthrough infections, and (e) 50% of hospitalizations were breakthroughs. $N = 20,000$ and $R_0^{\text{NPI}} = 4$ for all plots, with baseline VE and immunity parameters vs the delta variant (Materials and Methods, Supplementary Tables S2 and S3; no testing. See Fig. S10 for $R_0^{\text{NPI}} = 6$.

First, our results reinforce the fact that increased vaccination rates lead to decreased total infections and hospitalizations, both before and after the herd immunity threshold at $R_{\text{eff}} = 1$ (Fig. 3.1e,f). Moreover, when large proportions of the population are also partially protected by immunity from prior infection,

the vaccination levels required to reach $R_{\text{eff}} = 1$ decrease considerably (Fig. 3.2a). For instance, increasing prior infection rates from 35% to 50% decreases the required vaccination rate for $R_{\text{eff}} = 1$ from 87% to 80% under baseline modeling parameters. Combinations of immunity from past infection and vaccination thus have the potential to create a herd immunity frontier, beyond which transmission is no longer self-sustaining even in the absence of screening. We caution that although total infections and hospitalizations may appear equal along lines of constant R_{eff} (Fig. 3.2a,b), both actually decrease as vaccination rates increase, due to vaccines' superior protection, relative to prior infection, against infection and hospitalization.

Second, as vaccination rates increased, the fraction of infections classified as vaccine breakthroughs increased (Fig. 3.1e), creating a transition point such that when 68% of the population was vaccinated, 50% of all infections were breakthrough infections under our baseline modeling conditions for the delta variant. To determine whether this transition point of 68% was sensitive to the precise fraction of the population with immunity from past infection (35%, Fig. 3.1), we varied the fraction with infection-acquired immunity between 0% and 100%, finding that the 50/50 breakthrough infection transition occurred between 63% and 75% vaccine coverage (Fig. 3.2c). Because vaccines provide an additional level of protection against hospitalization VE_P, the 50/50 breakthrough hospitalization transition occurs at rates of vaccination of 90-96% (Figs. 3.1f and 3.2e). Thus, our results set the expectation that increasing vaccination rates will decrease total infections and hospitalizations, yet a higher proportion of both will be breakthroughs, irrespective of levels of immunity due to prior infection.

Third, as vaccination rates increased, the unvaccinated community ceased to be the primary driver of transmission. Under our baseline modeling conditions ($R_0^{\text{NPI}} = 4$, 35% with infection-acquired immunity), this transition occurred when 80% or more of the population was vaccinated (Fig. 3.1g). When we varied the fraction of the population with infection-acquired immunity between 0% and 100%, this transition point varied from 76% to 82% (Fig. 3.2d). Thus, while COVID-19 hospitalizations remain concentrated primarily in unvaccinated populations, only a minority of infections will occur in, and be driven by, the unvaccinated community when vaccine coverage is sufficiently high. Note that this implies that unvaccinated individuals living in highly vaccinated communities will still be exposed to SARS-CoV-2 and thus remain at risk of

infection and severe disease.

These findings are driven by reductions in susceptibility, disease severity, and infectiousness arising from vaccination, prior SARS-CoV-2 infection, or both. However, quantitative estimates of those reductions vary depending on which vaccine was administered [11], time since vaccination or SARS-CoV-2 infection [11, 40, 80], whether an additional "booster" dose was given [74], and the variant circulating at the time of the study [49, 175]. We therefore sought to determine how our findings might change under different sets of assumptions about vaccine effectiveness by comparing our baseline scenario ($\text{VE}_S = 0.65$, $\text{VE}_I = 0.35$, $\text{VE}_P = 0.86$) with a waning/low immunity scenario ($\text{VE}_S = 0.5$, $\text{VE}_I = 0.1$, $\text{VE}_P = 0.80$) and a boosted/high immunity scenario ($\text{VE}_S = 0.8$, $\text{VE}_I = 0.6$, $\text{VE}_P = 0.90$), as well as a scenario reflecting plausible VE values based on early observations for the omicron variant ($\text{VE}_S = 0.35$, $\text{VE}_I = 0.05$, $\text{VE}_P = 0.77$; [73, 230]). To explore the impact of these changes in vaccine effectiveness, we simulated outbreaks for all combinations of vaccination and infection-acquired immunity rates under the four VE scenarios. Across simulations, total infections and hospitalizations were well predicted by calculating R_{eff} at the start of each simulation (Eq. (3.3); Methods). In particular, outbreaks were small when vaccination or past infection rates crossed the herd immunity threshold ($R_{\text{eff}} < 1$). When $R_{\text{eff}} > 1$, total infections monotonically increased as R_{eff} increased (Fig. S9). The herd immunity threshold was impossible to cross with vaccination alone in the waning or omicron VE scenarios with partially mitigated transmission ($R_0^{\text{NPI}} = 4$, Fig. 3.3a,d; Fig. S9), and in waning, baseline, and omicron VE scenarios with unmitigated transmission ($R_0^{\text{NPI}} = 6$; Fig. S10), as evidenced by the fact that the $R_{\text{eff}} = 1$ curves either fail to intersect the vaccination rate axis or appear at all.

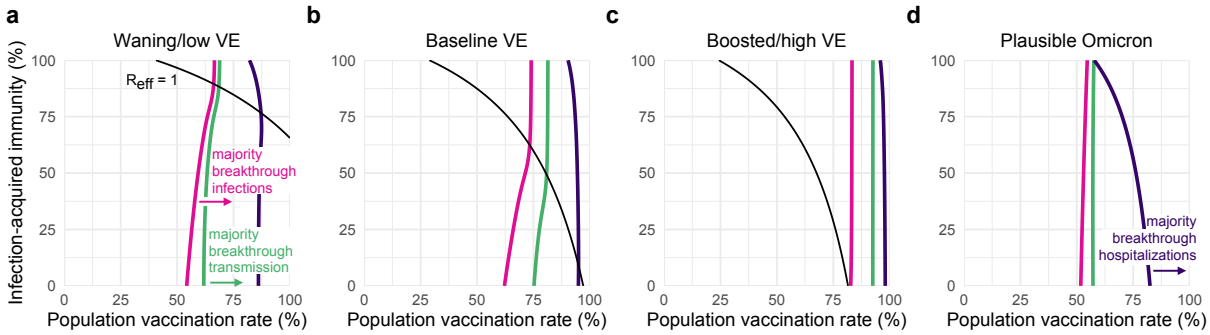

Figure 3.3: **Transition points for breakthrough infections, hospitalizations, and transmission.** All panels show curves representing the vaccination and prior infection rates infections (pink), transmission (green), and hospitalizations (purple) are composed of equal numbers of vaccinated an unvaccinated individuals, with majority-breakthrough regions to the right of each line as indicated, for (a) waning/low, (b) baseline, and (c) boosted/high VE vs the delta variant, and (d) plausible VE vs the omicron variant. Black lines indicate $R_{\text{eff}} = 1$ isoclines, which do not appear in panel (d) due to $R_{\text{eff}} > 1$. See Table S3 for immunity parameter values. $R_0^{\text{NPI}} = 4$ in all panels.

Waning, boosting, or omicron-specific assumptions altered the proportions of infections and hospitalizations occurring in, and transmission from, the unvaccinated vs vaccinated communities. All else being equal, waning or omicron VE led to increased fractions of breakthrough infections and hospitalizations, and increased transmission from the vaccinated community, while boosted VE led to decreases of all three. In turn, the population vaccination rates at which the majority of infections or hospitalizations were breakthroughs shifted down for waning or omicron VE (Fig. 3.3a,d), while the vaccination rate at which the majority of transmission was driven by vaccinated individuals shifted up for boosted VE (Fig. 3.3c).

Among the four transition points identified in transmission dynamics, we observe that, in each VE scenario, R_{eff} is driven by both vaccination and past infection rates, as evidenced by curvature in $R_{\text{eff}} = 1$ isoclines (Fig. 3.3, black lines). In contrast, isoclines representing the transition points between majority-unvaccinated vs majority-breakthrough infections (Fig. 3.3, pink lines), between majority-unvaccinated vs majority-breakthrough hospitalizations (Fig. 3.3, purple lines), and between majority-unvaccinated vs majority-breakthrough transmission (Fig. 3.3, green lines) are relatively insensitive to variation in rates of infection-acquired immunity, as evidenced by vertical or near-vertical isoclines. These findings suggest that the relative proportions of breakthrough infections, hospitalizations, and transmission are driven more by vaccination rates and VE, but not by rates of past infection or proximity to herd immunity; indeed, after the herd immunity threshold, all three isoclines show essentially no variation. These observations suggest that unvaccinated-only screening programs, which decrease rates of $U \to U$ and $U \to V$ transmission, may be highly effective only in regimes where transmission is driven by the unvaccinated (i.e. to the "left" of green isoclines, Fig. 3.3), an intuition we now explore in detail.

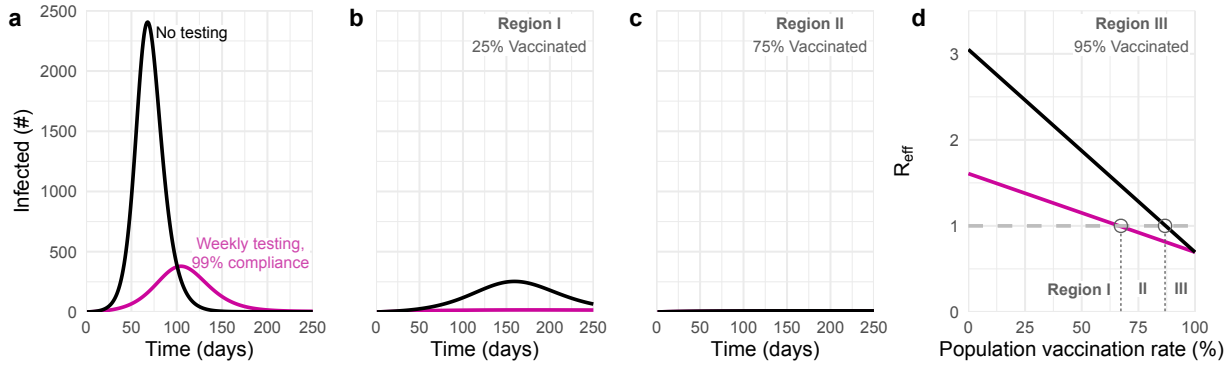

Figure 3.4: **The impact of unvaccinated-only screening corresponds to three distinct parameter regions.** Total number of infections with no screening (black) and weekly testing with 99% compliance (pink) are shown for (a) 25%, (b) 75%, and (c) 95% population vaccination rates. (d) Effective reproductive number over various population vaccination rates, where $R_{\text{eff}} = 1$ is denoted by gray dashed line. The impacts of screening fall into three categories (see text) depending on whether vaccination rate falls into region I, II, or III, as annotated. $R_0^{\text{NPI}} = 4$ and 35% rate of prior infection with baseline immunity parameters (Materials and Methods, Table S3).

3.2.2 The impacts of unvaccinated-only screening depend on population immunity, compliance, and VE

To explore the impact of unvaccinated-only screening on population transmission, we modified our simulations so that a positive test would result in an unvaccinated individual isolating to avoid infecting others [135, 136]. We considered test sensitivity equivalent to RT-PCR with a one-day delay between sample collection and diagnosis under three screening paradigms: weekly testing with 50% compliance—a value which reflects observed compliance with a weekly testing mandate in a university setting [21]—weekly testing with 99% compliance, and, specifically for the omicron variant, twice-weekly testing with 99% compliance.

Our analysis shows that the benefits of an unvaccinated-only screening program fall into one of three categories, depending on the population vaccination rate and transmission dynamics. These categories align

with three distinct regions in parameter space, denoted in Fig. 3.4 as regions I, II and III. In region I, screening is insufficient to fully control transmission, yet nevertheless markedly reduces the peak number of total infections, colloquially "flattening the curve" (Fig. 3.4a). In region II, screening successfully brings transmission under control (Fig. 3.4b). In region III, screening has little impact on transmission due to the fact that outbreaks are already mitigated by population immunity and other control measures (Fig. 3.4c). Unvaccinated-only screening is therefore impactful in the first two regions, sufficient for transmission control in only the second region, and largely inconsequential to transmission in the third.

The three regions that correspond to different impacts of screening on transmission are separated by boundaries which can be estimated from two analytical calculations of R_{eff}—one which includes the effects of screening and one which does not (Eq. 3.3, Methods). The boundary separating regions I and II is given by those parameters for which $R_{\text{eff}} = 1$ with screening, while the boundary separating regions II and III is given by those parameters for which $R_{\text{eff}} = 1$ without screening (Fig. 3.4d). Thus, the value of a screening testing program in reducing infections can be evaluated based on which of three regions the current vaccination rate, prior infection rate, and VE fall into.

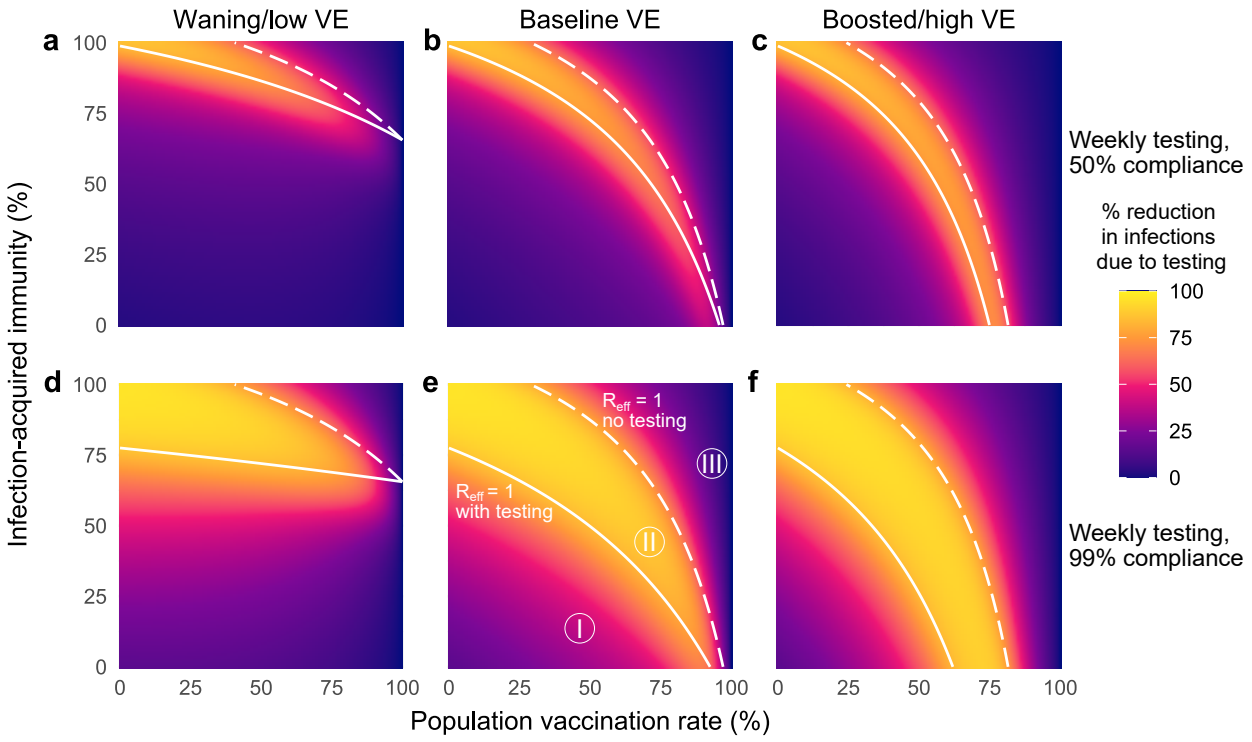

Figure 3.5: **The impacts of unvaccinated-only screening depend on population immunity, compliance, and vaccine effectiveness.** Percent reduction in cumulative infections due to screening over various population vaccination rates assuming waning/low (a, d), baseline (b, e), and boosted/high (c, f) VE with once-weekly screening at 50% (top row) and 99% (bottom row) compliance. White lines indicate the population immunity rate at which $R_{\text{eff}} = 1$ with screening (solid) and without screening (dashed), which divide the space into three regions, labeled I, II and III. See Table S1 and Table S3 for parameter values. $R_0^{\text{NPI}} = 4$ in all panels; see Fig. S11 for $R_0^{\text{NPI}} = 6$.

To illustrate the value of this R_{eff}-based analysis, we considered vaccination rates and prior infection rates ranging from 0-100% and varied VE between waning, baseline, and boosted scenarios for the delta variant. Across scenarios, dramatic relative reductions in cumulative infections are concentrated within the envelope between the boundaries of $R_{\text{eff}} = 1$ with and without screening, i.e., region II (Fig. 3.5). Outside of this effective screening envelope, percent reductions in cumulative infections decreased markedly, either because unvaccinated-only screening flattened the infection curve but had little impact on cumulative

infections (region I), or because existing population immunity prevented large outbreaks in the first place (region III). Assuming a 35% past infection rate and $R_0^{\text{NPI}} = 4$, region III appeared only for baseline and boosted vaccine effectiveness assumptions, and only when vaccination rates were approximately 90% or greater (baseline VE) or 75% or greater (boosted VE). Sensitivity analyses show that increasing R_0^{NPI} to 6, potentially representing pre-pandemic contact rates and the SARS-CoV-2 delta variant, cause region III to shrink further (Fig. S12). Thus continued screening for SARS-CoV-2 among the unvaccinated may be of limited value when vaccination rates are sufficiently high.

The role of compliance—the fraction of scheduled tests that are actually taken—can also be clarified by examining the three regions of screening testing impact. Both the simulations and equations for R_{eff} show that increasing compliance from 50% (Fig. 3.5, row 1) to 99% (Fig. 3.5, row 2) causes the lower boundary of the effective screening envelope to shift to lower vaccination and prior infection rates, decreasing the size of region I and increasing the size of region II. Moreover, increased compliance increases the magnitude of infection reductions within both regions, visible as an intensification of color in the infection reduction heatmaps (Fig. 3.5). As a result of these observations, we conclude that, in addition to test sensitivity, frequency, and turnaround time [136], high participation in screening programs is critical to expanding the impact of unvaccinated-only screening testing programs. However, we also note that compliance had little effect in region III where $R_{\text{eff}} < 1$, a result which parallels analysis of universal screening programs [156].

This R_{eff}-based analysis of transmission is not restricted to unvaccinated-only screening programs. To illustrate this, we considered an identical set of simulations as in Fig. 3.5 but with universal screening, i.e. screening via testing of the vaccinated and unvaccinated populations alike. Universal screening caused the boundary between regions I and II ($R_{\text{eff}} = 1$ with screening) to shift, expanding the size of the effective screening envelope (Fig. S13). While we present these results here for completeness, universal testing in mixed vaccination status populations have been investigated elsewhere prior to the present work [156].

The impact of screening on hospitalizations is also predicted well by the R_{eff}-based effective screening envelope. While hospitalizations were not identical across all equal-R_{eff} combinations of vaccination and

prior infection rates, dramatic relative reductions in cumulative hospitalizations were nevertheless clearly concentrated within region II, with decreasing relative reductions in regions I and III (Fig. S14). We therefore find that analysis based only on the effective screening envelope, calculated via Eq. (3.3) (Methods), is useful in predicting the impact of screening regimens—both unvaccinated-only and universal—on reductions in cumulative infections and hospitalizations alike.

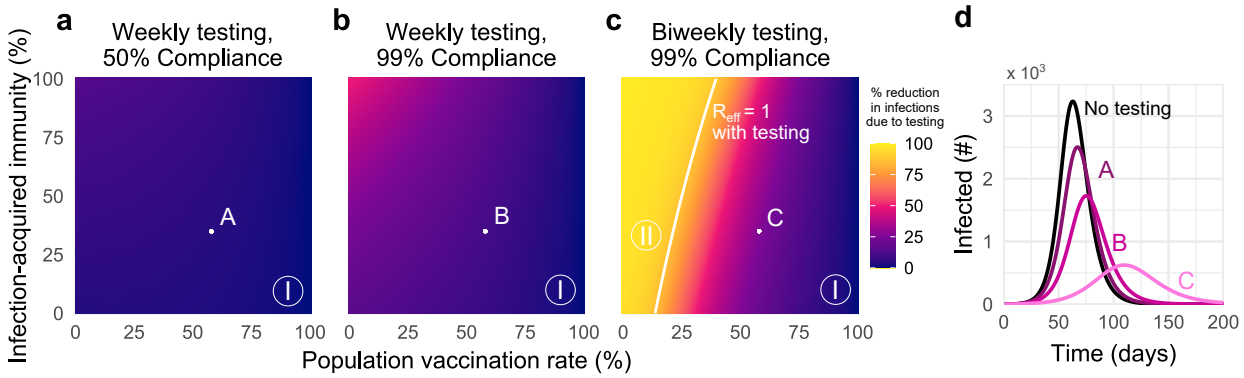

Figure 3.6: **Unvaccinated-only screening during omicron transmission cannot achieve $R_{\text{eff}} < 1$ except in low-vaccination and high-frequency regimes.** Percent reduction in cumulative infections due to screening over various population vaccination rates assuming plausible parameters for immunity versus the omicron variant, with (a) once-weekly screening at 50% compliance, (b) once-weekly screening at 99% compliance, and (c) twice-weekly screening at 99% compliance. (d) Number of individuals infected over time, under screening scenarios denoted A, B, C, compared with no screening (black) with 58% vaccination rate and 35% rate of prior infection. Solid white line indicates $R_{\text{eff}} = 1$ with screening; $R_{\text{eff}} = 1$ is not achievable without screening. See Table S2 and Table S3 for parameter values. $R_0^{\text{NPI}} = 4$ in all panels; see Fig. S12 for $R_0^{\text{NPI}} = 6$ and Fig. S13 for universal testing.

The omicron variant's rapid spread, and in particular its increased rates of reinfection and vaccine breakthrough, raise key questions about the role of unvaccinated-only screening programs and whether populations considering such policies may fall into region I, II, or III defined above. Because estimates of omicron-specific immunity parameters were either limited or nonexistent at the time of writing, we assumed

plausible lower values of each based on extant data [73, 230], alongside lower infection-hospitalization rates for omicron in general (Table Table S2 and Table S3). Under such assumptions, weekly unvaccinated-only screening with 50% compliance was ineffective at reducing cumulative infections even though screening reduced the peak magnitude of infections (Fig. 3.6d). Regardless of compliance, all prior infection and vaccination rate combinations with a weekly screening policy were in region I, indicating that magnitude of peak infections can be mitigated but impact on cumulative infections is low (Fig. 3.6a,b). Doubling the frequency of screening to twice weekly with 99% compliance creates a bifurcated landscape, with highly effective screening only in settings with 18-40% vaccination rates (Fig. 3.6c). For vaccination rates above 50%, even twice-weekly unvaccinated-only screening programs with near-perfect compliance are unlikely to dramatically impact the spread of the omicron variant (region I). Universal screening showed comparatively higher impact, yet, nevertheless, only twice-weekly testing regimens created broad region II regimes in which community spread was controlled (Fig. S13).

3.2.3 Unvaccinated-only screening shifts the balance of unvaccinated vs breakthrough transmission but not infection or hospitalization

By reducing transmission from unvaccinated individuals, screening programs specifically mitigate $U \to U$ and $U \to V$ transmission modes, thus diminishing the role of the unvaccinated population in transmission dynamics and amplifying the relative role of vaccine breakthrough transmission. As a consequence, we observe that in the presence of screening, the vaccination rates at which the unvaccinated cease to drive a majority of transmission decrease by up to 15 percentage points (Fig. 3.7b), with the largest decreases for 99% compliance and waning VE vs delta, and the smallest decreases for 50% compliance and boosted VE vs delta, or in all screening scenarios vs the omicron variant. Under waning/low, baseline and omicron VE scenarios, unvaccinated-only screening programs shrink the regime in which the unvaccinated population drives outbreaks.

In contrast, unvaccinated-only screening programs had little effect on the percentage of infections or hospitalizations that were vaccine breakthroughs. Instead, majority breakthrough regimes remained pri-

marily dependent on vaccination rates and vaccine effectiveness (Fig. 3.7a,c), with transitions to majority-breakthrough infection regimes beginning at 55 to 67% vaccination rates (waning VE, delta), 63 to 75% vaccination rates (baseline VE, delta), 83 to 84% vaccination rates (boosted VE, delta), and 50 to 55% vaccination rates (omicron). Transitions to majority-breakthrough hospitalizations occurred at 83 to 88% (waning VE, delta), 91 to 96% (baseline VE, delta), 96 to 99% vaccination rates (boosted VE, delta), and 58 to 83% vaccination rates (omicron), regardless of screening. We therefore conclude that unvaccinated-only screening programs do not markedly alter the expectations of majority-breakthrough infections or hospitalizations at high vaccination levels, particularly if VE is low or waning.

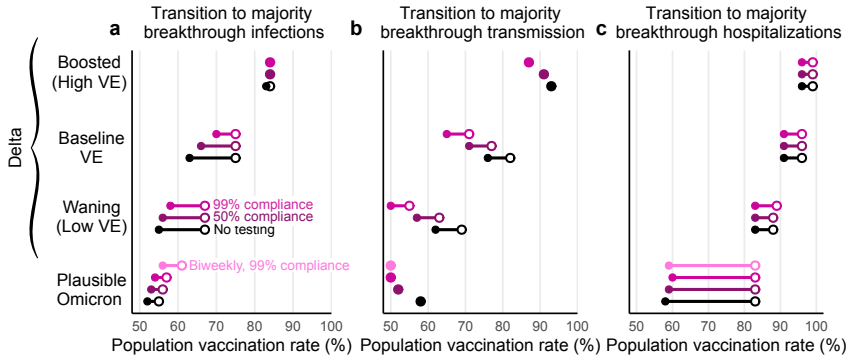

Figure 3.7: **Screening and vaccine effectiveness affect transition points to majority-breakthrough regimes.** The vaccination rates at which the vaccinated population makes up the majority of (a) infections, (b) transmission, and (c) hospitalizations for low, moderate, and high vaccine effectiveness scenarios. Minimum (filled circle) and maximum (open circle) endpoints show the variation in transition points over all combinations of vaccination and prior infection rates for no screening (black), 50% compliance (purple), 99% compliance (pink) over all possible values for past infection rates. $R_0^{\text{NPI}} = 4$ for all plots; see Fig. S15 for $R_0^{\text{NPI}} = 6$.

3.3 Discussion

In this analysis, we find that in communities with mixed vaccination status, routine SARS-CoV-2 screening programs focused only on the unvaccinated may reduce infections and hospitalizations, but in a manner dependent on two conditions. First, effective screening via testing requires high participation to be most impactful, reinforcing the need for mechanisms to encourage or enforce high participation. Second, when immunity from vaccination and past infection are high enough to curtail transmission on their own, or in concert with effective non-pharmaceutical interventions (NPIs) [91, 215], testing the remaining unvaccinated population averts few infections and hospitalizations in both relative and absolute terms. On the other hand, when transmission due to reinfection and/or vaccine breakthrough is sufficiently high, unvaccinated-only screening will at best "flatten the curve" of infections, but cannot adequately control infections and hospitalizations except when testing twice weekly with near-perfect participation in low vaccination communities. Once communities reach vaccination rates of $\sim$40% or more, even twice-weekly unvaccinated-only screening, with near-perfect compliance and isolation adherence, cannot control the omicron variant. Thus, targeted unvaccinated screening programs are highly effective only in a restricted region of epidemiological parameter space, results echoed by similar work analyzing universal screening programs [156].

Key to understanding this chapter are three observations and findings. First, an unvaccinated-only screening program simply tests fewer and fewer individuals as vaccination rates increase. Second, the relative role of the unvaccinated population in driving transmission decreases as vaccination rates increase, regardless of vaccine effectiveness. Third, when vaccine effectiveness against infection and transmission wanes, unvaccinated-only screening programs decrease in impact. As a consequence, our work broadly suggests that unvaccinated-only screening is most beneficial when a population is undervaccinated and is close to, but has not yet achieved, herd immunity—region II in our analyses—leading to the recommendation that such testing programs be used in conjunction with other NPIs. Indeed, our work finds that unvaccinated-only screening alone is generally insufficient to markedly reduce infections and hospitalizations when (i) the population is far from the herd immunity threshold, inclusive of existing NPIs, in either direction, (ii) vaccination rates are high, or (iii) testing is weekly and/or compliance is low. Against a backdrop of wan-

ing immunity and continued emergence of antigenically distinct variants, even herd immunity may be, at best, temporary. In this context, weekly unvaccinated-only screening programs alone are an insufficient countermeasure for the omicron variant.

Indeed, while our analysis focused on a single screening-based intervention in isolation, unvaccinated-only (or universal) screening programs are typically implemented alongside other NPIs [21,186,199]. These NPIs, including limitations on gatherings, increasing the availability of personal protective equipment, and school or restaurant closures, were estimated to have reduced the effective reproductive number R_{eff} by $0.1 - 0.2$ in 2020, particularly when implemented early [91], and by around 10% in 2021 [215]. In comparison, an unvaccinated-only weekly screening policy with a realistic (50%) compliance rate [21] and 58% vaccination rate, would reduce R_{eff} by an estimated 10.2% (Eq. (3.3)), decreasing further as vaccination rates increase, and compliance and isolation adherence decrease. Thus, while our analysis ranks vaccinate-or-test policies as potentially competitive with high-impact NPIs [91, 215], such screening will decrease in impact as vaccination rates inch higher. Because prior work has shown that pandemic countermeasures also vary in their impact depending on time, vaccination, and the presence of other NPIs or behaviors [215], an empirical assessment of vaccinate-or-test programs would be valuable. However, just as empirical estimates of NPIs' impacts on R_{eff} include wide uncertainty [91, 215], similar estimates for unvaccinated-only screening programs are also likely to be highly uncertain.

This chapter elucidates three critical transitions as vaccination rates increase. First, when vaccination rates are sufficiently high, a majority of the albeit reduced number of infections will be vaccine breakthrough infections. This fact should come as no surprise, as this transition must occur at some point for any vaccine below 100% effectiveness; for the delta variant, our modeling estimates it to take place between 63% and 75% vaccine coverage (baseline VE; 55-67% vaccinated with waning VE; 83-84% vaccinated with boosted VE), while for the omicron variant, we estimate it to take place between 55% and 59% vaccine coverage. Second, a transition to majority breakthrough hospitalizations will occur at some point greater than the transition to majority breakthrough infections, a natural consequence of $\text{VE}_P > 0$. Third, while community spread is driven by the unvaccinated at low vaccination rates, it is driven by the vaccinated population at

high vaccination rates (Fig. 3.3). These vaccination rate transition points separating majority-unvaccinated transmission and majority-breakthrough transmission are driven lower by unvaccinated-only screening programs (Fig. 3.7). Taken together, these results suggest that while the overall number of infections during an outbreak decreases as vaccination rates increase, assuming $\text{VE}_S > 0$, vaccine breakthrough infections and transmission events from vaccinated individuals should not be surprising in highly vaccinated populations—vaccine effectiveness is imperfect. Consequently, in anticipation of continued community transmission even in highly vaccinated communities, those at increased risk of severe COVID-19 should take additional precautions to limit their risk of infection or severe disease.

Our analyses identify two limitations of screening via testing programs in reducing community transmission which generalize beyond the specific scenarios investigated herein. First, the ability of a screening program to prevent community spread is restricted to a limited "envelope" of past infection rate and vaccination rate combinations such that R_{eff} without screening is greater than one, and R_{eff} with screening is less than one. Second, the width of that effective screening envelope, and thus the effectiveness of a screening program to control transmission more broadly, are highly sensitive to compliance and participation: weekly screening with 50% compliance—a rate which reflects observed compliance in a population with a weekly screening mandate [21]—is likely to be relatively ineffective. However, although our analyses focus on the benefits of testing in reducing transmission, testing also plays an important role in diagnosis and treatment, detection of variants, situational awareness and surveillance, and decreasing pressure on the healthcare system during outbreaks. Furthermore, testing focused on the unvaccinated population may provide additional incentives to get vaccinated and thus avoid regular testing. This work did not explore the benefits of unvaccinated-only testing mandates for these additional purposes.

Our analysis is limited in at least three different manners. First, our modeling incorporated fixed parameters that are difficult to estimate in practice. For instance, while our analysis considered boosted, baseline, and waning scenarios for vaccines' reductions in susceptibility VE_S, infectiousness VE_I, and hospitalization given infection VE_P based on ranges of estimates in the current literature, few studies are available to guide estimates of similar risk reductions associated with prior SARS-CoV-2 infection, with

or without vaccination (but see Refs. [25] and [74]). Moreover, real-time estimates for emerging variants of concern such as omicron require observational study and are thus unavailable for prospective policy analyses. Alternative parameter assumptions may be explored via the provided open-source code. Second, we assumed perfect isolation after receiving a positive test result. Were this assumption to be violated by imperfect or delayed isolation, we predict a proportional loss of screening impact across all scenarios. Third, our model assumes values of R_0^{NPI} and immunity associated with the delta variant and plausible values for the omicron variant, but other emerging variants may dramatically shift the values of these parameters. These limitations affect the exact vaccination and past infection rates at which the three transitions identified in this chapter occur, and thus our analyses describe fundamental phenomena but do not make projections or predictions for specific communities.

Our analysis also uses a well-mixed SEIR model framework, inheriting two key limitations which merit direct discussion. First, we assume that vaccination and past infection statuses are uncorrelated at the population level. In reality, they may be anticorrelated due to the protective effects of vaccination, or because those with past infection may choose to forgo subsequent vaccination. We similarly assumed no homophily in contact patterns based on vaccination status, following the well-mixed assumption of the SEIR model framework, yet those who choose to be vaccinated may be more likely to be situated in a social network with others who choose to be vaccinated, and vice versa [127]. Second, compartmental SEIR models such as ours assume uniform infectiousness in the I compartment, contrasting empirical observations [96] and more sophisticated models [135, 136]. While our model's latent and infectious periods are well aligned with other SEIR models [5, 41, 70, 156], they nevertheless lead to unrealistically long generation times. Decreasing these periods proportionally to achieve the same reproductive number while aligning more closely with generation time estimates [90] would change the time-scale across all simulations, but would not impact the cumulative metrics or dynamics discussed in our key results.

More broadly, our work is situated within a family of research which uses mathematical modeling to estimate the impact of targeted countermeasures or strategies in populations with heterogeneous susceptibility, transmissibility, and/or contact rates. Other areas of focus include the allocation of scarce personal pro-

tective equipment to reduce transmission [252], the prioritization of vaccines by subpopulation [30,154,157], proactive screening programs in specific workplace structures [190] or contact networks [156], immunity "passport" programs [135], or immune shielding strategies [248]. While our analyses are directed at SARS-CoV-2, this work illustrates contributes general principles to this literature by showing that screening programs focused on testing the unvaccinated may be less effective than hoped in the face of high vaccination rates, waning vaccine effectiveness, or low compliance with testing.

3.4 Materials and Methods

3.4.1 SEIR model

Our analyses are based on a continuous time ordinary differential equation compartmental model with Susceptible, Exposed, Infectious, and Recovered (SEIR) compartments, stratified into vaccinated V and unvaccinated U groups. In addition to tracking infections among these two groups separately, we also tracked infections from both groups separately, enabling us to investigate four modes of transmission: from U to U, from U to V, from V to U, and from V to V. In all simulations, we used a constant total population size of $N = 20,000$ and denoted the vaccinated fraction of the population with ϕ.

To incorporate the possibility that individuals may have experienced prior infections, we further subdivided U and V into SARS-CoV-2 naive and SARS-CoV-2 experienced subpopulations, such that a fraction ψ of each was assumed to be previously infected and $1 - \psi$ remains naive. For notation, we denote the subpopulations of U to be u (unvaccinated, naive) and x (unvaccinated, experienced/prior infection), and the subpopulations of V to be v (vaccinated, naive) and h (vaccinated, experienced). We assumed that vaccination and SARS-CoV-2 experience statuses were fixed at the start of each simulation and immutable throughout, such that there was no ongoing vaccination, and individuals who were infected and recovered during each simulation were not reassigned to SARS-CoV-2 experienced status [6].

We denote the protective effects of immunity as XE, VE, HE, expressed as reductions in risk due to prior infection alone (x), vaccination alone (v), or prior infection and vaccination (i.e. so-called "hybrid"

immunity; h), respectively. Immunity was modeled to (i) decrease the risk of infection upon exposure, (ii) decrease the risk of transmission upon infection, placing our vaccine and immunity model in the broader category of leaky models [88], and (iii) decrease the risk of disease progression (i.e., hospitalization) upon infection. Reductions in the risk of infection upon exposure (XE_S, VE_S, HE_S), reductions in the risk of transmission when infected (XE_I, VE_I, HE_I), and reductions in the risk of hospitalization when infected (XE_P, VE_P, HE_P) were parameterized separately, based on ranges of estimates from the literature. Note that VE_H, the reduction in risk of hospitalization due to vaccination, is more commonly reported in the literature than VE_P, the reduction in risk of hospitalization due to vaccination conditional on infection. So, we used the formula $\text{VE}_P = 1 - \frac{1-\text{VE}_H}{1-\text{VE}_S}$ to estimate values for VE_P. We used the same relationship to estimate XE_P. See Table S3. Due to broad uncertainty in these effects over time since exposure [6, 25] or vaccination [25, 40, 80], by vaccine manufacturer and schedule [11, 74, 84, 217], by context [87, 175], and by variant [74], our analyses intentionally consider a range of values. We assumed that hybrid immunity against infection, HE_S, and transmission, HE_I, would always be superior to either vaccination alone or prior infection alone, via the simple formula $\text{HE} = (1-\text{XE})\text{VE}+\text{XE}$ and hybrid immunity against hospitalization given infection $\text{HE}_P = \max\{\text{VE}_P, \text{XE}_P\}$.

Fig. S16 shows a model schematic diagram for the SEIR model used in this chapter, where solid and dashed lines denote movement and transmission between classes, respectively. In lieu of including hospitalization as a model compartment, we computed total hospitalizations in each immunity class via multiplication of total infections, variant-specific infection hospitalization rates and $(1 - RR_P)$, where RR_P is the risk reduction against progression to hospitalization given infection (i.e., 0, VE_P, XE_P, or HE_P) (Supplementary Tables S2 and S3).

To model a community with open boundaries, we included a uniform risk of exposure to infection from an external source at a rate of N^{-1} per person per day. For instance, in a completely naive population, S_u/N individuals would be infected per day. After including the protective effects of vaccination and past infection this resulted in importation of infections at per-capita rates of $(1 - \text{VE}_S)N^{-1}$, $(1 - \text{HE}_S)N^{-1}$, $(1 - \text{XE}_S)N^{-1}$, and N^{-1} new infections per day in the v, h, x, and u groups respectively.

All simulations were run for 270 days, and all individuals were initially in one of the susceptible compartments S_u, S_x, S_v, or S_h in proportions $(1-\phi)(1-\psi)$, $(1-\phi)\psi$, $\phi(1-\psi)$, and $\phi\psi$, respectively. Model equations were solved using *lsoda* solver from the package *deSolve*, R version 4.1.0.

3.4.2 Incorporation of community testing

Screening the unvaccinated population via community testing, and subsequent isolation of those testing positive, was modeled by increasing the rate at which infected individuals were removed from the unvaccinated I_u and I_x compartments. Similarly, universal screening regardless of vaccination status was modeled by increasing the rate at which infected individuals were removed from all I compartments, I_u, I_x, I_v and I_h. The effectiveness of screening tests was assumed to be equal for vaccinated and unvaccinated individuals. We estimated increased rates of removal taking into account (i) the calibrated trajectories of viral loads within individual infection [38], (ii) the relationship between viral load and infectiousness [136], (iii) the frequency of testing, (iv) the test's analytical sensitivity (i.e. limit of detection) and turnaround time [135], and (v) screening compliance and valid sample rates, i.e. the fraction of scheduled or mandated tests which actually produce a valid sample [21]. In particular, our adaptation takes a previous model [135, 136] and updates viral load dynamics for the delta variant of SARS-CoV-2 [23, 125], the dominant variant at the time of the present analysis. To incorporate the effectiveness of screening θ, we reduce the duration of infectiousness $1/\gamma$ by a factor $(1-\theta)$, where θ corresponds to testing effectiveness (TE) as presented in Chapter 2. Parameter values for θ are found in Table S2, and are based on weekly PCR testing with a one-day turnaround, analytical limit of detection of 10^3 RNA copies per ml sample, and compliance rates of 50% (as in [21]) or 99% (as in [186]). These values assume that individuals immediately and successfully isolate upon receiving a positive diagnosis. We note that estimated effects of rapid antigen tests (with higher analytical limits of detection, but zero turnaround time) are highly similar to PCR testing under the assumptions above, provided that the community testing program frequencies and compliance rates are identical [136].

3.4.3 Transmission modes and forces of infection

Inclusive of all effects introduced above, the forces of infection are given by

$$\lambda_u = \alpha \left(\frac{I_u}{N_u} c_{u\to u} + [1 - \mathrm{XE}_I] \frac{I_x}{N_x} c_{x\to u} + [1 - \mathrm{VE}_I] \frac{I_v}{N_v} c_{v\to u} + [1 - \mathrm{HE}_I] \frac{I_h}{N_h} c_{h\to u} \right) + \frac{1}{N} \tag{3.1}$$

$$\lambda_i = \left[\alpha \left(\frac{I_u}{N_u} c_{u\to i} + [1 - \mathrm{XE}_I] \frac{I_x}{N_x} c_{x\to i} + [1 - \mathrm{VE}_I] \frac{I_v}{N_v} c_{v\to i} + [1 - \mathrm{HE}_I] \frac{I_h}{N_h} c_{h\to i} \right) + \frac{1}{N} \right] [1 - (RR_S)_i] \,, \tag{3.2}$$

where $i = \{x, v, h\}$, and reductions in susceptibility due to immunity are given by $(RR_S)_i = \{\mathrm{XE}_S, \mathrm{VE}_S, \mathrm{HE}_S\}$, correspondingly. The parameter α is the probability an unvaccinated, SARS-CoV-2 naive individual is infected by an infectious contact, tuned to achieve the desired R_0^{NPI}, $c_{i\to j}$ is the number of times an individual in group j is contacted by individuals from group i per day, and N_j is a convenience variable representing the number of people in subpopulation j.

To produce counts of how many infections were caused by each of the transmission modes $U \to U$, $U \to V$, $V \to U$, and $V \to V$, we integrated the appropriate terms of Eqs. (3.1) and (3.2) over the duration of each simulation. For instance, the cumulative number of vaccinated infections caused by the unvaccinated population is given by integrating over the forces of infection from u and x to v and h,

$$\begin{aligned} U \to V = \alpha \int_0^{270} \Bigg[& \frac{I_u(t)}{N_u} \Big(c_{u\to v} S_v(t) [1 - \mathrm{VE}_S] + c_{u\to h} S_h(t) [1 - \mathrm{HE}_S] \Big) \ \ldots \\ & + [1 - \mathrm{XE}_I] \frac{I_x(t)}{N_x} \Big(c_{x\to v} S_v(t) [1 - \mathrm{VE}_S] + c_{x\to h} S_h(t) [1 - \mathrm{HE}_S] \Big) \Bigg] dt \end{aligned}$$

3.4.4 Reproductive number

The basic reproductive number R_0 is defined as the expected number of secondary infections created by a typical infector in an entirely susceptible population, in the absence of any non-pharmaceutical interventions. Given the variety of environments in which SARS-CoV-2 spreads, and the presence of various permanent or semi-permanent non-pharmaceutical interventions, we use R_0^{NPI} in this work to denote the reproductive number in an entirely susceptible population inclusive of varying levels of now-baseline NPIs for the delta, omicron, and future variants. We consider $R_0^{\mathrm{NPI}} = 4$ (Main and Supplementary Figures)

and $R_0^{\text{NPI}} = 6$ (Supplementary Figures). For unvaccinated-only screening programs, this model's effective reproductive number is given by

$$R_{\text{eff}} = R_0^{\text{NPI}} \left[f_u(1-\theta) + f_x r_x (1-\theta) + f_v r_v + f_h r_h \right] \ , \tag{3.3}$$

where $f_u = (1-\psi)(1-\phi)$, $f_x = \psi(1-\phi)$, $f_v = (1-\psi)\phi$, and $f_h = \phi\psi$ represent the fractions of the population in the unvaccinated, experienced, vaccinated, and hybrid immunity groups, respectively, and $r_x = (1-\text{XE}_I)(1-\text{XE}_S)$, $r_v = (1-\text{VE}_I)(1-\text{VE}_S)$, and $r_h = (1-\text{HE}_I)(1-\text{HE}_S)$ are the cumulative impacts of immunity on each group. Setting the above equation equal to a constant produces isoclines shown in plots throughout the paper. The reduction in R_{eff} due to screening is given by

$$R_{\text{no screening}} - R_{\text{screening}} = R_0^{\text{NPI}} \theta (1-\phi) \left[1 - \psi(1-r_x) \right] \ , \tag{3.4}$$

a function linear in each of its variables which goes to zero as the vaccination rate ϕ approaches 1.

For universal screening programs, similar calculations yield

$$R_{\text{eff}}^{\text{universal}} = R_0^{\text{NPI}} (1-\theta) \left[f_u + f_x r_x + f_v r_v + f_h r_h \right] \ , \tag{3.5}$$

differing from Eq. (3.3) only in the terms to which $(1-\theta)$ applies. For a complete derivation of these equations, see Appendix.

Chapter 4

Statistical Methods for Estimating the Protective Effects of Immune Markers Using Test-Negative Designs

4.1 Introduction

Antibodies are a key component of the adaptive immune system, equipping the host to quickly recognize and respond to pathogen invasion. Antibodies have been identified as a mediator of protection against infection or severe disease for pathogens such as flu [167], SARS-CoV-2 [32, 102, 119, 148, 179, 195], Ebola virus [212, 249], and HIV [153]. While the concentration of antibodies and other immune molecules can be qualitatively linked to decreased risks, establishing the quantitative relationship between immune markers and protection is more challenging.

Test-negative design (TND) studies provide cost-effective data to understand the risk reduction provided by potential correlates of protection, and have been a common tool to estimate vaccine effectiveness in real-world settings [50, 71, 109, 111, 144]. TNDs recruit individuals who seek care for a particular symptom set, such as influenza-like illness (ILI) or fever. All sampled individuals are tested for a pathogen of interest, and the results of the test are reported alongside potential correlates of protection, such as vaccination status. These methods have been extended to understand the association between immunological assays, such as antibody titer, and risk reduction [32, 102, 148, 167, 179, 195].

TNDs typically use logistic regression to estimate the associations between continuous covariates and risk [32, 102, 148, 167, 179, 195]. Logistic regression provides a powerful statistical tool to estimate the

odds of a binary outcome, such as observable disease, given covariates such as antibody titer. However, little work has been done to understand the ability of logistic regression to recover commonly assumed antibody-protection relationships.

In this chapter, we make progress on the problem by first showing which types of relationships may be well suited for inference using logistic regression in TND studies, and which may not. Importantly, while the protective effects of antibodies are typically assumed to be sigmoidal in the literature [81, 120, 218], we demonstrate that standard logistic regression applied to TND data inherently limits the ability to accurately recover these relationships. We then extend the scaled logit model introduced by Dunning [58] to TND data, demonstrating its ability to recover commonly assumed protection functions from TND studies, with only a small mathematical change. We explore the accuracy of the scaled logit model for inference of various protection functions, identify conditions under which it may still fail, and provide practical guidance for researchers to adopt this model as a new standard for estimating the protective effects of immunological assays in TND studies.

4.2 Results

4.2.1 Standard logistic regression recovers only exponential protection from TND data

Test-negative designs (TNDs) are commonly used to estimate vaccine effectiveness (VE), defined as the reduction in risk of disease due to vaccination. In TNDs, VE is estimated using the odds ratio (OR) of disease among vaccinated versus unvaccinated individuals, i.e. $VE = 1 - OR$ [109, 144]. Logistic regression is a convenient statistical tool for inferring log-odds from data, and is often employed to learn this relationship from TND data [50,71,111,144,225]. In a logistic regression model, the log-odds of disease given vaccination status and other covariates are modeled as:

$$\text{logit}\, p = \beta_0 + \beta_1 V + \beta_2 \theta, \tag{4.1}$$

where p is the probability of disease, V is the vaccination status (e.g., 1 if vaccinated, 0 if not), and θ represents other covariates. The coefficient β_1 represents the change in log-odds of disease associated with

vaccination, meaning the odds ratio is described by: $OR = e^{\beta_1}$. Therefore, vaccine effectiveness is defined as:

$$VE = 1 - e^{\beta_1}. \tag{4.2}$$

When analyzing scalar correlates of protection, such as antibody titers, an intuitive substitution is to simply replace the binary vaccination status V with a measured titer A, and proceed with typical logistic regression [32, 102, 148, 167, 179, 195]. Assuming a baseline risk of $A = 0$, this replacement yields the following protection function, which describes the fraction by which risk is reduced as a function of A:

$$\Phi(A) = 1 - e^{\beta_1 A}, \tag{4.3}$$

where β_1 is the predicted change in log-odds of risk given a one unit increase in antibody titer using logistic regression.

Equation 4.3 provides the exact functional form of the resulting protection function when logistic regression is used to learn from TND data. Consequently, logistic regression is well suited to recovering this particular functional relationship between titers A and protection Φ. Hereafter, we refer to this as an exponential protection function.

To illustrate how logistic regression accurately recovers exponential protection functions, we developed a straightforward synthetic TND data testbed. First, we specify the shape of a protection function, and here we assume the exponential form (Fig. 4.1A). Second, we use this protection function to simulate infected (red circles) and uninfected (gray circles) antibody titer distributions (Fig. 4.1B). As a base case, we assume a large sample size ($N = 100,000$) and perfect diagnostic sensitivity and specificity for assigning infected status. Third, we use logistic regression to estimate risk of infection from the simulated data (Fig. 4.1C, purple curve). Lastly, we use this risk estimate to compute the odds ratio, with $A = 0$ as the baseline risk, and arrive at an estimated protection function (Fig. 4.1D, purple curve). The result of this simulation (Fig. 4.1D) illustrates what we have shown mathematically: using logistic regression to infer protection (purple curve) can recover true protection when the true protection function is exponential (black dashed curve).

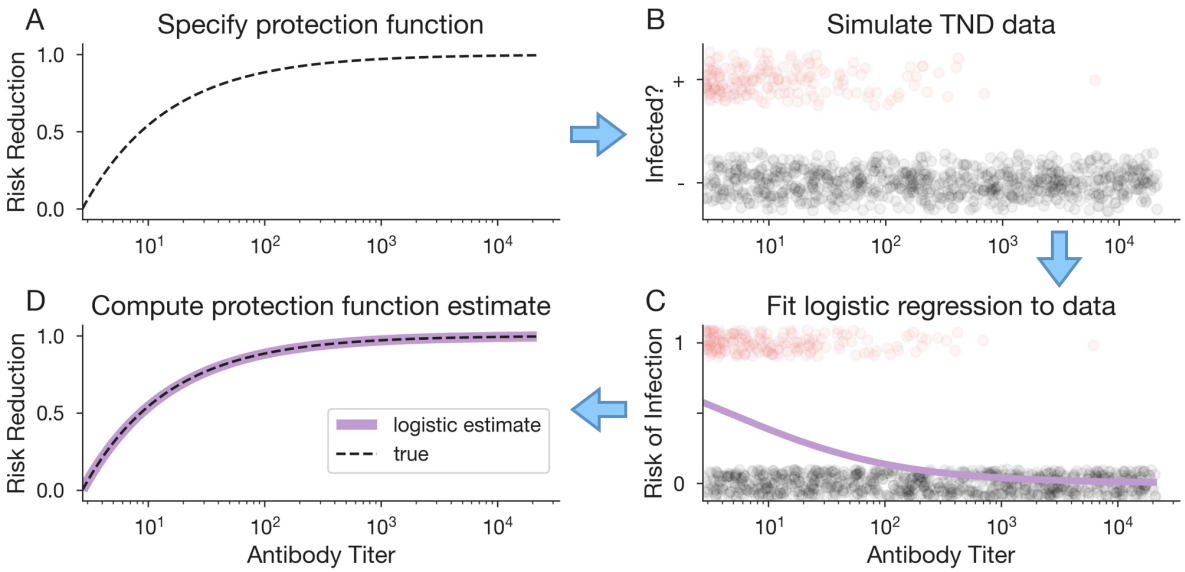

Figure 4.1: **Logistic regression provides an accurate estimate of antibody protection for an exponential protection function.** (A) First, we specify a protection function. (B) Next, we simulate TND data using this protection function to produce antibody distributions for test-positive (red circles) and test-negative (gray circles) individuals (subset of data shown here). (C) Logistic regression is used to estimate risk of infection from the simulated data. (D) Lastly, we compute the estimated protection function from the logistic regression model results (purple curve), which we compare to the true protection function (black dashed curve).

4.2.2 Logistic regression is poorly suited to recover a general protection function

The fact that logistic regression leads to an estimated protection function defined by a single-parameter exponential (Eq. 4.3) raises an important question: what if the true protection function is not exponential? We illustrate this type of mismatch between model and data – a model misspecification problem – through a second simulation experiment which follows the same four step procedure illustrated above. However, in this experiment, we generate data according to a plausible (but non-exponential) alternative protection function, and then fit a logistic regression model to the data.

Rather than an exponential protection function, we used a sigmoidal shape (Fig. 4.2B; black dashed curve), as is commonly assumed in the literature [81,120,218]. We simulated TND data using this sigmoidal protection function (Fig. 4.2A, red and black circles), and fit a logistic regression model to the synthetic data. The inferred risk (Fig. 4.2A) and resulting estimated protection function (Fig. 4.2B) are shown in purple.

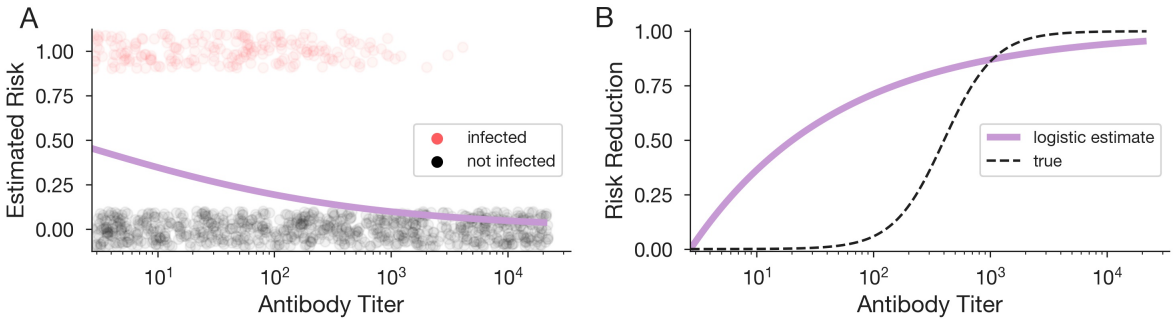

Figure 4.2: **Logistic regression does not provide an accurate estimate for a sigmoidal protection function.** (A) Logistic regression fit to simulated data. Circles show a subset of infected (red) and uninfected (gray) simulated individuals at various antibody titers used to train the model. (B) Estimated protection function from logistic regression (purple curve) compared to true protection function (dashed black curve).

Logistic regression fails to recover the true sigmoidal protection function used to generate the data, as evidenced by the mismatch between the estimated and true curves. These results are not unexpected: the logistic regression model is restricted to exponential protection functions (Eq. 4.3) and thus cannot recover other functional forms, even when applied to an ideal dataset with large sample size and no measurement error. Consequently, this model is incapable of capturing other intuitive functional forms, even under ideal data conditions. To infer a general, unknown relationship between antibodies and protection, a different statistical approach is required.

4.2.3 The scaled logit model can recover many functional relationships between antibody titers and risk reduction from TND data

A few alternatives to logistic regression have been proposed for inferring correlates of protection, which we briefly review. Zhang et al. showed that rescaling model inputs such that logit $p \sim ln(1 - X)$ for rescaled titers $X \in [0, 1]$ can recover a linear protection function, and matching the power of X to the protection function can recover polynomial functions [259]. However, the functional form of the risk reduction curve must be known a priori in order to use this method.

One might also consider using a polynomial expansion in our logistic regression model such that

$$\text{logit p} = \beta_0 + \beta_1 A + \beta_2 A^2 + ... + \beta_n A^n, \tag{4.4}$$

an approach commonly employed when the relationship between the predictor and log-odds is nonlinear. While this approach can approximate more complicated functional forms of protection, it has the drawback of overfitting data and requires model selection techniques to determine the optimal number of polynomial terms (n) to employ. Thus, polynomial logistic regression is not an ideal alternative for current practices.

Dunning proposed a scaled logit model to describe the relationship between immunological assay values and subsequent development of disease in case-control data [58]. This approach defines the probability of observing a case as

$$\text{Pr(disease)} = \lambda(1 - \pi(A \mid \theta)), \tag{4.5}$$

where λ denotes the probability a susceptible individual develops disease, and $\pi(A \mid \theta)$ describes the probability that an individual with titer A is protected, given model parameters θ. If a logistic protection function is assumed for $\pi(A)$, this results in the following risk of disease:

$$\text{Pr(disease)} = \frac{\lambda}{1 + e^{\beta_0 + \beta_1 A}}. \tag{4.6}$$

Thus, the scaled logit model has a similar shape to the logistic, but parameter λ reduces the expected force of exposure for individuals with low antibody titer. We refer to this model as the scaled logit, mirroring Dunning's original language.

We extend the scaled logit model for use in test-negative designs (TNDs) by substituting the risk function in Eq. 4.6 into the protection function estimator, i.e. one minus the odds ratio of protection at titer A vs titer $A = 0$. This yields a protection function of

$$\Phi_S(A) = 1 - \frac{1 - \lambda + e^{\beta_0}}{1 - \lambda + e^{\beta_0 + \beta_1 A}}, \tag{4.7}$$

where subscript S identifies this as the protection function using the scaled logit model. Importantly, the use of the scaled logit model requires estimation of only one more parameter (λ) than traditional logistic regression, and this, in turn, produces a protection function with three parameters β_0, β_1, and λ (Eq. 4.7) instead of only one parameter β_1 given by logistic regression (Eq. 4.3). Consequently, we should expect protection functions resulting from the scaled logit model to be substantially more flexible in modeling correlates of protection.

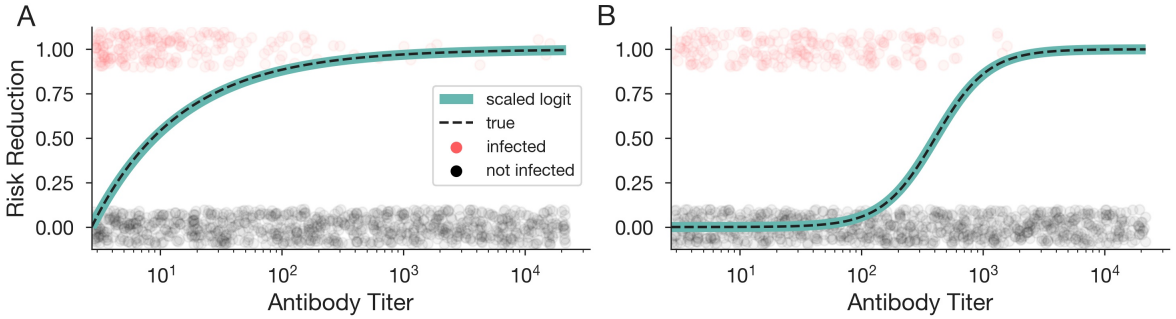

Figure 4.3: **The scaled logit model can recover complicated antibody protection functions.** Estimated protection function using the scaled logit model (green curve) trained on data generated using exponential (A) and sigmoidal (B) protection functions (dashed black curve). Circles show a subset of infected (red) and uninfected (gray) simulated individuals at various antibody titers used to train the model.

To demonstrate the flexibility of a scaled logit for TND studies, we simulated TND data under both exponential and sigmoidal protection functions (Fig. 4.3A,B; black dashed curves), and used the scaled logit model to estimate the protection function (green curves) for each simulated data set. We observe that the scaled logit model has high accuracy for estimating both exponential and sigmoidal protection. These results demonstrate that the scaled logit model can recover not only exponential protection, which logistic regression can recover, but also sigmoidal protection functions, which logistic regression cannot capture.

To further explore the ability of these models to accurately recover a variety of protection function scenarios, we subjected both the scaled logit and logistic models to several additional synthetic data sets generated from distinct protection functions. We found that the scaled logit, again, was able to accurately recover protection functions that logistic regression was unable to (Fig. S17). In further tests, we restricted the range of antibody titers such that few individuals had high or low titers, to challenge the scaled logit model's ability to recover protection functions from less optimal data, but its high accuracy was unaffected (Fig. S18).

These results demonstrate that introducing a single additional parameter in a scaled logit model enables inference of a broader range of functional forms, including sigmoidal risk reduction, which standard logistic regression cannot capture. Adopting this scaled logit model as the standard approach for estimating

the protective effects of immunological assays from TND data would allow for inference of a broader set of possible protection functions.

4.2.4 Scaled logit model accuracy depends on sample size

Studies vary widely in the total number of individuals sampled, as well as the proportion of samples that are cases versus controls [32,102,148,167,179,195]. Factors such as study duration, disease prevalence, and specificity of the symptoms which trigger enrollment into the study may impact sample size and case-to-control ratios. To explore how sample attributes impact the accuracy with which we can infer a protection function, we simulated TND data from a range of sample sizes and case-to-control ratios using a sigmoidal protection function, and the simulated data was used to estimate the protection function from both the scaled logit and logistic regression models. For each scenario, we computed error as the discrete ℓ_2 norm of the difference between the best-fit model $\hat{\Phi}(A)$ and the true protection function $\Phi_{\text{true}}(A)$, given by

$$\|\hat{\Phi} - \Phi_{\text{true}}\|_{\ell_2} = \left(\sum_{i=1}^{N} (\hat{\Phi}(A_i) - \Phi_{\text{true}}(A_i))^2 \right)^{\frac{1}{2}}, \tag{4.8}$$

where $\{A_i\}_{i=1}^{N}$ is the set of all potential antibody titers in the population. This norm corresponds to the Euclidean distance between the predicted and true values. To account for stochasticity in the generation of synthetic data, the mean error was calculated for 50 simulations per scenario.

When the scaled logit model is used to estimate protection, we observe higher error for smaller sample sizes (Fig. 4.4A). This is a result of model fitting estimating a threshold-type relationship between antibody titer and risk when sample size is low (see panel I), and thus poorly approximate the sigmoid used in synthetic data generation. As sample size increases, model fits more closely resemble the true protection function on average (panels I, III). Furthermore, we observe lower error when a higher proportion of total samples are cases (lighter colored curves), especially at low sample sizes. This demonstrates that cases typically provide more information to model inference than controls.

The same analysis of error in protection function estimation using logistic regression shows a higher error across all scenarios (Fig. 4.4B), which does not approach 0 as sample size increases. These results

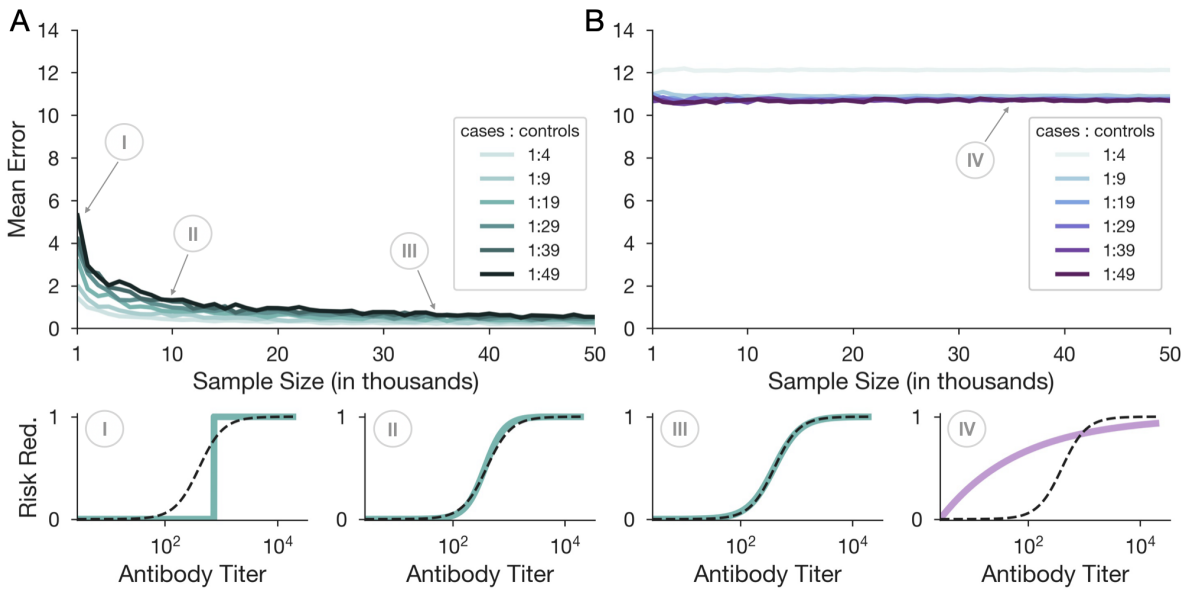

Figure 4.4: **The scaled logit model is better specified to recover sigmoidal protection from TND data than logistic regression.** Average error over 50 simulations per scenario for various sample sizes and case-to-control ratios using the scaled logit model (A) and logistic regression (B). Error was defined as the discrete ℓ_2 norm (Euclidean distance) between the modeled and true protection functions. Darker-colored lines represent scenarios with more controls per case. Insets show protection function estimates (colored curves) compared with the true protection function (black dashed curve) from a single simulation when $N = 1$, 10, and 35 thousand for the scaled logit (I-III) and 35 thousand for the logistic model (IV) using a $1:49$ case-to-control ratio.

reflect the large discrepancy between the inferred and true protection functions when using logistic regression (panel IV). This observation offers further support that logistic regression is poorly suited to recover a sigmoidal protection function, regardless of sample size, and the scaled logit model should be preferentially used to recover this functional form. However, the scaled logit model's high level of flexibility may also result in high error when large sample sizes are not feasible (see Figs. S19, S20).

4.2.5 The scaled logit model has poor accuracy if antibodies do not provide perfect protection

While the addition of a scaling constant λ allows for more flexible protection function estimates, Φ_S still approaches 1 as $A \to \infty$ (Eq. 4.7) for typical monotonically decreasing risk parameterization (i.e. $\beta_0 < 0$, $\beta_1 > 0$). Because of this, the model may be ill suited to recover scenarios where protection is imperfect, or where perfect protection exists but is simply not in the sampled population.

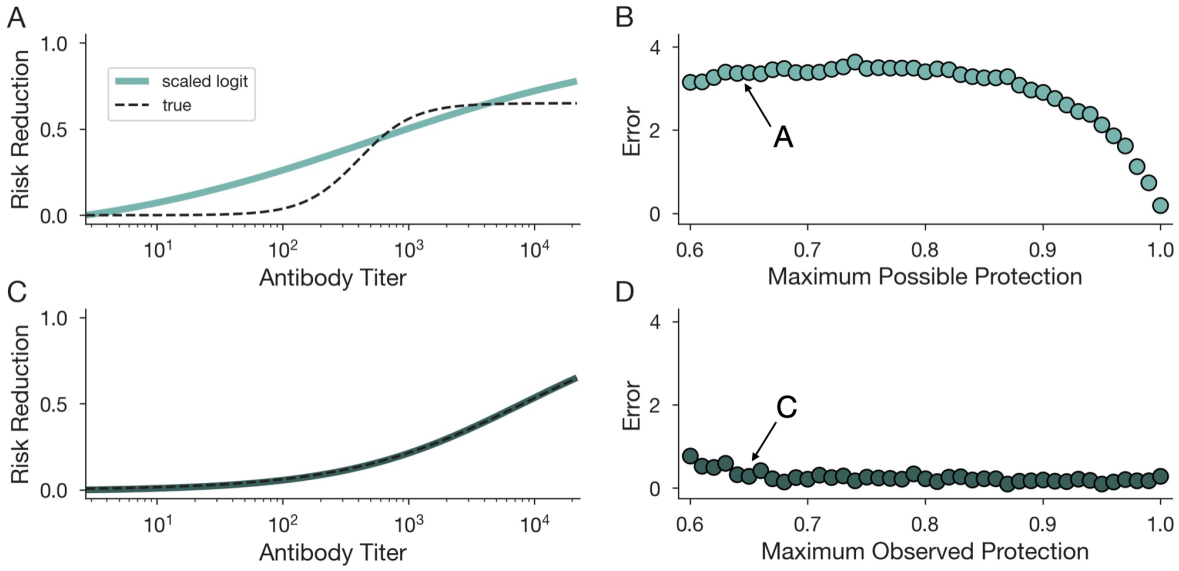

Figure 4.5: **Scaled logit model has reduced accuracy if antibodies do not provide perfect protection.** The scaled logit model is fit to TND data generated from a sigmoidal protection function which does not saturate to 1 (A,B) and when individuals with near-perfectly protective antibody titers are not sampled among controls (C,D). (A,C) Predicted protection functions from the scaled logit model (green curves) versus true protection (black dashed curves) for a maximum protection of 0.65. (B,D) Prediction error (Euclidean distance between predicted and true protection) under varying maximum protection levels.

We conducted two numerical experiments, each of which explores a different scenario in which the scaled logit may have poor accuracy. In the first experiment, we asked what happens if the protection function does not saturate to one — that is, to perfect protection — as antibody titers grow large. We simulated TND data under a sigmoidal protection function which saturates at 65% (Fig. 4.5A, black dashed curve), such that individuals with high antibody titers still have a 25% chance of infection if they are exposed. We then estimated the protection function using the scaled logit model (green curve). The best-fit protection function overestimates protection at both low and high antibody titer, and approaches 1 as titer values increase. Varying the saturation point, or maximum possible protection, we observe relatively stable error estimates until the maximum possible protection surpasses 90%, at which point error approaches 0 (Fig. 4.5B).

In the second experiment, we asked what happens if individuals with near-perfectly protective antibody titers are simply not sampled among the controls. To simulate this, we generate TND data where the

maximum sampled antibody titer is A_{max}, but the slope of the sigmoidal protection function is reduced such that risk reduction is perfect only for values $A \gg A_{\text{max}}$ (Fig. 4.5C, dark green curve). For this scenario, we observe an estimated protection function (green curve) that nearly perfectly estimates the true protection function (black dashed curve; note curves are overlapping). Varying the maximum observed protection shows that error is low and nearly constant across scenarios (Fig. 4.5D). Comparing across experiments, we observe higher error for saturating protection (Fig. 4.5B) than for unsampled perfect protection (Fig. 4.5D). Distinguishing between these two scenarios may facilitate a better understanding of confidence in model fits.

4.3 Discussion

Our results establish the scaled logit model as a more flexible alternative to typical logistic regression methods for protection as a function of scalar immunological assays in test-negative design (TND) studies. Using simulated data, we see that the scaled logit model can recover not only an exponential protection function, which logistic regression can recover, but also a sigmoidal protection function, which logistic regression fails to recover. Despite its increased flexibility, we demonstrate that the scaled logit model may not consistently recover the true protection function for sample sizes below $\approx 10,000$, and that model accuracy drops off steeply for sample sizes $< 1,000$. Furthermore, we show that if protection does not saturate to 1, model accuracy may suffer.

These results lead us to recommend the adoption of the scaled logit model for estimating the protective effects of immunological assays from TND data. This model allows for flexible inference of a variety of protection functions. If researchers are faced with small sample sizes, for which we demonstrate low accuracy of the scaled logit model, we note that performance would be greatly improved by implementing regularization to prevent parameter β_1 from predicting steep transitions. This work omits regularization to explore the utility of the scaled logit model with minimal prior knowledge of the protection function. Alternative models with greater flexibility to capture protection functions which do not saturate to 1, exhibit asymmetry, or are characterized by extremely steep transitions have been previously explored [59]. How-

ever, differentiating between model options requires model selection methods or prior knowledge of the expected shape of the protection curve. Thus, we recommend the scaled logit model as a simple alternative to logistic regression methods, exhibiting greater flexibility without the need for model selection.

Our methods are subject to a number of limitations. First, we simulate data under ideal sampling scenarios, exploring limitations of sample sizes and case-to-control ratio variations, but not sensitivity and specificity of diagnostic tests or noise in immunological assay measurements. Second, we do not consider the effects of demographic covariates, such as age and sex, or immunity covariates, such as time since last infection or other immunological assays [171]. While these covariates may impact protection estimates, we posit that the scaled logit model can be used to control for their effects as effectively as logistic regression. Third, our exploration of protection functions is limited to functions which start at 0 when $A = 0$ and monotonically increase with increasing titer. These functions do not account for immune imprinting [243] or antigenic drift which may lead to decreasing protection functions. Lastly, we do not account for differences in care-seeking behavior that may be correlated with titer values, i.e. due to changes in symptom prevalence or timing, nor do we account for potential cross-protection between circulating pathogens in our synthetic data pipeline. These factors, as well as differential depletion of susceptibles, have been shown to potentially bias the protection estimates inferred using test-negative designs for vaccine effectiveness studies [109, 144].

Quantifying the relationship between assay value and risk reduction is an important task to understand the utility of immunological assays. Informative immunological assays may open up new data streams to model heterogeneous susceptibility in immune-experienced populations [33, 161], vaccination strategies [123, 166], and other epidemiological endpoints. Furthermore, understanding the strength of correlations between titer values and protection could be used to predict vaccine efficacy from titers alone instead of following a cohort in vaccine trials, reducing costs and increasing the speed at which trials may be performed. The scaled logit model, in combination with test-negative designs, can provide an accurate road-map of which immunological measurements predict protection levels, opening the door for immunological assays to inform infectious disease modeling efforts. Once the functional relationship connecting immune assays to protection is understood, the norms of the field may evolve from sharing only binary

serology results to a more granular view of serology data [137].

4.4 Materials and Methods

The purpose of this study is to evaluate statistical methods used to infer correlates of protection in test-negative design (TND) studies. These studies seek to establish a quantitative link between an immunological assay and risk reduction – we call this relationship the protection function, i.e. the reduction in risk of disease associated with a particular immunological assay value. Here, we focus on antibody titer A as a commonly utilized quantitative immunological assay, but methods may be extended to other scalar assays as well.

In TNDs, protection is estimated using the odds ratio (OR) of disease among individuals with titer A versus individuals with titer $A = 0$, mirroring the estimator used predict the direct protective effects of vaccination in vaccine effectiveness studies [109, 144]. A statistical model is used to infer the relationship between titer and risk of disease from data. Given the inferred relationship between titer and risk, $p(A)$, the estimated protection function is defined as

$$\hat{\Phi}(A) = 1 - \text{OR} = 1 - \frac{\frac{p(A)}{1-p(A)}}{\frac{p(A=0)}{1-p(A=0)}}. \tag{4.9}$$

We wish to evaluate the ability of a particular inference method, such as logistic regression, to learn this protection function from TND data. To accomplish this, we will simulate data where the protection function we wish to infer is known a priori, allowing for comparison between the known relationship (Φ_{true}) and the predicted relationship ($\hat{\Phi}$) under different inference methods.

Our methodology follows a four step routine. First, we first specify the shape of a protection function (e.g. exponential protection in Fig. 4.1A). Second, we use this protection function to simulate infected (red circles) and uninfected (gray circles) antibody titer distributions (Fig. 4.1B), which produces a synthetic test-negative design data set under the specified protection function. Third, we use a statistical model to estimate the relationship between titer and risk (p(A)) from the simulated data (Fig. 4.1C, purple curve). Lastly, we utilize this risk estimate to compute the estimated protection function from Equation 4.9 (Fig. 4.1D, purple curve), and compare the inferred protection function to the true protection function used to generate the data.

The methods for each step are explained in detail below.

4.4.1 Simulating test-negative design (TND) data

TND studies typically recruit all individuals who report a particular symptom or set of symptoms. Recruited individuals are tested for a pathogen of interest, with data reported on: (1) test result for pathogen of interest (positive or negative), (2) value of covariate(s) assumed to be associated with infection risk (i.e. vaccination status or immunological assay), and (3) other variables which may impact risk (i.e. age, sex). Our synthetic data will focus on quantitative antibody titer A as the covariate of interest, but other scalar immunological assay values may be easily substituted.

We begin by defining the protection function $\Phi_{\text{true}}(A)$ that will be used to generate TND data. The protection function is defined such that Pr(disease $\mid A$) $= (1 - \Phi_{\text{true}}(A)) \cdot$ Pr(disease $\mid A = 0$). High values of $\Phi_{\text{true}}(A)$ are thus associated with a low probability of infection. Multiple functional forms for this relationship were explored in our analyses, including: (1) no relationship, (2) threshold: perfect protection above a given titer, (3) exponential, and (4) sigmoidal (Fig. S21).

Next, we simulate a large population of individuals with known log antibody titers ($log(A)$). For main-text analyses, $log(A) \sim$ log-uniform$(1, 10)$, representing raw antibody titers on the interval of approximately $A \in [0, 22000]$, distributed uniformly on a log-scale. Titer values are meant to represent a quantitative assay, such as Enzyme-Linked Immunosorbent Assay (ELISA). However, the authors note that antibody titer distributions vary widely depending on the pathogen and population-level immunity. Given that this manuscript seeks to evaluate whether statistical methods can recover known protection functions from data, we use this arbitrary distribution of titers not to reflect reality for any given pathogen but simply to establish an assumed relationship.

Next, we draw from this pool of individual antibody titers to simulate $N = 100,000$ synthetic TND samples, made up of cases who test positive for the pathogen of interest and controls who test negative. The ratio of cases to controls varies widely across studies, depending on factors such as disease prevalence,

symptom specificity, and immunity levels. Thus, we specify the number of controls per case ($c = 4$) and explore the effects of different ratios in the main text. For a specified number of samples (N) and controls-per-case value (c), we generate $n_{cases} = N/(c+1)$ cases and $n_{controls} = N - n_{cases}$ controls.

Under the assumption that antibodies provide no protection from other non-focal pathogens or conditions which may cause symptoms, we may reasonably assume that our controls are a random sample of the total population who experience symptoms for reasons other than infection with the pathogen of interest. Thus, antibody titers for $n_{controls}$ are drawn uniformly at random from the simulated antibody titers without replacement.

Since antibody titers may provide protection to disease from the pathogen of interest according to the pre-defined relationship $\Phi_{\text{true}}(A)$, we must consider individual antibody titer levels A when simulating cases. Thus, cases are randomly selected from the population with probability $1 - \Phi_{\text{true}}(A)$ until n_{cases} is achieved. The resulting simulated data contains [titer, case designation] pairs for N individuals as a result of a synthetic test-negative design study.

4.4.2 Estimating protection function

TND studies provide samples of linked covariates (i.e. antibody titer) and outcomes (i.e. observed infections). TNDs define protection using the ratio of infection odds with and without an intervention [144]. For scalar antibody titers A, the protection function is given by Equation 4.9. A statistical model is needed to estimate odds, or equivalently risk, from data.

4.4.2.1 Using logistic regression to estimate risk

In practice, logistic regression is often employed as a convenient statistical tool to estimate odds of an outcome given data [32, 102, 148, 167, 179, 195]. For antibody titers, the logistic model defines risk as $\text{logit}\, p = \beta_0 + \beta_1 A$. Computing risk reduction ($\hat{\Phi}_{\text{logistic}}$) from this estimate using the odds ratio definition gives

$$\hat{\Phi}_{\text{logistic}} = 1 - e^{\beta_1 A}. \tag{4.10}$$

Computationally, we perform maximum likelihood estimation (MLE) for logistic model parameters using `sklearn` in python 3.8.11 without regularization (see code availability for model training code). Parameters are fit to logged titer data, following the norms of the field [32, 102, 148, 167]. The protection function was then computed using Equation 4.10 by computing the odds of disease at each logged titer compared to the baseline odds when $A = 0$ under the logistic model.

4.4.2.2 Using a scaled logit to estimate risk

Dunning presented a model called the scaled logit model for estimating immunological correlates of protection from case-control studies [58]. This approach defines the probability of observing a case as

$$\text{Pr(disease)} = \lambda(1 - \pi(A \mid \theta)), \tag{4.11}$$

where λ denotes the probability a susceptible individual develops disease, and $\pi(A \mid \theta)$ is a smooth function on the interval [0,1] describing the probability an individual with titer A is protected, given model parameters θ. If a logistic protection function is assumed for $\pi(A)$, this results in a risk function of:

$$p_{\text{scaled}}(A) = \frac{\lambda}{1 + e^{\beta_0 + \beta_1 A}}. \tag{4.12}$$

If we extend this model for use in test-negative designs using Equation 4.9, risk reduction (Φ_{scaled}) can be computed as:

$$\Phi_{\text{scaled}}(A) = 1 - \frac{1 - \lambda + e^{\beta_0}}{1 - \lambda + e^{\beta_0 + \beta_1 A}}. \tag{4.13}$$

Importantly, the use of the scaled logit model requires estimation of only one more parameter (λ) than traditional logistic regression, which results in two more parameters describing the protection function.

4.4.2.3 Fitting a scaled logit model

The scaled logit model defined in Eq. 4.12 was fit to data using maximum likelihood estimation (MLE). Unlike standard logistic regression, typical programming languages do not have built-in model fitting for atypical functions such as the scaled logit. Thus, we present our fitting method and code to assist researchers in adapting the scaled logit model for their own work.

The likelihood of observing a given data set is given by

$$\mathcal{L}(\lambda, \beta_0, \beta_1; \{y_i, A_i\}) = \prod_i \left(\frac{\lambda}{1 + e^{(\beta_0 + \beta_1 A_i)}} \right)^{y_i} \left(1 - \frac{\lambda}{1 + e^{(\beta_0 + \beta_1 A_i)}} \right)^{(1-y_i)}, \tag{4.14}$$

where A_i denotes individual antibody titers and $y_i = 1/0$ denotes an observed infection or non-infection, respectively. We wish to find the parameters $(\lambda, \beta_0, \beta_1)$ which maximize this likelihood function, or equivalently the parameters that minimize the negative log-likelihood:

$$\mathcal{NLL}(\lambda, \beta_0, \beta_1; \{y_i, A_i\}) = \sum_i \left[-y_i \log \left(\frac{\lambda}{1 + e^{(\beta_0 + \beta_1 A_i)}} \right) - (1 - y_i) \log \left(1 - \frac{\lambda}{1 + e^{(\beta_0 + \beta_1 A_i)}} \right) \right]. \tag{4.15}$$

The latter form is preferable for computational methods, given limitations of machine epsilon when computing extremely small values.

We use the built in `scipy.minimize` function in python, implemented with the Nelder-Mead minimization algorithm and options to increase the number of iterations before convergence, to find the optimal parameterization which minimizes the negative log-likelihood. Sample code is provided for MLE in both python and R in the Appendix.

Chapter 5

Conclusion

The chapters of this dissertation highlight how multi-scale modeling can be used to inform public health decision making. Chapter 2 utilizes a simultaneous integration framework informed by within-host viral kinetics modeling to estimate the impact of diagnostic testing and subsequent isolation on transmission reduction. Chapter 3 extends these results into a compartmental modeling framework to estimate the impact of vaccinate-or-test programs for COVID-19 using a serial integration framework. Chapter 4 considers a different type of within-host data: immune markers, such as antibody titers, which may predict one's level of susceptibility to infection or severe disease. This chapter uses simulated antibody titer data to show the limitations of common statistical methods for estimating correlates of protection, and introduces an alternative model with increased flexibility.

5.1 Significance

The work completed in this thesis has numerous applications furthering the field of infectious disease modeling and public health decision making. Chapter 2 introduces a novel approach to multi-scale modeling for the impact of testing on disease transmission. This chapter builds on work comparing COVID-19 testing strategies by Larremore et al. [136], formalizing the mathematics to predict testing effectiveness for any virus. This simultaneous integration framework mirrors the mathematics developed by Fraser to estimate the effects of symptomatic isolation and contact tracing [69] and could be further extended to other interventions. Furthermore, the results of this model predict reduction in transmission due to testing, and can

therefore be incorporated into a compartmental model to analyze the impact of targeted testing strategies, as in Chapter 3. This provides a more accurate estimate of testing effectiveness than traditional compartmental methods given its reliance on viral kinetics data, but is more computationally efficient than performing the same estimates using a multi-domain integration framework, as in [136]. The results of this study were published in multiple news outlets to inform COVID-19 at-home testing recommendations [97, 172, 224].

Chapter 3 incorporates the results from Chapter 2 into a serial integration framework, estimating the effects of vaccinate-or-test policies for COVID-19. As COVID-19 vaccines rolled out in 2021, schools, institutions, and governments considered reallocating diagnostic testing resources towards unvaccinated populations. Our results showed that the effectiveness of vaccinate-or-test policies would vary depending on population immunity levels for early variants of COVID-19. Furthermore, results elucidated that these policies would be ineffective toward the omicron variant, which swept America as the manuscript was in press, due to higher levels of immune escape from the omicron variant. These results were used to inform testing policies on CU Boulder campus.

Chapter 4 uses simulated data to evaluate common statistical methods used to infer correlates of protection from test-negative design data. These methods have been used to estimate the protective effects of antibodies towards SARS-CoV-2 [32, 102, 148, 179] and influenza [167, 195]. Our results show that more flexible statistical methods open the door to more realistic protection functions. This work provides a framework for learning how within-host immune markers are associated with reductions in susceptibility, proven mathematically and through simulation studies. This chapter lays an important groundwork to change the models we use to understand correlates of protection, a necessary step towards future studies that use within-host immunological models to inform susceptibility levels in between-host transmission models.

5.2 Limitations

The studies presented in this thesis are subject to a number of common limitations. First, pathogens evolve over time, and the models presented here do not necessarily predict the impact of this evolution. Chapters 2 and 3 each consider multiple distinct variants of SARS-CoV-2. However, the aggregation of

genotypes into variants is limited in itself, and our ability to characterize distinct attributes (such as viral kinetics, symptom timing, test sensitivity, etc.) to each variant was limited by the information available at the time during a rapidly changing pandemic. Similarly, Chapter 4 results may change depending on if currently circulating variants are highly mutated compared to the immune marker being measured in the study.

Second, human behavior is an important component of transmission dynamics, which we do not directly consider in our studies. None of the three chapters consider how differences in behavior may reduce transmission. This simplification omits observed differences in contacts based on attributes such as age or occupation [170, 192, 227], as well as potential differences in preventative behaviors, such as mask wearing [226] or vaccination refusal [147], across a population. Inclusion of this heterogeneity may lead to differentially distributed infectious potential (Chapters 2 and 3) or potential for exposure (Chapter 4) in the population.

Lastly, the number of potential infectious disease endpoints is vast and often difficult to measure. Chapter 2 considers how testing can reduce transmission, and therefore the number of infections. This does not explore how testing may reduce other important endpoints, such as the likelihood of an outbreak or importation of a disease [29]. Similarly, Chapter 4 explores the statistical methods used to estimate probability of disease, or symptomatic infection, but cannot be used to estimate the probability of infection itself. This endpoint would require a different study design, which is not conducive to test-negative design.

5.3 Future research

5.3.1 Estimating individual infectiousness profiles

In Chapter 2, we use viral load as a proxy for infectious potential. Viral load is measured using quantitative reverse transcription polymerase chain reaction (RT-qPCR), which amplifies viral genomic ribonucleic acid (RNA) to quantify even small concentrations of genetic material. However, this method does not differentiate between replicating virus, which is considered potentially infectious, and non-viable

viral fragments. To approximate infectious viral concentrations, researchers may use assays such as focus-forming/plaque assays [121] or viral titers [13, 95, 141] which aim to capture only the virus that can actively replicate in-vitro.

Chapters 2 and 3 rely on the assumption that a higher viral load is associated with a higher transmission potential given contact with a susceptible person, which is supported by the literature [7, 7, 21, 72, 86, 113, 116, 188], albeit not perfectly [86, 115, 116]. Some studies show higher correlation between viral load and replicating virus in the early days of an infection [116], i.e. the proliferation period. This phenomenon may be explained by neutralizing antibodies, cytotoxic T cells, phagocytic cells, or other immune responders preventing viral replication without necessarily clearing viral RNA.

This idea could be incorporated into a within-host model that simulates virus interactions with cells and immune molecules (Figure 5.1A). This model seeks to replicate infectious virus (V) interactions with host target cells (T), which become infected (I) and stimulate the production of immune responders (A) and more virus particles. If viral-immune interactions lead to reductions in infectious virus without immediate reductions in viral RNA, we may observe differential peaks for infectious virus (Figure 5.1, red curve) and total viral RNA as measured by RT-qPCR ($V + R$, black curve). Fitting this model to viral load (black curve) and viral titer (red curve) data may allow us to infer the rate at which the immune response effectively stunts viral replication (i.e. parameter σ). If this parameter value is consistent across individuals or even pathogens, we may realize a future where viral load measurements can be easily be mapped to infectious potential without the need for time consuming titer or plaque assays.

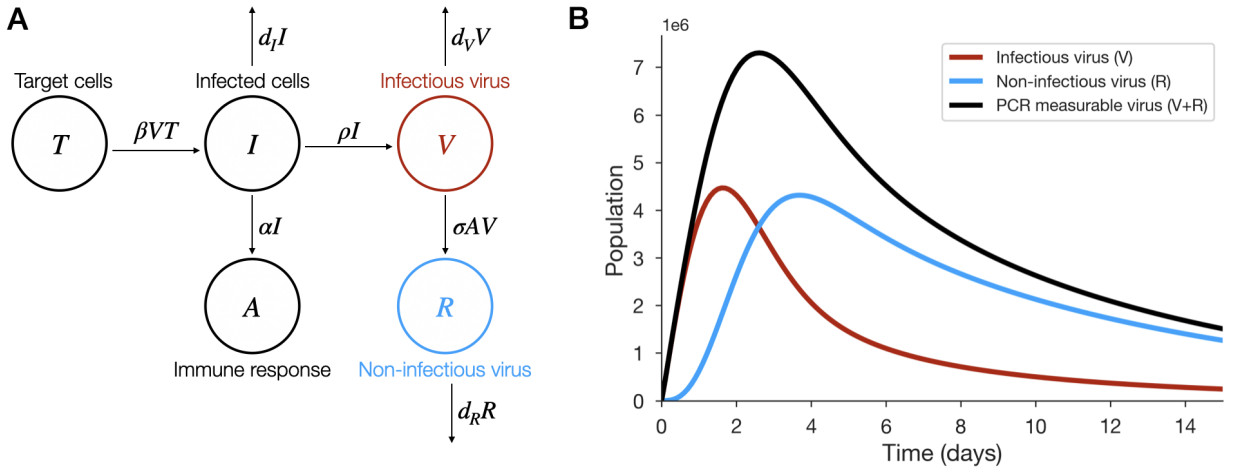

Figure 5.1: **Within-host modeling can help differentiate infectious virus from non-infectious virus**. (A) Model diagram depicting within-host compartments of target cells (T), infected cells (I), infectious virus particles (V), non-infectious virus particles (R), and immune response (A). (B) Example kinetics for infectious (red curve), non-infectious (blue curve), and total (black curve) virus populations.

The approach depicted in Figure 5.1 focuses on within-host data, but we may also learn the relationship between viral load and infectious potential using between-host data, or observed transmissions. These observations are complicated by veils of stochasticity, individual behaviors, and individual susceptibility levels. However, we may gain some traction by comparing the distribution of observed secondary infections to the distribution of individual infectiousness under some model (i.e. the logarithm of viral load above some threshold). Infectiousness models which replicate observed transmission distributions are likely good candidate models to infer infectiousness from viral load data. Increased model complexity may also consider how expected behaviors, such as heterogeneous contact patterns and symptomatic self-isolation, change these results.

5.3.2 Incorporating serology data into epidemiology models

The methods presented in Chapter 4 are one of several ways to infer the protective effects of quantitative immunological assays. These methods can link assay values, such as antibody titers, to observed

reductions in risk of infection, severe disease, transmission, or death. Understanding this functional link between assay values and risk reduction is the first step to incorporating quantitative cross-sectional sero-surveys into epidemiological modeling efforts.

This adds another layer of complexity to individual heterogeneity that can change modeling results. Theoretical work has demonstrated that heterogeneous host susceptibility generally dampens infection counts [33], reduces epidemic final size and herd immunity threshold estimates [33, 161, 166], and may change optimal vaccination policies [123]. Realistically modeling this heterogeneity requires both serology data and the protection function which links serology data to observed reductions in risk. Given this understanding, future work could easily incorporate serological data into a simple SSIR-type model, where multiple susceptible compartments provide varying levels of protection from infection given exposure.

5.4 Concluding remarks

This dissertation demonstrates the power of multi-scale modeling to bridge the gap between individual-level viral and immune dynamics and population-level transmission and protection outcomes. By integrating viral kinetics with testing and isolation strategies, evaluating vaccinate-or-test policies, and examining statistical methods to estimate correlates of protection, this work advances our ability to predict and mitigate infectious disease transmission. While some limitations remain, such as the availability of large-scale immune response data and the complexity of real-world transmission dynamics, these findings provide a strong foundation for future research on testing policies, vaccine evaluation, and multi-scale infectious disease modeling. Ultimately, this work demonstrates the value of multi-scale modeling to inform public health decision-making and improve epidemic preparedness.

Bibliography

[1] Cost-effectiveness of preventing AIDS complications (CEPAC) model. https://www.massgeneral.org/medicine/mpec/research/cpac-model. Accesed: 11-29-2023.

[2] Evaluating the roadmap out of lockdown: modelling step 4 of the roadmap in the context of B.1.617.2. https://assets.publishing.service.gov.uk/government/uploads/system/uploads/attachment_data/file/993427/S1289_Imperial_Roadmap_Step_4.pdf, 2021. Accessed: August 11, 2021.

[3] What we now know about the SARS-CoV-2 delta variant that's wreaking havoc globally. https://scitechdaily.com/what-we-now-know-about-the-{SARS-CoV-2}-delta-variant-thats-wreaking-havoc-globally/, Aug 4, 2021. Accessed: August 11, 2021.

[4] Puranik A, Lenehan PJ, Silvert E, Niesen MJM, Corchado-Garcia J, O'Horo JC, Virk A, Swift MD, Halamka J amd Badley AD, Venkatakrishnan AJ, and Soundararajan V. Comparison of two highly-effective mRNA vaccines for COVID-19 during periods of alpha and delta variant prevalence. medRxiv, 2021.

[5] Gavin M. Abernethy and David H Glass. Optimal COVID-19 lockdown strategies in an age-structured SEIR model of Northern Ireland. J. R. Soc. Interface, 2022.

[6] Laith J Abu-Raddad, Hiam Chemaitelly, Peter Coyle, Joel A Malek, Ayeda A Ahmed, Yasmin A Mohamoud, Shameem Younuskunju, Houssein H Ayoub, Zaina Al Kanaani, Einas Al Kuwari, et al. SARS-CoV-2 antibody-positivity protects against reinfection for at least seven months with 95% efficacy. EClinicalMedicine, 35:100861, 2021.

[7] Soha Al Bayat, Jesha Mundodan, Samina Hasnain, Mohamed Sallam, Hayat Khogali, Dina Ali, Saif Alateeg, Mohamed Osama, Aiman Elberdiny, Hamad Al-Romaihi, and Mohammed Hamad J. Al-Thani. Can the cycle threshold (Ct) value of RT-PCR test for SARS CoV2 predict infectivity among close contacts? Journal of Infection and Public Health, 14(9):1201–1205, Sep 2021.

[8] Heba Altarawneh, Hiam Chemaitelly, Patrick Tang, Mohammad R. Hasan, Suelen Qassim, Houssein H. Ayoub, Sawsan AlMukdad, Hadi M. Yassine, Fatiha M. Benslimane, Hebah A. Al Khatib, Peter Coyle, Zaina Al Kanaani, Einas Al Kuwari, Andrew Jeremijenko, Anvar Hassan Kaleeckal, Ali Nizar Latif, Riyazuddin Mohammad Shaik, Hanan F. Abdul Rahim, Gheyath K. Nasrallah, Mohamed Ghaith Al Kuwari, Adeel A. Butt, Hamad Eid Al Romaihi, Mohamed H. Al-Thani, Abdul-

latif Al Khal, Roberto Bertollini, and Laith J. Abu-Raddad. Protection afforded by prior infection against SARS-CoV-2 reinfection with the omicron variant. medRxiv, 2022.

[9] Avnika B Amin, Matt D T Hitchings, Otavio T Ranzani, Jason R Andrews, Derek A T Cummings, Albert I Ko, Julio Croda, and Natalie E Dean. Severity-dependent test-seeking behaviors and test-negative designs: impact on estimated vaccine effectiveness and utility of analytic and design choices. American Journal of Epidemiology, page kwae303, August 2024.

[10] Nick Andrews, Julia Stowe, Freja Kirsebom, Samuel Toffa, Tim Rickeard, Eileen Gallagher, Charlotte Gower, Meaghan Kall, Natalie Groves, Anne-Marie O'Connell, David Simons, Paula B. Blomquist, Asad Zaidi, Sophie Nash, Nurin Iwani Binti Abdul Aziz, Simon Thelwall, Gavin Dabrera, Richard Myers, Gayatri Amirthalingam, Saheer Gharbia, Jeffrey C. Barrett, Richard Elson, Shamez N Ladhani, Neil Ferguson, Maria Zambon, Colin NJ Campbell, Kevin Brown, Susan Hopkins, Meera Chand, Mary Ramsay, and Jamie Lopez Bernal. Effectiveness of COVID-19 vaccines against the omicron (B.1.1.529) variant of concern. medRxiv, 2021.

[11] Nick Andrews, Elise Tessier, Julia Stowe, Charlotte Gower, Freja Kirsebom, Ruth Simmons, Eileen Gallagher, Meera Chand, Kevin Brown, Shamez Ladhani, et al. Vaccine effectiveness and duration of protection of Comirnaty, Vaxzevria and Spikevax against mild and severe COVID-19 in the UK. medRxiv, 2021.

[12] Nick Andrews, Elise Tessier, Julia Stowe, Charlotte Gower, Freja Kirsebom, Ruth Simmons, Eileen Gallagher, Simon Thelwall, Natalie Groves, Gavin Dabrera, Richard Myers, Colin N.J. Campbell, Gayatri Amirthalingam, Matt Edmunds, Maria Zambon, Kevin Brown, Susan Hopkins, Meera Chand, Shamez N. Ladhani, Mary Ramsay, and Jamie Lopez Bernal. Duration of protection against mild and severe disease by Covid-19 vaccines. NEJM, 386(4):340–350, 2022.

[13] Bindiya Bagga, Christopher W Woods, Timothy H Veldman, Anthony Gilbert, Alex Mann, Ganesh Balaratnam, Robert Lambkin-Williams, John S Oxford, Micah T McClain, Tom Wilkinson, Brad P Nicholson, Geoffrey S Ginsburg, and John P DeVincenzo. Comparing influenza and RSV viral and disease dynamics in experimentally infected adults predicts clinical effectiveness of RSV antivirals. Antiviral Therapy, 18(6):785–792, Aug 2013.

[14] Jean-Louis Bayart, Jonathan Degosserie, Julien Favresse, Constant Gillot, Marie Didembourg, Happy Phanio Djokoto, Valérie Verbelen, Gatien Roussel, Céline Maschietto, François Mullier, Jean-Michel Dogné, and Jonathan Douxfils. Analytical sensitivity of six SARS-CoV-2 rapid antigen tests for omicron versus delta variant. Viruses, 14(44):654, Apr 2022.

[15] Meriem Bekliz, Kenneth Adea, Olha Puhach, Francisco Perez-Rodriguez, Stéfane Marques Melancia, Stephanie Baggio, Anna-Rita Corvaglia, Frederique Jacquerioz, Catia Alvarez, Manel Essaidi-Laziosi, Camille Escadafal, Laurent Kaiser, and Isabella Eckerle. Analytical sensitivity of eight different SARS-CoV-2 antigen-detecting rapid tests for omicron-BA.1 variant. Microbiology Spectrum, 10(4):e00853–22, Aug 2022.

[16] Ted Bergstrom, Carl T Bergstrom, and Haoran Li. Frequency and accuracy of proactive testing for COVID-19. MedRxiv, pages 2020–09, 2020.

[17] Daniel Bernoulli. Essai d'une nouvelle analyse de la mortalité causée par la petite vérole et des avantages de l'inoculation pour la prévenir. Mémoires de Mathématique et de Physique de l'Académie Royale des Sciences, pages 1–45, 1760. Reprinted in: Bradley, L., ed. (1971). *Smallpox Inoculation: An Eighteenth Century Mathematical Controversy*.

[18] David I Bernstein, Asuncion Mejias, Barbara Rath, Christopher W Woods, and Jamie Phillips Deeter. Summarizing study characteristics and diagnostic performance of commercially available tests for respiratory syncytial virus: A scoping literature review in the COVID-19 era. The Journal of Applied Laboratory Medicine, 8(2):353–371, 2023.

[19] Matthew T. Berry, Shanchita R. Khan, Timothy E. Schlub, Adriana Notaras, Mohana Kunasekaran, Andrew E. Grulich, C. Raina MacIntyre, Miles P. Davenport, and David S. Khoury. Predicting vaccine effectiveness for mpox. 15:3856, May 2024.

[20] Michel Bielecki, Giovanni Andrea Gerardo Crameri, Patricia Schlagenhauf, Thomas Werner Buehrer, and Jeremy Werner Deuel. Body temperature screening to identify SARS-CoV-2 infected young adult travellers is ineffective. Travel Medicine and Infectious Disease, 37, 09 2020. Copyright - ©2020. Elsevier Ltd; Last updated - 2020-10-17.

[21] Kristen K Bjorkman, Tassa K Saldi, Erika Lasda, Leisha Conners Bauer, Jennifer Kovarik, Patrick K Gonzales, Morgan R Fink, Kimngan L Tat, Cole R Hager, Jack C Davis, et al. Higher viral load drives infrequent severe acute respiratory syndrome coronavirus 2 transmission between asymptomatic residence hall roommates. The Journal of Infectious Diseases, 224(8):1316–1324, 2021.

[22] François Blanquart, Clémence Abad, Joevin Ambroise, Mathieu Bernard, Gina Cosentino, Jean-Marc Giannoli, and Florence Débarre. Spread of the delta variant, vaccine effectiveness against PCR-detected infections and within-host viral load dynamics in the community in France. July 2021. working paper or preprint.

[23] François Blanquart, Clémence Abad, Joevin Ambroise, Mathieu Bernard, Gina Cosentino, Jean-Marc Giannoli, and Florence Débarre. Spread of the delta variant, vaccine effectiveness against PCR-detected infections and within-host viral load dynamics in the community in France. HAL archives-ouvertes, 2021.

[24] Erin Bodine, Erin Deery, and Casey Middleton. The potential impact of using vaccination and insect repellent to control the spread of yellow fever. Spora: A Journal of Biomathematics, 4(1):15–24, April 2018.

[25] Toon Braeye, Laura Cornelissen, Lucy Catteau, Freek Haarhuis, Kristiaan Proesmans, Karin De Ridder, Achille Djiena, Romain Mahieu, Frances De Leeuw, Alex Dreuw, Naima Hammami, Sophie Quoilin, Herman Van Oyen, Chloé Wyndham-Thomas, and Dieter Van Cauteren. Vaccine effectiveness against infection and onwards transmission of COVID-19: Analysis of Belgian contact tracing data, January-June 2021. Vaccine, 39(39):5456–5460, Sep 2021.

[26] Cara E. Brook, Graham R. Northrup, Alexander J. Ehrenberg, Jennifer A. Doudna, and Mike Boots. Optimizing COVID-19 control with asymptomatic surveillance testing in a university environment. Epidemics, 37:100527, Dec 2021.

[27] Kate M Bubar, Casey E Middleton, Kristen K Bjorkman, Roy Parker, and Daniel B Larremore. SARS-CoV-2 transmission and impacts of unvaccinated-only screening in populations of mixed vaccination status. Nature Communications, 13(2777), 2022.

[28] Kate M Bubar, Casey E Middleton, and Daniel B Larremore. Code repository for: SARS-CoV-2 Transmission and Impacts of Unvaccinated-Only Screening in Populations of Mixed Vaccination Status. 2022. https://zenodo.org/badge/latestdoi/419096560.

[29] Kate M. Bubar, Casey E. Middleton, Daniel B. Larremore, and Katelyn M. Gostic. Fundamental limits to the effectiveness of traveler screening with molecular tests. medRxiv, page 2024.07.11.24310291, July 2024.

[30] Kate M. Bubar, Kyle Reinholt, Stephen M. Kissler, Marc Lipsitch, Sarah Cobey, Yonatan H. Grad, and Daniel B. Larremore. Model-informed COVID-19 vaccine prioritization strategies by age and serostatus. Science, 371(6532):916–921, Feb 2021.

[31] Daniel J Butler, Christopher Mozsary, Cem Meydan, David Danko, Jonathan Foox, Joel Rosiene, Alon Shaiber, Ebrahim Afshinnekoo, Matthew MacKay, Fritz J Sedlazeck, et al. Shotgun transcriptome and isothermal profiling of SARS-CoV-2 infection reveals unique host responses, viral diversification, and drug interactions. BioRxiv, 2020.

[32] Michal Canetti, Noam Barda, Yaniv Lustig, Yael Weiss-Ottolenghi, Victoria Indenbaum, Yovel Peretz, Neta Zuckerman, Keren Asraf, Sharon Amit, Yitshak Kreiss, and Gili Regev-Yochay. Risk factors and correlates of protection against XBB SARS-CoV-2 infection among health care workers. Vaccine, 42(26):126308, December 2024.

[33] Marcus Carlsson, Jens Wittsten, and Cecilia Söderberg-Nauclér. A note on variable susceptibility, the herd-immunity threshold and modeling of infectious diseases. PLOS ONE, 18(2):e0279454, 2023.

[34] Fabrice Carrat, Elisabeta Vergu, Neil M. Ferguson, Magali Lemaitre, Simon Cauchemez, Steve Leach, and Alain-Jacques Valleron. Time lines of infection and disease in human influenza: A review of volunteer challenge studies. American Journal of Epidemiology, 167(7):775–785, 01 2008.

[35] Fabrice Carrat, Elisabeta Vergu, Neil M. Ferguson, Magali Lemaitre, Simon Cauchemez, Steve Leach, and Alain-Jacques Valleron. Time lines of infection and disease in human influenza: A review of volunteer challenge studies. American Journal of Epidemiology, 167(7):775–785, Apr 2008.

[36] Bernard Cazelles, Benjamin Nguyen Van Yen, Clara Champagne, and Catherine Comiskey. Dynamics of the COVID-19 epidemic in Ireland under mitigation. BMC Infectious Diseases, 21(735), 2021.

[37] Ohio Supercomputer Center. Reed-frost epidemic model. https://www.osc.edu/education/si/projects/epidemic. Accessed: 2025-03-12.

[38] Muge Cevik, Matthew Tate, Ollie LLoyd, Alberto Enciro Maraolo, Jenna Schafers, and Antonia Ho. SARS-CoV-2, SARS-CoV, and MERS-CoV viral load dynamics, duration of viral shedding, and infectiousness: a systematic review and meta-analysis. The Lancet Microbe, 2(1), January 1 2021.

[39] Bozio CH, Grannis SJ, Naleway AL, Ong TC, Butterfield KA, DeSilva MB, Natarajan K, Yang DH, Rao S, et al. Laboratory-confirmed COVID-19 among adults hospitalized with COVID-19-like illness with infection-induced or mRNA vaccine-induced SARS-CoV-2 immunity - nine states, January-September 2021. MMWR Morb Mortal Wkly Rep., 70(44):1539–1544, 2021.

[40] Hiam Chemaitelly, Patrick Tang, Mohammad R Hasan, Sawsan AlMukdad, Hadi M Yassine, Fatiha M Benslimane, Hebah A Al Khatib, Peter Coyle, Houssein H Ayoub, Zaina Al Kanaani, et al. Waning of BNT162b2 vaccine protection against SARS-CoV-2 infection in Qatar. New England Journal of Medicine, 2021.

[41] Lauren Childs, David W Dick, Zhilan Feng, Jane M Heffernan, Jing Li, and Gergely Röst. Modeling waning and boosting of COVID-19 in Canada with vaccination. medRxiv, 2021.

[42] Melanie H. Chitwood, Ted Cohen, Kenneth Gunasekera, Joshua Havumaki, Fayette Klaassen, Nicolas A. Menzies, Virginia E. Pitzer, Marcus Russi, Joshua Salomon, Nicole Swartwood, Joshua L. Warren, and Daniel M. Weinberger. COVID estim - COVID-19 nowcasting. https://covidestim.org/. Accessed: Sept. 22, 2021.

[43] A. A. Chughtai, Q. Wang, T. C. Dung, and C. R. MacIntyre. The presence of fever in adults with influenza and other viral respiratory infections. Epidemiology and Infection, 145(1):148–155, 2017.

[44] Hsing-Yi Chung, Ming-Jr Jian, Chih-Kai Chang, Jung-Chung Lin, Kuo-Ming Yeh, Chien-Wen Chen, Sheng-Kang Chiu, Yi-Hui Wang, Shu-Jung Liao, Shih-Yi Li, et al. Novel dual multiplex real-time RT-PCR assays for the rapid detection of SARS-CoV-2, influenza A/B, and respiratory syncytial virus using the BD MAX open system. Emerging Microbes & Infections, 10(1):161–166, 2021.

[45] Anne Condon and Richard M Karp. Algorithms for graph partitioning on the planted partition model. Random Structures & Algorithms, 18(2):116–140, 2001.

[46] Laurent Coudeville, Fabrice Bailleux, Benjamin Riche, Françoise Megas, Philippe Andre, and René Ecochard. Relationship between haemagglutination-inhibiting antibody titres and clinical protection against influenza: development and application of a bayesian random-effects model. BMC Medical Research Methodology, 10(1):18, 2010.

[47] Tinglong Dai, Ronghuo Zheng, and Katia Sycara. Mask or no mask for covid-19: A public health and market study. PLOS ONE, 15(8):e0237691, 2020.

[48] Nicholas Davies, Petra Klepac, Yang Liu, Kiesha Prem, Mark Jit, and Rosalind M Eggo. Age-dependent effects in the transmission and control of COVID-19 epidemics. Nature Medicine, 26(1205-1211), 2020.

[49] Chris Davis, Nicola Logan, Grace Tyson, Richard Orton, William Harvey, John Haughney, Jon Perkins, Thomas Peacock, Wendy S Barclay, Peter Cherepanov, et al. Reduced neutralisation of the delta (B. 1.617. 2) SARS-CoV-2 variant of concern following vaccination. PLOS Pathogens, 2021.

[50] Natalie E. Dean, Joseph W. Hogan, and Mireille E. Schnitzer. Covid-19 vaccine effectiveness and the test-negative design. New England Journal of Medicine, 385(15):1431–1433, 2021.

[51] Julia Deichmann, Noam Barda, Michal Canetti, Yovel Peretz, Yael Ottolenghi, Yaniv Lustig, Gili Regev-Yochay, and Marc Lipsitch. Predicting antibody kinetics and duration of protection against SARS-CoV-2 following vaccination from sparse serological data. medRxiv, page 2025.02.10.25322008, February 2025.

[52] John DeVincenzo, Dereck Tait, John Efthimiou, Julie Mori, Young-In Kim, Elaine Thomas, Lynn Wilson, Rachel Harland, Neil Mathews, Stuart Cockerill, Kenneth Powell, and Edward Littler. A randomized, placebo-controlled, respiratory syncytial virus human challenge study of the antiviral efficacy, safety, and pharmacokinetics of RV521, an inhibitor of the RSV-F protein. Antimicrobial Agents and Chemotherapy, 64(2):e01884–19, 2020.

[53] John P. DeVincenzo, Tom Wilkinson, Akshay Vaishnaw, Jeff Cehelsky, Rachel Meyers, Saraswathy Nochur, Lisa Harrison, Patricia Meeking, Alex Mann, Elizabeth Moane, John Oxford, Rajat Pareek, Ryves Moore, Ed Walsh, Robert Studholme, Preston Dorsett, Rene Alvarez, and Robert Lambkin-Williams. Viral load drives disease in humans experimentally infected with respiratory syncytial virus. Am J Respir Crit Care Med, 182(10):1305–1314, 2010.

[54] Klaus Dietz and J. A. P. Heesterbeek. Daniel Bernoulli's epidemiological model revisited. Mathematical Biosciences, 180(1):1–21, November 2002.

[55] Hana M. Dobrovolny, Micaela B. Reddy, Mohamed A. Kamal, Craig R. Rayner, and Catherine A. A. Beauchemin. Assessing mathematical models of influenza infections using features of the immune response. PLOS ONE, 8(2):1–20, 02 2013.

[56] Amiel A. Dror, Netanel Eisenbach, Shahar Taiber, Nicole G. Morozov, Matti Mizrachi, Asaf Zigron, Samer Srouji, and Eyal Sela. Vaccine hesitancy: the next challenge in the fight against COVID-19. European Journal of Epidemiology, 35(8):775–779, Aug 2020.

[57] Jamie Ducharme. We need to start thinking differently about breakthrough infections. https://time.com/6130704/breakthrough-infections-omicron/. Accessed: Dec. 21, 2021.

[58] Andrew J. Dunning. A model for immunological correlates of protection. Statistics in Medicine, 25(9):1485–1497, May 2006.

[59] Andrew J. Dunning, Jennifer Kensler, Laurent Coudeville, and Fabrice Bailleux. Some extensions in continuous models for immunological correlates of protection. BMC Medical Research Methodology, 15(1):107, December 2015.

[60] Brown DW, Warrener L, Scobie HM, Donadel M, Waku-Kouomou D, Mulders MN, and Rota PA. rapid diagnostic tests to address challenges for global measles surveillance. Curr Opin Virol, 41:77–84, 2020.

[61] Steffen E. Eikenberry, Marina Mancuso, Enahoro Iboi, Tin Phan, Keenan Eikenberry, Yang Kuang, Eric Kostelich, and Abba B. Gumel. To mask or not to mask: Modeling the potential for face mask use by the general public to curtail the COVID-19 pandemic. Infectious Disease Modelling, 5:293–308, 2020.

[62] Hana M. El Sahly, Lindsey R. Baden, Brandon Essink, Susanne Doblecki-Lewis, Judith M. Martin, Evan J. Anderson, Thomas B. Campbell, Jesse Clark, Lisa A. Jackson, Carl J. Fichtenbaum, Marcus Zervos, Bruce Rankin, Frank Eder, Gregory Feldman, Christina Kennelly, Laurie Han-Conrad, Michael Levin, Kathleen M. Neuzil, Lawrence Corey, Peter Gilbert, Holly Janes, Dean Follmann, Mary Marovich, Laura Polakowski, John R. Mascola, Julie E. Ledgerwood, Barney S. Graham, Allison August, Heather Clouting, Weiping Deng, Shu Han, Brett Leav, Deb Manzo, Rolando Pajon, Florian Schödel, Joanne E. Tomassini, Honghong Zhou, and Jacqueline Miller. Efficacy of the mRNA-1273 SARS-CoV-2 vaccine at completion of blinded phase. New England Journal of Medicine, Sep 2021.

[63] Public Health England (PHE). SARS-CoV-2 variants of concern and variants under investigation - technical briefing 15; London: PHE; 2021. https://assets.publishing.service.gov.uk/government/uploads/system/uploads/attachment_data/file/993879/Variants_of_Concern_VOC_Technical_Briefing_15.pdf. Accessed: Aug 6, 2021.

[64] David W Eyre, Donald Taylor, Mark Purver, David Chapman, Tom Fowler, Koen B Pouwels, A Sarah Walker, and Tim EA Peto. Effect of Covid-19 vaccination on transmission of alpha and delta variants. NEJM, 386:744–756, 2022.

[65] M.D. Falsey, Ann R., R.N. Hennessey, Patricia A., M.S. Formica, Maria A., PhD. Cox, Christopher, and M.D. Walsh, Edward E. Respiratory syncytial virus infection in elderly and high-risk adults. The New England journal of medicine, 352(17):1749–59, Apr 28 2005.

[66] Sindew M Feleke, Emily N Reichert, Hussein Mohammed, Bokretsion G Brhane, Kalkidan Mekete, Hassen Mamo, Beyene Petros, Hiwot Solomon, Ebba Abate, Chris Hennelly, et al. Plasmodium falciparum is evolving to escape malaria rapid diagnostic tests in Ethiopia. Nature Microbiology, 6(10):1289–1299, 2021.

[67] Salim Ferrani, Thierry Prazuck, Stéphane Béchet, Fabien Lesne, Robert Cohen, and Corinne Levy. Diagnostic accuracy of a rapid antigen triple test (SARS-CoV-2, respiratory syncytial virus, and influenza) using anterior nasal swabs versus multiplex RT-PCR in children in an emergency department. Infectious Diseases Now, page 104769, 2023.

[68] Christophe Fraser, T. Déirdre Hollingsworth, Ruth Chapman, Frank de Wolf, and William P. Hanage. Variation in HIV-1 set-point viral load: epidemiological analysis and an evolutionary hypothesis. Proceedings of the National Academy of Sciences, 104(44):17441–17446, 2007.

[69] Christophe Fraser, Steven Riley, Roy M Anderson, and Neil M Ferguson. Factors that make an infectious disease outbreak controllable. Proceedings of the National Academy of Sciences, 101(16):6146–6151, 2004.

[70] Peter I. Frazier, J. Massey Cashore, Ning Duan, Shane G. Henderson, Alyf Janmohamed, Brian Liu, David B. Shmoys, Jiayue Wan, and Yujia Zhang. Modeling for COVID-19 college reopening decisions: Cornell, a case study. Proceedings of the National Academy of Sciences, 119(2):e2112532119, 2022.

[71] Wakaba Fukushima and Yoshio Hirota. Basic principles of test-negative design in evaluating influenza vaccine effectiveness. Vaccine, 35(36):4796–4800, 2017.

[72] Emily N. Gallichotte, Kendra M. Quicke, Nicole R. Sexton, Emily Fitzmeyer, Michael C. Young, Ashley J. Janich, Karen Dobos, Kristy L. Pabilonia, Gregory Gahm, Elizabeth J. Carlton, Gregory D. Ebel, and Nicole Ehrhart. Early adoption of longitudinal surveillance for SARS-CoV-2 among staff in long-term care facilities: Prevalence, virologic and sequence analysis. Microbiology Spectrum, 9(3):e01003–21, Nov 2021.

[73] Billy J. Gardner and A. Marm Kilpatrick. Estimates of reduced vaccine effectiveness against hospitalization, infection, transmission and symptomatic disease of a new SARS-CoV-2 variant, omicron (B.1.1.529), using neutralizing antibody titers. medRxiv, 2021.

[74] Billy J Gardner and A Marm Kilpatrick. Third doses of COVID-19 vaccines reduce infection and transmission of SARS-CoV-2 and could prevent future surges in some populations. medRxiv, 2021.

[75] Billy J. Gardner and A. Marm Kilpatrick. Validation of neutralizing antibody titers for estimating vaccine effectiveness for the omicron SARS-CoV-2 variant, BA.1. medRxiv, 2023.

[76] Billy J. Gardner and A. Marm Kilpatrick. Predicting vaccine effectiveness for hospitalization and symptomatic disease for novel SARS-CoV-2 variants using neutralizing antibody titers. Viruses, 16(33):479, March 2024.

[77] Winston Garira. A complete categorization of multiscale models of infectious disease systems. Journal of Biological Dynamics, 11(1):378–435, Jan 2017.

[78] Subhas Kumar Ghosh and Sachchit Ghosh. A mathematical model for COVID-19 considering waning immunity, vaccination and control measures. Scientific Reports, 13(1):3610, March 2023.

[79] Dishit P Ghumra, Nishit Shetty, Kevin R McBrearty, Joseph V Puthussery, Benjamin J Sumlin, Woodrow D Gardiner, Brookelyn M Doherty, Jordan P Magrecki, David L Brody, Thomas J Esparza, et al. Rapid direct detection of SARS-CoV-2 aerosols in exhaled breath at the point of care. ACS Sensors, 2023.

[80] Yair Goldberg, Micha Mandel, Yinon M Bar-On, Omri Bodenheimer, Laurence S Freedman, Eric Haas, Ron Milo, Sharon Alroy-Preis, Nachman Ash, and Amit Huppert. Waning immunity of the BNT162b2 vaccine: A nationwide study from Israel. NEJM, 2021.

[81] Ana P. Goncalvez, Cheng-Hsin Chien, Kamolchanok Tubthong, Inna Gorshkova, Carrie Roll, Olivia Donau, Peter Schuck, Sutee Yoksan, Sy-Dar Wang, Robert H. Purcell, and Ching-Juh Lai. Humanized monoclonal antibodies derived from chimpanzee fabs protect against japanese encephalitis virus in vitro and in vivo. Journal of Virology, 82(14):7009–7021, July 2008.

[82] Nicholas C Grassly, Margarita Pons-Salort, Edward PK Parker, Peter J White, Neil M Ferguson, Kylie Ainslie, Marc Baguelin, Samir Bhatt, Adhiratha Boonyasiri, Nick Brazeau, et al. Comparison of molecular testing strategies for COVID-19 control: a mathematical modelling study. The Lancet Infectious Diseases, 20(12):1381–1389, 2020.

[83] World Health Organization Writing Group. Nonpharmaceutical interventions for pandemic influenza, international measures. Emerging Infectious Diseases, 12:81–87, 2006.

[84] Brian Grunau, David M Goldfarb, Michael Asamoah-Boaheng, Liam Golding, Tracy L Kirkham, Paul A Demers, and Pascal M Lavoie. Immunogenicity of extended mRNA SARS-CoV-2 vaccine dosing intervals. JAMA.

[85] Christoforos Hadjichrysanthou, Emilie Cauët, Emma Lawrence, Carolin Vegvari, Frank de Wolf, and Roy Anderson. Understanding the within-host dynamics of influenza A virus: From theory to clinical implications. Journal of The Royal Society Interface, 13, 06 2016.

[86] Seran Hakki, Jie Zhou, Jakob Jonnerby, Anika Singanayagam, Jack L Barnett, Kieran J Madon, Aleksandra Koycheva, Christine Kelly, Hamish Houston, Sean Nevin, Joe Fenn, Rhia Kundu, Michael A Crone, Timesh D Pillay, Shazaad Ahmad, Nieves Derqui-Fernandez, Emily Conibear, Paul S Freemont, Graham P Taylor, Neil Ferguson, Maria Zambon, Wendy S Barclay, Jake Dunning, Ajit Lalvani, Anjna Badhan, Robert Varro, Constanta Luca, Valerie Quinn, Jessica Cutajar, Niamh Nichols, Jessica Russell, Holly Grey, Anjeli Ketkar, Giulia Miserocchi, Chitra Tejpal, Harriet Catchpole, Koji Nixon, Berenice Di Biase, Tamara Hopewell, Janakan Sam Narean, Jada Samuel, Kristel Timcang, Eimear McDermott, Samuel Bremang, Sarah Hammett, Samuel Evetts, and Alexandra Kondratiuk. Onset and window of SARS-CoV-2 infectiousness and temporal correlation with symptom onset: a prospective, longitudinal, community cohort study. The Lancet Respiratory Medicine, 10(11):1061–1073, Nov 2022.

[87] Victoria Jane Hall, Sarah Foulkes, Ayoub Saei, Nick Andrews, Blanche Oguti, Andre Charlett, Edgar Wellington, Julia Stowe, Natalie Gillson, Ana Atti, et al. COVID-19 vaccine coverage in health-care workers in England and effectiveness of BNT162b2 mRNA vaccine against infection (SIREN): a prospective, multicentre, cohort study. The Lancet, 397(10286):1725–1735, 2021.

[88] M. Elizabeth Halloran, Michael Haber, and Jr. Longini, Ira M. Interpretation and estimation of vaccine efficacy under heterogeneity. American Journal of Epidemiology, 136(3):328–343.

[89] Christian Holm Hansen, Astrid Blicher Schelde, Ida Rask Moustsen-Helm, Hanne-Dorthe Emborg, Tyra Grove Krause, Kare Molbak, and Palle Valentiner-Branth. Vaccine effectiveness against SARS-CoV-2 infection with the Omicron or Delta variants following a two-dose or booster BNT162b2 or mRNA-1273 vaccination series: A Danish cohort study. medRxiv, 2021.

[90] William S Hart, Elizabeth Miller, Nick J Andrew, Pauline Waight, Phillip K Maini, Sebastian Funk, et al. Generation time of the alpha and delta SARS-CoV-2 variants: an epidemiological analysis. The Lancet Infectious Diseases, 2022.

[91] Nils Haug, Lukas Geyrhofer, Alessandro Londei, Elma Dervic, Amélie Desvars-Larrive, Vittorio Loreto, Beate Pinior, Stefan Thurner, and Peter Klimek. Ranking the effectiveness of worldwide COVID-19 government interventions. Nature human behaviour, 4(12):1303–1312, 2020.

[92] Jason S Haukoos, Emily Hopkins, Amy A Conroy, Morgan Silverman, Richard L Byyny, Sheri Eisert, Mark W Thrun, Michael L Wilson, Angela B Hutchinson, Jessica Forsyth, et al. Routine opt-out rapid HIV screening and detection of HIV infection in emergency department patients. Jama, 304(3):284–292, 2010.

[93] James A Hay, Lee Kennedy-Shaffer, Sanjat Kanjilal, Niall J Lennon, Stacey B Gabriel, Marc Lipsitch, and Michael J Mina. Estimating epidemiologic dynamics from cross-sectional viral load distributions. Science, 373(6552):eabh0635, 2021.

[94] James A Hay, Stephen M Kissler, Joseph R Fauver, Christina Mack, et al. Quantifying the impact of immune history and variant on SARS-CoV-2 viral kinetics and infection rebound: A retrospective cohort study. eLife, 11:e81849, Nov 2022.

[95] F. G. Hayden, R. Fritz, M. C. Lobo, W. Alvord, W. Strober, and S. E. Straus. Local and systemic cytokine responses during experimental human influenza A virus infection. Relation to symptom formation and host defense., Feb 1998.

[96] Xi He, Eric H. Y. Lau, Peng Wu, Xilong Deng, Jian Wang, Xinxin Hao, Yiu Chung Lau, Jessica Y. Wong, Yujuan Guan, Xinghua Tan, Xiaoneng Mo, Yanqing Chen, Baolin Liao, Weilie Chen, Fengyu Hu, Qing Zhang, Mingqiu Zhong, Yanrong Wu, Lingzhai Zhao, Fuchun Zhang, Benjamin J. Cowling, Fang Li, and Gabriel M. Leung. Temporal dynamics in viral shedding and transmissibility of COVID-19. Nature, 26(5):672–675, Apr 2020.

[97] HealthDay. Feel sick? waiting at least 2 days before COVID test is best. https://www.usnews.com/news/health-news/articles/2024-06-26/feel-sick-waiting-at-least-2-days-before-covid-test-is-best. Accessed: March 17, 2025.

[98] J.m. Heffernan and M.j. Keeling. Implications of vaccination and waning immunity. Proceedings of the Royal Society B: Biological Sciences, 276(1664):2071–2080, March 2009.

[99] Joel Hellewell, Sam Abbott, Amy Gimma, Nikos I Bosse, Christopher I Jarvis, Timothy W Russell, James D Munday, Adam J Kucharski, W John Edmunds, Fiona Sun, et al. Feasibility of controlling COVID-19 outbreaks by isolation of cases and contacts. The Lancet Global Health, 8(4):e488–e496, 2020.

[100] R. I. Hickson and M. G. Roberts. How population heterogeneity in susceptibility and infectivity influences epidemic dynamics. Journal of Theoretical Biology, 350:70–80, 2014.

[101] Scobie HM, Johnson AG, Suthar AB, et al. Monitoring incidence of COVID-19 cases, hospitalizations, and deaths, by vaccination status — 13 U.S. jurisdictions, April 4–July 17, 2021. MMWR Morb Mortal Wkly Rep, 70(1):284–1290, 2021.

[102] Alexandra B. Hogan, Patrick Doohan, Sean L. Wu, Daniela Olivera Mesa, Jaspreet Toor, Oliver J. Watson, Peter Winskill, Giovanni Charles, Gregory Barnsley, Eleanor M. Riley, David S. Khoury, Neil M. Ferguson, and Azra C. Ghani. Estimating long-term vaccine effectiveness against SARS-CoV-2 variants: a model-based approach. Nature Communications, 14(1):4325, July 2023.

[103] Inga Holmdahl, Rebecca Kahn, James A Hay, Caroline O Buckee, and Michael J Mina. Estimation of transmission of COVID-19 in simulated nursing homes with frequent testing and immunity-based staffing. JAMA Network Open, 4(5):e2110071–e2110071, 2021.

[104] David Holtz, Michael Zhao, Seth G Benzell, Cathy Y Cao, Mohammad Amin Rahimian, Jeremy Yang, Jennifer Allen, Avinash Collis, Alex Moehring, Tara Sowrirajan, et al. Interdependence and the cost of uncoordinated responses to COVID-19. Proceedings of the National Academy of Sciences, 117(33):19837–19843, 2020.

[105] Jason Horowitz. Italy puts in force tough new law requiring workers to test or vaccinate. The New York Times. Accessed: Oct. 15, 2021.

[106] Timothy S. Howard, Lynn H. Hoffman, Paul E. Stang, and Eric A.F. Simoes. Respiratory syncytial virus pneumonia in the hospital setting: Length of stay, charges, and mortality. The Journal of Pediatrics, 137(2):227–232, 2000.

[107] James M Hyman, Jia Li, and E Ann Stanley. Modeling the impact of random screening and contact tracing in reducing the spread of HIV. Mathematical biosciences, 181(1):17–54, 2003.

[108] Dennis K. M. Ip, Lincoln L. H. Lau, Kwok-Hung Chan, Vicky J. Fang, Gabriel M. Leung, Malik J. S. Peiris, and Benjamin J. Cowling. The dynamic relationship between clinical symptomatology and viral shedding in naturally acquired seasonal and pandemic influenza virus infections. Clinical Infectious Diseases, 62(4):431–437, Feb 2016.

[109] Michael L. Jackson and Jennifer C. Nelson. The test-negative design for estimating influenza vaccine effectiveness. Vaccine, 31(17):2165–2168, April 2013.

[110] Michael A. Johansson, Talia M. Quandelacy, Sarah Kada, Pragati Venkata Prasad, Molly Steele, John T. Brooks, Rachel B. Slayton, Matthew Biggerstaff, and Jay C. Butler. SARS-CoV-2 transmission from people without COVID-19 symptoms. JAMA Network Open, 4(1):e2035057, Jan 2021.

[111] Erik K. Johnson, Rebecca Kahn, Yonatan H. Grad, Marc Lipsitch, and Daniel B. Larremore. Test negative designs with uncertainty, sensitivity, and specificity. medRxiv, page 2021.06.24.21259495, June 2021.

[112] Kaitlyn E. Johnson, Remy Pasco, Spencer Woody, Michael Lachmann, Maureen Johnson-Leon, Darlene Bhavnani, Jessica Klima, A. David Paltiel, Spencer J. Fox, and Lauren Ancel Meyers. Optimizing covid-19 testing strategies on college campuses: Evaluation of the health and economic costs. PLOS Computational Biology, 19(12):e1011715, December 2023.

[113] Terry C. Jones, Guido Biele, Barbara Mühlemann, Talitha Veith, Julia Schneider, Jörn Beheim-Schwarzbach, Tobias Bleicker, Julia Tesch, Marie Luisa Schmidt, Leif Erik Sander, Florian Kurth, Peter Menzel, Rolf Schwarzer, Marta Zuchowski, Jörg Hofmann, Andi Krumbholz, Angela Stein, Anke Edelmann, Victor Max Corman, and Christian Drosten. Estimating infectiousness throughout SARS-CoV-2 infection course. Science, 373(6551), Jul 2021.

[114] Min Kang, Hualei Xin, Jun Yuan, Sheikh Taslim Ali, Zimian Liang, Jiayi Zhang, Ting Hu, Eric H. Y. Lau, Yingtao Zhang, Meng Zhang, Benjamin J. Cowling, Yan Li, and Peng Wu. Transmission dynamics and epidemiological characteristics of delta variant infections in China. medRxiv, page 2021.08.12.21261991, Aug 2021.

[115] Ruian Ke, Pamela P. Martinez, Rebecca L. Smith, Laura L. Gibson, Chad J. Achenbach, Sally McFall, Chao Qi, Joshua Jacob, Etienne Dembele, Camille Bundy, Lacy M. Simons, Egon A. Ozer, Judd F. Hultquist, Ramon Lorenzo-Redondo, Anita K. Opdycke, Claudia Hawkins, Robert L. Murphy, Agha Mirza, Madison Conte, Nicholas Gallagher, Chun Huai Luo, Junko Jarrett, Abigail Conte, Ruifeng Zhou, Mireille Farjo, Gloria Rendon, Christopher J. Fields, Leyi Wang, Richard Fredrickson, Melinda E. Baughman, Karen K. Chiu, Hannah Choi, Kevin R. Scardina, Alyssa N. Owens, John Broach, Bruce Barton, Peter Lazar, Matthew L. Robinson, Heba H. Mostafa, Yukari C. Manabe, Andrew Pekosz, David D. McManus, and Christopher B. Brooke. Longitudinal analysis of SARS-CoV-2 vaccine breakthrough infections reveal limited infectious virus shedding and restricted tissue distribution. Open Forum Infectious Diseases, Apr 2022.

[116] Ruian Ke, Pamela P Martinez, Rebecca L Smith, Laura L Gibson, Agha Mirza, Madison Conte, Nicholas Gallagher, Chun Huai Luo, Junko Jarrett, Ruifeng Zhou, et al. Daily longitudinal sampling of SARS-CoV-2 infection reveals substantial heterogeneity in infectiousness. Nature Microbiology, 7(5):640–652, 2022.

[117] Ruian Ke, Carolin Zitzmann, David D. Ho, Ruy M. Ribeiro, and Alan S. Perelson. In vivo kinetics of SARS-CoV-2 infection and its relationship with a person's infectiousness. Proceedings of the National Academy of Sciences, 118(49):e2111477118, Dec 2021.

[118] William Ogilvy Kermack and Anderson G McKendrick. A contribution to the mathematical theory of epidemics. Proceedings of the Royal Society of London. Series A, Containing Papers of a Mathematical and Physical Character, 115(772):700–721, 1927.

[119] David S. Khoury, Deborah Cromer, Arnold Reynaldi, Timothy E. Schlub, Adam K. Wheatley, Jennifer A. Juno, Kanta Subbarao, Stephen J. Kent, James A. Triccas, and Miles P. Davenport. Neutralizing antibody levels are highly predictive of immune protection from symptomatic SARS-CoV-2 infection. Nature Medicine, 27(7):1205–1211, July 2021.

[120] David S. Khoury, Timothy E. Schlub, Deborah Cromer, Megan Steain, Youyi Fong, Peter B. Gilbert, Kanta Subbarao, James A. Triccas, Stephen J. Kent, , and Miles P. Davenport. Correlates of protection, thresholds of protection, and immunobridging among persons with SARS-CoV-2 infection. Emerging Infectious Diseases journal - CDC, 29(2), 2023.

[121] Ben Killingley, Alex J Mann, Mariya Kalinova, Alison Boyers, Niluka Goonawardane, Jie Zhou, Kate Lindsell, Samanjit S Hare, Jonathan Brown, Rebecca Frise, et al. Safety, tolerability and viral kinetics during SARS-CoV-2 human challenge in young adults. Nature Medicine, 28(5):1031–1041, 2022.

[122] Natalie N Kinloch, Gordon Ritchie, Chanson J Brumme, Winnie Dong, Weiyan Dong, Tanya Lawson, R Brad Jones, Julio S G Montaner, Victor Leung, Marc G Romney, Aleksandra Stefanovic, Nancy Matic, Christopher F Lowe, and Zabrina L Brumme. Suboptimal biological sampling as a probable cause of false-negative COVID-19 diagnostic test results. The Journal of Infectious Diseases, 222(6):899–902, 06 2020.

[123] Eva Kisdi. Optimal vaccination strategies for imperfect vaccines and variable host susceptibility. Journal of Theoretical Biology, 594:111899, 2024.

[124] Stephen M. Kissler, Joseph R. Fauver, Christina Mack, Scott W. Olesen, Caroline Tai, Kristin Y. Shiue, Chaney C. Kalinich, Sarah Jednak, Isabel M. Ott, Chantal B. F. Vogels, Jay Wohlgemuth, James Weisberger, John DiFiori, Deverick J. Anderson, Jimmie Mancell, David D. Ho, Nathan D. Grubaugh, and Yonatan H. Grad. Viral dynamics of acute SARS-CoV-2 infection and applications to diagnostic and public health strategies. PLOS Biology, 19(7):1–17, 07 2021.

[125] Stephen M. Kissler, Joseph R. Fauver, Christina Mack, Caroline G. Tai, Mallery I. Breban, Anne E. Watkins, Radhika M. Samant, Deverick J. Anderson, Jessica Metti, Gaurav Khullar, Rachel Baits, Matthew MacKay, Daisy Salgado, Tim Baker, Joel T. Dudley, Christopher E. Mason, David D. Ho, Nathan D. Grubaugh, and Yonatan H. Grad. Viral dynamics of SARS-CoV-2 variants in vaccinated and unvaccinated persons. NEJM, 2021.

[126] Stephen M Kissler, Nishant Kishore, Malavika Prabhu, Dena Goffman, Yaakov Beilin, Ruth Landau, Cynthia Gyamfi-Bannerman, Brian T Bateman, Jon Snyder, Armin S Razavi, et al. Reductions in commuting mobility correlate with geographic differences in SARS-CoV-2 prevalence in New York City. Nature Communications, 11(1):4674, 2020.

[127] Pinelopi Konstantinou, Katerina Georgiou, Navin Kumar, Maria Kyprianidou, Christos Nicolaides, Maria Karekla, and Angelos P Kassianos. Transmission of vaccination attitudes and uptake based on social contagion theory: A scoping review. Vaccines, 9(6):607, 2021.

[128] Tanya Kostova. Persistence of viral infections on the population level explained by an immunoepidemiological model. Mathematical Biosciences, 206(2):309–319, Apr 2007.

[129] Adam J Kucharski, Petra Klepac, Andrew JK Conlan, Stephen M Kissler, Maria L Tang, Hannah Fry, Julia R Gog, W John Edmunds, Jon C Emery, Graham Medley, et al. Effectiveness of isolation, testing, contact tracing, and physical distancing on reducing transmission of SARS-CoV-2 in different settings: a mathematical modelling study. The Lancet Infectious Diseases, 20(10):1151–1160, 2020.

[130] Lauren M. Kucirka, Stephen A. Lauer, Oliver Laeyendecker, Denali Boon, and Justin Lessler. Variation in false-negative rate of reverse transcriptase polymerase chain reaction–based SARS-CoV-2 tests by time since exposure. Annals of Internal Medicine, 173(4):262–267, 2020. PMID: 32422057.

[131] Bernard La Scola, Marion Le Bideau, Julien Andreani, Clio Grimaldier, Philippe Colson, Philippe Gautret, Didier Raoult, et al. Viral RNA load as determined by cell culture as a management tool for discharge of SARS-CoV-2 patients from infectious disease wards. European Journal of Clinical Microbiology & Infectious Diseases, 39(6):1059–1061, 2020.

[132] Suzanne E Landis, Victor J Schoenbach, David J Weber, Manjoo Mittal, Baldev Krishan, Karen Lewis, and Gary G Koch. Results of a randomized trial of partner notification in cases of HIV infection in North Carolina. New england Journal of medicine, 326(2):101–106, 1992.

[133] Daniel Larremore, Derek Toomre, and Roy Parker. Modeling the effectiveness of olfactory testing to limit SARS-CoV-2 transmission. Nature Communications, 12(1), June 16 2021.

[134] Daniel B Larremore, Kate M Bubar, and Yonatan H Grad. Implications of test characteristics and population seroprevalence on "immune passport" strategies. Clinical Infectious Diseases, 72(9):e412–e414, 2021.

[135] Daniel B. Larremore, Derek Toomre, and Roy Parker. Modeling the effectiveness of olfactory testing to limit SARS-CoV-2 transmission. Nature Communications 2021 12:1, 12(1):1–9, Jun 2021.

[136] Daniel B. Larremore, Bryan Wilder, Evan Lester, Soraya Shehata, James M. Burke, James A. Hay, Milind Tambe, Michael J. Mina, and Roy Parker. Test sensitivity is secondary to frequency and turnaround time for COVID-19 screening. Science Advances, 7(1), January 1 2021.

[137] Sophie L. Larsen, Junke Yang, Huibin Lv, Yang Wei Huan, Qiwen Teo, Tossapol Pholcharee, Ruipeng Lei, Akshita B Gopal, Evan K. Shao, Logan Talmage, Chris K. P. Mok, Saki Takahashi, Alicia N. M. Kraay, Nicholas C. Wu, and Pamela P. Martinez. Reimagining the serocatalytic model for infectious diseases: a case study of common coronaviruses. medRxiv, 2024.

[138] Lincoln L. H. Lau, Benjamin J. Cowling, Vicky J. Fang, Kwok-Hung Chan, Eric H. Y. Lau, Marc Lipsitch, Calvin K. Y. Cheng, Peter M. Houck, Timothy M. Uyeki, J. S. Malik Peiris, and Gabriel M. Leung. Viral shedding and clinical illness in naturally acquired influenza virus infections. The Journal of Infectious Diseases, 201(10):1509–1516, 05 2010.

[139] Shelah Leader and Kimmie Kohlhase. Recent trends in severe respiratory syncytial virus (rsv) among US infants, 1997 to 2000. The Journal of Pediatrics, 143(5, Supplement):127–132, 2003.

[140] Chun K. Lee, Hong K. Lee, Tze P. Loh, Florence Y. L. Lai, Paul A. Tambyah, Lily Chiu, Evelyn S. C. Koay, and Julian W. Tang. Comparison of pandemic (H1N1) 2009 and seasonal influenza viral loads, Singapore. Emerging Infectious Diseases, 17(2):287–291, 2011.

[141] F. Eun-Hyung Lee, Edward E. Walsh, Ann R. Falsey, Robert F. Betts, and John J. Treanor. Experimental infection of humans with A2 respiratory syncytial virus. Antiviral Research, 63(3):191–196, Sep 2004.

[142] Einav G. Levin, Yaniv Lustig, Carmit Cohen, Ronen Fluss, Victoria Indenbaum, Sharon Amit, Ram Doolman, Keren Asraf, Ella Mendelson, Arnona Ziv, Carmit Rubin, Laurence Freedman, Yitshak Kreiss, and Gili Regev-Yochay. Waning immune humoral response to BNT162b2 Covid-19 vaccine over 6 months. New England Journal of Medicine, 385(24):e84, December 2021.

[143] Joseph A. Lewnard, Vennis X. Hong, Manish M. Patel, Rebecca Kahn, Marc Lipsitch, and Sara Y. Tartof. Clinical outcomes among patients infected with omicron (b.1.1.529) SARS-CoV-2 variant in southern California. medRxiv, 2022.

[144] Joseph A Lewnard, Christine Tedijanto, Benjamin J Cowling, and Marc Lipsitch. Measurement of vaccine direct effects under the test-negative design. American Journal of Epidemiology, 187(12):2686–2697, December 2018.

[145] You Li, Xin Wang, Dianna M Blau, Mauricio T Caballero, Daniel R Feikin, Christopher J Gill, Shabir A Madhi, Saad B Omer, Eric AF Simões, Harry Campbell, et al. Global, regional, and national disease burden estimates of acute lower respiratory infections due to respiratory syncytial virus in children younger than 5 years in 2019: a systematic analysis. The Lancet, 399(10340):2047–2064, 2022.

[146] Baisheng Li1, Aiping Deng1, Kuibiao Li, Yao Hu1, Zhencui Lil, Qianling Xiong, Zhe Liu, Qianfang Guo, Lirong Zou, Huan Zhang, Meng Zhang, Fangzhu Ouyang, Juan Su, Wenzhe Su, Jing Xu, Huifang Lin1, Jing Sun, Jinju Peng, Huiming Jiang, Pingping Zhou, Ting Hu, Min Luo, Yingtao Zhang, Huanying Zheng, Jianpeng Xiao, Tao Liu1, Rongfei Che, Hanri Zeng, Zhonghua Zheng, Yushi, Jianxiang Yu, Lina Yi, Jie Wu, Jingdiao Chen, Haojie Zhong, Xiaoling Deng, Min Kang, Oliver G. Pybus, Matthew Hall, Katrina A. Lythgoe, Yan Li1, Jun Yuan, Jianfeng He1, and Jing Lu. Viral infection and transmission in a large, well-traced outbreak caused by the SARS-CoV-2 delta variant. medRxiv, 2021.

[147] Tracy A Lieu, G Thomas Ray, Nicola P Klein, Cindy Chung, and Martin Kulldorff. Geographic clusters in underimmunization and vaccine refusal. Pediatrics, 135(2):280–289, 2015.

[148] Can Liu, Jiawei Zhang, Yongbin Zeng, Chun Huang, Falin Chen, Yingping Cao, Siying Wu, Donghong Wei, Zhong Lin, Yali Zhang, Ling Zhang, Jing Teng, Zishun Li, Guolin Hong, Tianci Yang, Huiming Ye, Haijian Tu, Yupeng Xiao, Lishan Huang, Caorui Lin, Tianbin Chen, Yanqin Deng, Qishui Ou, and Jinming Li. Effectiveness of SARS-CoV-2-inactivated vaccine and the correlation to neutralizing antibodies: A test-negative case–control study. Journal of Medical Virology, 95(1):e28280, 2023.

[149] James O Lloyd-Smith, Sebastian J Schreiber, P Ekkehard Kopp, and Wayne M Getz. Superspreading and the effect of individual variation on disease emergence. Nature, 438(7066):355–359, 2005.

[150] Jamie Lopez Bernal, Nick Andrews, Charlotte Gower, Eileen Gallagher, Ruth Simmons, Simon Thelwall, Julia Stowe, Elise Tessier, Natalie Groves, Gavin Dabrera, et al. Effectiveness of COVID-19 vaccines against the B. 1.617. 2 (delta) variant. New England Journal of Medicine, pages 585–594, 2021.

[151] George Macdonald. The Epidemiology and Control of Malaria. Oxford University Press, London, 1957.

[152] Maia Martcheva, Necibe Tuncer, and Colette St Mary. Coupling within-host and between-host infectious diseases models. BIOMATH, 4(22):ID: 1510091–ID: 1510091, Oct 2015.

[153] John R Mascola. Passive transfer studies to elucidate the role of antibody-mediated protection against HIV-1. Vaccine, 20(15):1922–1925, May 2002.

[154] Laura Matrajt, Julia Eaton, Tiffany Leung, and Elizabeth R Brown. Vaccine optimization for COVID-19: Who to vaccinate first? Science Advances, 7(6):eabf1374, 2021.

[155] Brian E McGarry, Ashvin D Gandhi, and Michael L Barnett. COVID-19 surveillance testing and resident outcomes in nursing homes. New England Journal of Medicine, 388(12):1101–1110, 2023.

[156] Ryan S. McGee, Julian R. Homburger, Hannah E. Williams, Carl T. Bergstrom, and Alicia Y. Zhou. Proactive COVID-19 testing in a partially vaccinated population. medRxiv, 2021.

[157] Jan Medlock and Alison P Galvani. Optimizing influenza vaccine distribution. Science, 325(5948):1705–1708, 2009.

[158] Tigist F Menkir and Christl A Donnelly. The impact of repeated rapid test strategies on the effectiveness of at-home antiviral treatments for SARS-CoV-2. Nature Communications, 13(1):5283, 2022.

[159] Joanna Merckx, Rehab Wali, Ian Schiller, Chelsea Caya, Genevieve C Gore, Caroline Chartrand, Nandini Dendukuri, and Jesse Papenburg. Diagnostic accuracy of novel and traditional rapid tests for influenza infection compared with reverse transcriptase polymerase chain reaction: a systematic review and meta-analysis. Annals of Internal Medicine, 167(6):394–409, 2017.

[160] Nicholas R Meyerson, Qing Yang, Stephen K Clark, Camille L Paige, Will T Fattor, Alison R Gilchrist, Arturo Barbachano-Guerrero, and Sara L Sawyer. A community-deployable SARS-CoV-2 screening test using raw saliva with 45 minutes sample-to-results turnaround. MedRxiv, 2020.

[161] Joel C. Miller. Epidemic size and probability in populations with heterogeneous infectivity and susceptibility. Physical Review E, 76(1):010101, 2007.

[162] Michael J Mina, Roy Parker, and Daniel B Larremore. Rethinking COVID-19 test sensitivity—a strategy for containment. New England Journal of Medicine, 383(22):e120, 2020.

[163] Sho Miyamoto, Takeshi Arashiro, Yu Adachi, Saya Moriyama, Hitomi Kinoshita, Takayuki Kanno, Shinji Saito, Harutaka Katano, Shun Iida, Akira Ainai, Ryutaro Kotaki, Souichi Yamada, Yudai Kuroda, Tsukasa Yamamoto, Keita Ishijima, Eun-Sil Park, Yusuke Inoue, Yoshihiro Kaku, Minoru Tobiume, Naoko Iwata-Yoshikawa, Nozomi Shiwa-Sudo, Kenzo Tokunaga, Seiya Ozono, Takuya Hemmi, Akira Ueno, Noriko Kishida, Shinji Watanabe, Kiyoko Nojima, Yohei Seki, Takuo Mizukami, Hideki Hasegawa, Hideki Ebihara, Ken Maeda, Shuetsu Fukushi, Yoshimasa Takahashi, and Tadaki Suzuki. Vaccination-infection interval determines cross-neutralization potency to SARS-CoV-2 omicron after breakthrough infection by other variants. medRxiv, 2022.

[164] Petra Mlcochova, Steven Kemp, Mahesh Shanker Dhar, et al. SARS-CoV-2 B.1.617.2 Delta variant emergence and vaccine breakthrough. Research Square, 22 June 2021.

[165] Seyed M. Moghadas, Meagan C. Fitzpatrick, Pratha Sah, Abhishek Pandey, Affan Shoukat, Burton H. Singer, and Alison P. Galvani. The implications of silent transmission for the control of COVID-19 outbreaks. Proceedings of the National Academy of Sciences, 117(30):17513–17515, Jul 2020.

[166] Antonio Montalbán, Rodrigo M. Corder, and M. Gabriela M. Gomes. Herd immunity under individual variation and reinfection. Journal of Mathematical Biology, 85(2), 2022.

[167] Arnold S. Monto, Joshua G. Petrie, Rachel T. Cross, Emileigh Johnson, Merry Liu, Weimin Zhong, Min Levine, Jacqueline M. Katz, and Suzanne E. Ohmit. Antibody to influenza virus neuraminidase: An independent correlate of protection. The Journal of Infectious Diseases, 212(8):1191–1199, October 2015.

[168] SG Moon, YK Kim, WS Son, JH Kim, J Choi, BJ Na, B Park, and BY Choi. Time-variant reproductive number of COVID-19 in Seoul, Korea. Epidemiol Health, 42, 2020.

[169] Sam Moore, Edward M. Hill, Louise Dyson, Michael J. Tildesley, and Matt J. Keeling. Modelling optimal vaccination strategy for SARS-CoV-2 in the UK. PLOS Computational Biology, 17(5):e1008849, May 2021.

[170] Joël Mossong, Niel Hens, Mark Jit, Philippe Beutels, Kari Auranen, Rafael Mikolajczyk, Marco Massari, Stefania Salmaso, Gianpaolo Scalia Tomba, Jacco Wallinga, Janneke Heijne, Malgorzata Sadkowska-Todys, Magdalena Rosinska, and W. John Edmunds. Social contacts and mixing patterns relevant to the spread of infectious diseases. PLOS Medicine, 5(3):e74, March 2008.

[171] Alexander Muik, Bonny Gaby Lui, Jasmin Quandt, Huitian Diao, Yunguan Fu, Maren Bacher, Jessica Gordon, Aras Toker, Jessica Grosser, Orkun Ozhelvaci, Katharina Grikscheit, Sebastian Hoehl, Niko Kohmer, Yaniv Lustig, Gili Regev-Yochay, Sandra Ciesek, Karim Beguir, Asaf Poran, Isabel Vogler, Özlem Türeci, and Ugur Sahin. Progressive loss of conserved spike protein neutralizing antibody sites in omicron sublineages is balanced by preserved T cell immunity. Cell Reports, 42(8), August 2023.

[172] Ernie Mundell. Feel sick? waiting at least 2 days before COVID test is best. https://www.healthday.com/health-news/infectious-disease/feel-sick-waiting-at-least-2-days-before-covid-test-is-best. Accessed: March 17, 2025.

[173] Patrick K. Munywoki, Dorothy C. Koech, Charles N. Agoti, Ann Bett, Patricia A. Cane, Graham F. Medley, and D. James Nokes. Frequent asymptomatic respiratory syncytial virus infections during an epidemic in a rural Kenyan household cohort. The Journal of Infectious Diseases, 212(11):1711–1718, Dec 2015.

[174] James M. Musser, Paul A. Christensen, Randall J. Olsen, S. Wesley Long, Sishir Subedi, James J. Davis, Parsa Hodjat, Debbie R. Walley, Jacob C. Kinskey, and Jimmy Gollihar. Delta variants of SARS-CoV-2 cause significantly increased vaccine breakthrough COVID-19 cases in Houston, Texas. medRxiv, 2021.

[175] Srinivas Nanduri, Tamara Pilishvili, Gordana Derado, Minn Minn Soe, Philip Dollard, Hsiu Wu, Qunna Li, Suparna Bagchi, Heather Dubendris, Ruth Link-Gelles, et al. Effectiveness of Pfizer-BioNTech and Moderna vaccines in preventing SARS-CoV-2 infection among nursing home residents before and during widespread circulation of the SARS-CoV-2 B. 1.617. 2 (delta) variant—national healthcare safety network, March 1–August 1, 2021. Morbidity and Mortality Weekly Report, 70(34):1163, 2021.

[176] Ital Nemet, Limor Kliker, Yaniv Lustig, Neta Zuckerman, Oran Erster, Carmit Cohen, Yitshak Kreiss, Sharon Alroy-Preis, Gili Regev-Yochay, Ella Mendelson, and Michal Mandelboim. Third BNT162b2 vaccination neutralization of SARS-CoV-2 omicron infection. New England Journal of Medicine, 386(5):492–494, February 2022.

[177] Stephen C. Newbold, Madison Ashworth, David Finnoff, Jason F. Shogren, and Linda Thunström. Physical distancing versus testing with self-isolation for controlling an emerging epidemic. Scientific Reports, 13(11):8185, May 2023.

[178] Sophia Ng, Roger Lopez, Guillermina Kuan, Lionel Gresh, Angel Balmaseda, Eva Harris, and Aubree Gordon. The timeline of influenza virus shedding in children and adults in a household transmission study of influenza in Managua, Nicaragua. The Pediatric infectious disease journal, 35(5):583–586, May 2016.

[179] Eric J. Nilles, Cecilia Then Paulino, Michael de St Aubin, William Duke, Petr Jarolim, Isaac Miguel Sanchez, Kristy O Murray, Colleen L Lau, Emily Zielinski Gutiérrez, Ronald Skewes Ramm, Marietta Vasquez, and Adam Kucharski. Tracking immune correlates of protection for emerging SARS-CoV-2 variants. Lancet Infectious Diseases, 2023.

[180] Martin A. Nowak and Robert M. May. Mathematical biology of HIV infections: Antigenic variation and diversity threshold. Mathematical Biosciences, 106(1):1–21, 1991.

[181] Nadège Néant, Guillaume Lingas, Quentin Le Hingrat, Jade Ghosn, Ilka Engelmann, Quentin Lepiller, Alexandre Gaymard, Virginie Ferré, Cédric Hartard, Jean-Christophe Plantier, Vincent Thibault, Julien Marlet, Brigitte Montes, Kevin Bouiller, François-Xavier Lescure, Jean-François Timsit, Emmanuel Faure, Julien Poissy, Christian Chidiac, François Raffi, Antoine Kimmoun, Manuel Etienne, Jean-Christophe Richard, Pierre Tattevin, Denis Garot, Vincent Le Moing, Delphine Bachelet, Coralie Tardivon, Xavier Duval, Yazdan Yazdanpanah, France Mentré, Cédric Laouénan, Benoit Visseaux, Jérémie Guedj, French COVID Cohort Investigators, and French Cohort Study groups. Modeling SARS-CoV-2 viral kinetics and association with mortality in hospitalized patients from the French COVID cohort. Proceedings of the National Academy of Sciences of the United States of America, 118(8):e2017962118, Feb 2021.

[182] Sean Wei Xiang Ong, Calvin J. Chiew, Li Wei Ang, Tze-Minn Mak, Lin Cui, Matthias Paul HS Toh, Yi Ding Lim, Pei Hua Lee, Tau Hong Lee, Po Ying Chia, Sebastian Maurer-Stroh, Raymond Tzer Pin Lin, Yee-Sin Leo, Vernon J. Lee, David Chien Lye, and Barnaby E. Young. Clinical and virological features of SARS-CoV-2 variants of concern: A retrospective cohort study comparing B.1.1.7 (alpha), B.1.315 (beta), and B.1.617.2 (delta). 2021. preprint.

[183] World Health Organization. WHO coronavirus (COVID-19) dashboard. https://covid19.who.int/, 2020. Accessed: Dec. 31, 2020.

[184] A David Paltiel, Kenneth A Freedberg, Callie A Scott, Bruce R Schackman, Elena Losina, Bingxia Wang, George R Seage, Caroline E Sloan, Paul E Sax, and Rochelle P Walensky. HIV preexposure prophylaxis in the United States: impact on lifetime infection risk, clinical outcomes, and cost-effectiveness. Clinical Infectious Diseases, 48(6):806–815, 2009.

[185] A David Paltiel, Amy Zheng, and Rochelle P Walensky. Assessment of SARS-CoV-2 screening strategies to permit the safe reopening of college campuses in the United States. JAMA Network Open, 3(7):e2016818–e2016818, 2020.

[186] Martin Pavelka, Kevin Van-Zandvoort, Sam Abbott, Katharine Sherratt, Marek Majdan, CMMID COVID-19 working group, Inštitút Zdravotných Analýz, Pavol Jarčuška, Marek Krajčí, Stefan Flasche, and Sebastian Funk. The impact of population-wide rapid antigen testing on SARS-CoV-2 prevalence in Slovakia. Science, 372(6542):635–641, 2021.

[187] Joseph Sriyal Malik Peiris, Chung-Ming Chu, Vincent Chi-Chung Cheng, KS Chan, IFN Hung, Leo LM Poon, Kin-Ip Law, BSF Tang, TYW Hon, CS Chan, et al. Clinical progression and viral load in a community outbreak of coronavirus-associated SARS pneumonia: a prospective study. The Lancet, 361(9371):1767–1772, 2003.

[188] Andrew Pekosz, Valentin Parvu, Maggie Li, Jeffrey C Andrews, Yukari C Manabe, Salma Kodsi, Devin S Gary, Celine Roger-Dalbert, Jeffry Leitch, and Charles K Cooper. Antigen-based testing but not real-time polymerase chain reaction correlates with severe acute respiratory syndrome coronavirus 2 viral culture. Clinical Infectious Diseases, 73(9):e2861–e2866, Nov 2021.

[189] Alan S. Perelson, Andrew U. Neumann, Martin Markowitz, John M. Leonard, and David D. Ho. Hiv-1 dynamics in vivo: Virion clearance rate, infected cell life-span, and viral generation time. Science, 271(5255):1582–1586, 1996.

[190] Rowland W Pettit, Bo Peng, Patrick Yu, Peter Matos, Alexander L Greninger, Julie McCashin, and Christopher Ian Amos. Optimized post-vaccination strategies and preventative measures for SARS-CoV-2. medRxiv, 2021.

[191] David K Plate and Rapid HIV Test Evaluation Working Group. Evaluation and implementation of rapid HIV tests: the experience in 11 African countries. AIDS research and human retroviruses, 23(12):1491–1498, 2007.

[192] Kiesha Prem, Kevin van Zandvoort, Petra Klepac, Rosalind M. Eggo, Nicholas G. Davies, Centre for the Mathematical Modelling of Infectious Diseases COVID-19 Working Group, Alex R. Cook, and Mark Jit. Projecting contact matrices in 177 geographical regions: An update and comparison with empirical data for the COVID-19 era. PLOS Computational Biology, 17(7):e1009098, July 2021.

[193] Caitlin Prendergast and Jesse Papenburg. Rapid antigen-based testing for respiratory syncytial virus: moving diagnostics from bench to bedside? Future Microbiology, 8(4):435–44, 04 2013.

[194] Carel Pretorius, John Stover, Lori Bollinger, Nicolas Bacaër, and Brian Williams. Evaluating the cost-effectiveness of pre-exposure prophylaxis (PrEP) and its impact on HIV-1 transmission in South Africa. PLOS ONE, 5(11):e13646, Nov 2010.

[195] Li Qin, Peter B. Gilbert, Lawrence Corey, M. Juliana McElrath, and Steven G. Self. A framework for assessing immunological correlates of protection in vaccine trials. The Journal of Infectious Diseases, 196(9):1304–1312, November 2007.

[196] Kendra Quicke, Emily Gallichotte, Nicole Sexton, Michael Young, Ashley Janich, Gregory Gahm, Elizabeth J Carlton, Nicole Ehrhart, and Gregory D Ebel. Longitudinal surveillance for SARS-CoV-2 RNA among asymptomatic staff in five colorado skilled nursing facilities: epidemiologic, virologic and sequence analysis. MedRxiv, 2020.

[197] Quidel. QuickVue RSV10 rapid antigen test product specification. https://www.quidel.com/sites/default/files/product/documents/EF1179501EN01.pdf. Accessed: February 2, 2022.

[198] Romain Ragonnet, James M. Trauer, Justin T. Denholm, Nicholas L. Geard, Margaret Hellard, and Emma S. McBryde. Vaccination programs for endemic infections: Modelling real versus apparent impacts of vaccine and infection characteristics. Scientific Reports, 5(1):15468, October 2015.

[199] Diana Rose E Ranoa, Robin L Holland, Fadi G Alnaji, Kelsie J Green, Leyi Wang, Richard L Fredrickson, Tong Wang, George N Wong, Johnny Uelmen, Sergei Maslov, et al. Mitigation of SARS-CoV-2 transmission at a large public university. medRxiv, 2021.

[200] Diana Rose E Ranoa, Robin L Holland, Fadi G Alnaji, Kelsie J Green, Leyi Wang, Richard L Fredrickson, Tong Wang, George N Wong, Johnny Uelmen, Sergei Maslov, et al. Mitigation of SARS-CoV-2 transmission at a large public university. Nature Communications, 13(1):3207, 2022.

[201] Diana Rose E. Ranoa, Robin L. Holland, et al. Mitigation of SARS-CoV-2 transmission at a large public university. medRxiv, 2021.

[202] Hannah Ritchie, Edouard Mathieu, Lucas Rodés-Guirao, Cameron Appel, Charlie Giattino, Esteban Ortiz-Ospina, Joe Hasell, Bobbie Macdonald, Diana Beltekian, and Max Roser. Coronavirus pandemic (COVID-19). https://ourworldindata.org/coronavirus.

[203] Alexis Robert, Anne M. Suffel, and Adam J. Kucharski. Long-term waning of vaccine-induced immunity to measles in England. medRxiv, page 2024.04.18.24306028, April 2024.

[204] Katie Rogers and Sheryl Gay Stolberg. Biden mandates vaccines for workers, saying, 'Our patience is wearing thin'. https://www.nytimes.com/2021/09/09/us/politics/biden-mandates-vaccines.html. Accessed: Sept. 9, 2021.

[205] Christopher Rose, Andrew J Medford, C Franklin Goldsmith, Tejs Vegge, Joshua S Weitz, and Andrew A Peterson. Heterogeneity in susceptibility dictates the order of epidemic models. Journal of Theoretical Biology, 528:110839, 2021.

[206] Ronald Ross. The Prevention of Malaria. John Murray, London, 1911.

[207] James L. Rudolph, Christopher W. Halladay, Malisa Barber, Kevin W. McConeghy, Vince Mor, Aman Nanda, and Stefan Gravenstein. Temperature in nursing home residents systematically tested for SARS-CoV-2. Journal of the American Medical Directors Association, 21(7):895–899.e1, 2020.

[208] Timothy W Russell, Hermaleigh Townsley, Sam Abbott, Joel Hellewell, Edward J Carr, Lloyd Chapman, Rachael Pung, Billy J Quilty, David Hodgson, Ashley Fowler, et al. Within-host SARS-CoV-2 viral kinetics informed by complex life course exposures reveals different intrinsic properties of omicron and delta variants. medRxiv, pages 2023–05, 2023.

[209] Chadi M. Saad-Roy, Sinead E. Morris, Mike Boots, Rachel E. Baker, Bryan L. Lewis, Jeremy Farrar, Madhav V. Marathe, Andrea L. Graham, Simon A. Levin, Caroline E. Wagner, C. Jessica E. Metcalf, and Bryan T. Grenfell. Impact of waning immunity against SARS-CoV-2 severity exacerbated by vaccine hesitancy. PLOS Computational Biology, 20(8):e1012211, August 2024.

[210] Jerald Sadoff, Els De Paepe, John DeVincenzo, Efi Gymnopoulou, Joris Menten, Bryan Murray, Arangassery Rosemary Bastian, An Vandebosch, Wouter Haazen, Nicolas Noulin, Christy Comeaux, Esther Heijnen, Kingsley Eze, Anthony Gilbert, Rob Lambkin-Williams, Hanneke Schuitemaker, and Benoit Callendret. Prevention of respiratory syncytial virus infection in healthy adults by a single immunization of Ad26.RSV.preF in a human challenge study. The Journal of Infectious Diseases, 226(3):396–406, Jan 2021.

[211] Yuko Sakai-Tagawa, Seiya Yamayoshi, and Yoshihiro Kawaoka. Sensitivity of commercially available influenza rapid diagnostic tests in the 2018–2019 influenza season. Frontiers in Microbiology, 10, 10 2019.

[212] Erica Ollmann Saphire, Sharon L. Schendel, Bronwyn M. Gunn, Jacob C. Milligan, and Galit Alter. Antibody-mediated protection against Ebola virus. Nature Immunology, 19(11):1169–1178, November 2018.

[213] Beate Schmoele-Thoma, Agnieszka M. Zareba, Qin Jiang, Mohan S. Maddur, Rana Danaf, Alex Mann, Kingsley Eze, Juin Fok-Seang, Golam Kabir, Andrew Catchpole, Daniel A. Scott, Alejandra C. Gurtman, Kathrin U. Jansen, William C. Gruber, Philip R. Dormitzer, and Kena A. Swanson. Vaccine efficacy in adults in a respiratory syncytial virus challenge study. New England Journal of Medicine, 386(25):2377–2386, Jun 2022.

[214] Anoop S.V. Shah, Ciara Gribben, Jennifer Bishop, Peter Hanlon, David Caldwell, Rachael Wood, Martin Reid, Jim McMenamin, David Goldberg, Diane Stockton, Sharon Hutchinson, Chris Robertson, Paul M. McKeigue, Helen M. Colhoun, and David A. McAllister. Effect of vaccination on transmission of SARS-CoV-2. New England Journal of Medicine, Sep 2021.

[215] Mrinank Sharma, Sören Mindermann, Charlie Rogers-Smith, Gavin Leech, Benedict Snodin, Janvi Ahuja, Jonas B Sandbrink, Joshua Teperowski Monrad, George Altman, Gurpreet Dhaliwal, et al. Understanding the effectiveness of government interventions against the resurgence of COVID-19 in Europe. Nature communications, 12(1):1–13, 2021.

[216] David K. Shay, Robert C. Holman, Robert D. Newman, Lenna L. Liu, James W. Stout, and Larry J. Anderson. Bronchiolitis-associated hospitalizations among US children, 1980-1996. JAMA, 282(15):1440–1446, 10 1999.

[217] Madhumita Shrotri, Maria Krutikov, Tom Palmer, Rebecca Giddings, Borscha Azmi, Sathyavani Subbarao, Christopher Fuller, Aidan Irwin-Singer, Daniel Davies, Gokhan Tut, et al. Vaccine effectiveness of the first dose of ChAdOx1 nCoV-19 and BNT162b2 against SARS-CoV-2 infection in residents of long-term care facilities in England (vivaldi): a prospective cohort study. The Lancet Infectious Diseases, 2021.

[218] George R. Siber, Ih Chang, Sherryl Baker, Philip Fernsten, Katherine L. O'Brien, Mathuram Santosham, Keith P. Klugman, Shabir A. Madhi, Peter Paradiso, and Robert Kohberger. Estimating the protective concentration of anti-pneumococcal capsular polysaccharide antibodies. Vaccine, 25(19):3816–3826, May 2007.

[219] Eric A.F. Simoes. Respiratory syncytial virus and subsequent lower respiratory tract infections in developing countries: A new twist to an old virus. The Journal of Pediatrics, 135(6):657–661, 1999.

[220] Susan E. Sloan, Kristy J. Szretter, Bharathi Sundaresh, Kristin M. Narayan, Patrick F. Smith, David Skurnik, Sylvain Bedard, José M. Trevejo, David Oldach, and Zachary Shriver. Clinical and virological responses to a broad-spectrum human monoclonal antibody in an influenza virus challenge study. Antiviral Research, 184:104763, Dec 2020.

[221] Louise E Smith, R Amlôt, Helen Lambert, Isabel Oliver, Charlotte Robin, Lucy Yardley, and G James Rubin. Factors associated with adherence to self-isolation and lockdown measures in the UK: a cross-sectional survey. Public Health, 187:41–52, 2020.

[222] Rebecca L Smith, Laura L Gibson, Pamela P Martinez, Ruian Ke, Agha Mirza, Madison Conte, Nicholas Gallagher, Abigail Conte, Leyi Wang, Richard Fredrickson, Darci C Edmonson, Melinda E Baughman, Karen K Chiu, Hannah Choi, Tor W Jensen, Kevin R Scardina, Shannon Bradley, Stacy L Gloss, Crystal Reinhart, Jagadeesh Yedetore, Alyssa N Owens, John Broach, Bruce Barton, Peter Lazar, Darcy Henness, Todd Young, Alastair Dunnett, Matthew L Robinson, Heba H Mostafa, Andrew Pekosz, Yukari C Manabe, William J Heetderks, David D McManus, and Christopher B Brooke. Longitudinal assessment of diagnostic test performance over the course of acute SARS-CoV-2 infection. The Journal of Infectious Diseases, 224(6):976–982, Sep 2021.

[223] John Snow and Benjamin Ward Richardson. Snow on cholera: being a reprint of two papers. Commonwealth Fund, 1936.

[224] Infection Control Today Editorial Staff. Evaluating the impact of testing and timely diagnosis on disease transmission. https://www.infectioncontroltoday.com/view/evaluating-impact-testing-timely-diagnosis-disease-transmission. Accessed: March 17, 2025.

[225] Sheena G. Sullivan and Benjamin J. Cowling. Crude vaccine effectiveness is a misleading term in test-negative studies of influenza vaccine effectiveness. Epidemiology, 26(5):e60, September 2015.

[226] Juliana C. Taube, Zachary Susswein, and Shweta Bansal. Spatiotemporal trends in self-reported mask-wearing behavior in the United States: Analysis of a large cross-sectional survey. JMIR Public Health and Surveillance, 9(1):e42128, March 2023.

[227] Juliana C. Taube, Zachary Susswein, Vittoria Colizza, and Shweta Bansal. Characterizing us contact patterns relevant to respiratory transmission from a pandemic to baseline: Analysis of a large cross-sectional survey. medRxiv, page 2024.04.26.24306450, December 2024.

[228] Viet Loan Dao Thi, Konrad Herbst, Kathleen Boerner, Matthias Meurer, Lukas PM Kremer, Daniel Kirrmaier, Andrew Freistaedter, Dimitrios Papagiannidis, Carla Galmozzi, Megan L Stanifer, et al. A colorimetric RT-LAMP assay and LAMP-sequencing for detecting SARS-CoV-2 RNA in clinical samples. Science translational medicine, 12(556), 2020.

[229] Mark G. Thompson, Jefferey L. Burgess, Allison L. Naleway, Harmony Tyner, Sarang K. Yoon, Jennifer Meece, Lauren E.W. Olsho, Alberto J. Caban-Martinez, Ashley L. Fowlkes, Karen Lutrick, Holly C. Groom, Kayan Dunnigan, Marilyn J. Odean, Kurt Hegmann, Elisha Stefanski, Laura J. Edwards, Natasha Schaefer-Solle, Lauren Grant, Katherine Ellingson, Jennifer L. Kuntz, Tnelda Zunie, Matthew S. Thiese, Lynn Ivacic, Meredith G. Wesley, Julie Mayo Lamberte, Xiaoxiao Sun, Michael E. Smith, Andrew L. Phillips, Kimberly D. Groover, Young M. Yoo, Joseph Gerald, Rachel T. Brown, Meghan K. Herring, Gregory Joseph, Shawn Beitel, Tyler C. Morrill, Josephine Mak, Patrick Rivers, Brandon P. Poe, Brian Lynch, Yingtao Zhou, Jing Zhang, Anna Kelleher, Yan Li, Monica Dickerson, Erika Hanson, Kyley Guenther, Suxiang Tong, Allen Bateman, Erik Reisdorf, John Barnes, Eduardo Azziz-Baumgartner, Danielle R. Hunt, Melissa L. Arvay, Preeta Kutty, Ali-

cia M. Fry, and Manjusha Gaglani. Prevention and Attenuation of COVID-19 with the BNT162b2 and mRNA-1273 Vaccines. New England Journal of Medicine, 385(4):320–329, Jun 2021.

[230] Mark G. Thompson, Karthik Natarajan, Stephanie A. Irving, Elizabeth A. Rowley, Eric P. Griggs, Manjusha Gaglani, Nicola P. Klein, Shaun J. Grannis, Malini B. DeSilva, Edward Stenehjem, Sarah E. Reese, et al. Effectiveness of a third dose of mRNA vaccines against COVID-19–associated emergency department and urgent care encounters and hospitalizations among adults during periods of delta and omicron variant predominance — VISION network, 10 states, August 2021–January 2022. MMWR Morb Mortal Wkly Rep., 71, 2021.

[231] William W. Thompson, David K. Shay, Eric Weintraub, Lynnette Brammer, Nancy Cox, Larry J. Anderson, and Keiji Fukuda. Mortality associated with influenza and respiratory syncytial virus in the United States. JAMA, 289(2):179–186, 01 2003.

[232] Ingrid Torjesen. COVID-19: Peak of viral shedding is later with omicron variant, Japanese data suggest. BMJ, 376:89, Jan 2022.

[233] Kuo-Chien Tsaoa, Yung-Bin Kuob, Chung-Guei Huanga, Shao-Wen Chaue, and Err-Cheng Chan. Performance of rapid-test kits for the detection of the pandemic influenza A/H1N1 virus. Journal of Virological Methods, 173:387–389, February 2011.

[234] Henry C. Tuckwell, Laurent Toubiana, and Jean-Francois Vibert. Spatial epidemic network models with viral dynamics. Physical Review E, 57(2):2163–2169, Feb 1998.

[235] Ana Cecilia Ulloa, Sarah A. Buchan, Nick Daneman, and Kevin A Brown. Early estimates of SARS-CoV-2 omicron variant severity based on a matched cohort study, Ontario, Canada. medRxiv, 2022.

[236] U.S. Centers for Disease Control and Prevention. COVID-19 Vaccinations in the United States. https://covid.cdc.gov/covid-data-tracker/#vaccinations_vacc-total-admin-rate-total. Accessed: Sept. 22, 2021.

[237] U.S. Centers for Disease Control and Prevention. Guidance for COVID-19 prevention in K-12 schools. https://www.cdc.gov/coronavirus/2019-ncov/community/schools-childcare/k-12-guidance.html. Accessed: Oct. 14, 2021.

[238] U.S. Centers for Disease Control and Prevention. Isolation and precautions for people with COVID-19. https://www.cdc.gov/coronavirus/2019-ncov/your-health/isolation.html. Accessed: May 11, 2023.

[239] U.S. Centers for Disease Control and Prevention. Preliminary estimated influenza illnesses, medical visits, hospitalizations, and deaths in the United States – 2021-2022 influenza season. https://www.cdc.gov/flu/about/burden/2021-2022.htm. Accessed: October 4, 2022.

[240] Timothy M. Uyeki, Ramakrishna Prasad, Charles Vukotich, Samuel Stebbins, Charles R. Rinaldo, Yu-hui Ferng, Stephen S. Morse, Elaine L. Larson, Allison E. Aiello, Brian Davis, and Arnold S. Monto. Low sensitivity of rapid diagnostic test for influenza. Clinical Infectious Diseases, 48(9):e89–e92, 05 2009.

[241] T Van Effelterre, N Hens, L J White, S Gravenstein, A R Bastian, N Buyukkaramikli, C Y Cheng, J Hartnett, G Krishnarajah, K Weber, and L Hernandez Pastor. Modeling respiratory syncytial virus adult vaccination in the United States with a dynamic transmission model. Clinical Infectious Diseases, 77(3):480–489, 2023.

[242] Inonge van Twillert, Wanda G. H. Han, and Cécile A. C. M. van Els. Waning and aging of cellular immunity to Bordetella pertussis. Pathogens and Disease, 73(8):ftv071, November 2015.

[243] Avni Vatti, Diego M. Monsalve, Yair Pacheco, Chia Chang, Juan-Manuel Anaya, and M. Eric Gershwin. Original antigenic sin: A comprehensive review. Journal of Autoimmunity, 83:12–21, 2017.

[244] Gary M. Vilke, Jesse J. Brennan, Alexandrea O. Cronin, and Edward M. Castillo. Clinical features of patients with COVID-19: is temperature screening useful? Journal of Emergency Medicine, 59(6):952–956, 2020.

[245] Chantal BF Vogels, Anderson F Brito, Anne L Wyllie, Joseph R Fauver, Isabel M Ott, Chaney C Kalinich, Mary E Petrone, Arnau Casanovas-Massana, M Catherine Muenker, Adam J Moore, et al. Analytical sensitivity and efficiency comparisons of SARS-CoV-2 RT–qPCR primer–probe sets. Nature Microbiology, 5(10):1299–1305, 2020.

[246] Jacco Wallinga and Peter Teunis. Different epidemic curves for severe acute respiratory syndrome reveal similar impacts of control measures. American Journal of Epidemiology, 160(6):509–516, 2004.

[247] M Wathuo, GF Medley, DJ Nokes, and PK Munywoki. Quantification and determinants of the amount of respiratory syncytial virus (RSV) shed using real time PCR data from a longitudinal household study. Wellcome Open Res, 1(27), 2017.

[248] Joshua S Weitz, Stephen J Beckett, Ashley R Coenen, David Demory, Marian Dominguez-Mirazo, Jonathan Dushoff, Chung-Yin Leung, Guanlin Li, Andreea Măgălie, Sang Woo Park, et al. Modeling shield immunity to reduce COVID-19 epidemic spread. Nature medicine, 26(6):849–854, 2020.

[249] Julie A. Wilson, Michael Hevey, Russell Bakken, Shawn Guest, Mike Bray, Alan L. Schmaljohn, and Mary Kate Hart. Epitopes involved in antibody-mediated protection from Ebola virus. Science, 287(5458):1664–1666, March 2000.

[250] Roman Wölfel, Victor M Corman, Wolfgang Guggemos, Michael Seilmaier, Sabine Zange, Marcel A Müller, Daniela Niemeyer, Terry C Jones, Patrick Vollmar, Camilla Rothe, et al. Virological assessment of hospitalized patients with COVID-2019. Nature, 581(7809):465–469, 2020.

[251] Mark EJ Woolhouse, C Dye, J-F Etard, T Smith, JD Charlwood, GP Garnett, P Hagan, JLK Hii, PD Ndhlovu, RJ Quinnell, et al. Heterogeneities in the transmission of infectious agents: implications for the design of control programs. Proceedings of the National Academy of Sciences, 94(1):338–342, 1997.

[252] Colin J. Worby and Hsiao-Han Chang. Face mask use in the general population and optimal resource allocation during the COVID-19 pandemic. Nature Communications, 11(4049), 2020.

[253] World Health Organization. Statement on the fifteenth meeting of the IHR (2005) emergency committee on the COVID-19 pandemic. https://www.who.int/news/item/05-05-2023-statement-on-the-fifteenth-meeting-of-the-international-health-regulations-(2005)-emergency-committee-regarding-the-coronavirus-disease-({COVID-19})-pandemic. Accessed: May 5, 2023.

[254] Luojun Yang, Bryan T Grenfell, and Michael J Mina. Waning immunity and re-emergence of measles and mumps in the vaccine era. Current Opinion in Virology, 40:48–54, February 2020.

[255] Qing Yang, Tassa K. Saldi, Patrick K. Gonzales, Erika Lasda, Carolyn J. Decker, Kimngan L. Tat, Morgan R. Fink, Cole R. Hager, Jack C. Davis, Christopher D. Ozeroff, Denise Muhlrad, Stephen K. Clark, Will T. Fattor, Nicholas R. Meyerson, Camille L. Paige, Alison R. Gilchrist, Arturo Barbachano-Guerrero, Emma R. Worden-Sapper, Sharon S. Wu, Gloria R. Brisson, Matthew B. McQueen, Robin D. Dowell, Leslie Leinwand, Roy Parker, and Sara L. Sawyer. Just 2% of SARS-CoV-2 positive individuals carry 90% of the virus circulating in communities. Proceedings of the National Academy of Sciences, 118(21):e2104547118, May 2021.

[256] Yazdan Yazdanpanah, Caroline E Sloan, Cécile Charlois-Ou, Stéphane Le Vu, Caroline Semaille, Dominique Costagliola, Josiane Pillonel, Anne-Isabelle Poullié, Olivier Scemama, Sylvie Deuffic-Burban, et al. Routine HIV screening in france: clinical impact and cost-effectiveness. PloS one, 5(10):e13132, 2010.

[257] Sam Zhang, Patrick R. Heck, Michelle N. Meyer, Christopher F. Chabris, Daniel G. Goldstein, and Jake M. Hofman. An illusion of predictability in scientific results: Even experts confuse inferential uncertainty and outcome variability. Proceedings of the National Academy of Sciences, 120(33):e2302491120, 2023.

[258] Shengyuan Zhang, Akosua A Agyeman, Christoforos Hadjichrysanthou, and Joseph F Standing. SARS-CoV-2 viral dynamic modelling to inform model selection and timing and efficacy of antiviral therapy. CPT: Pharmacometrics & Systems Pharmacology, 2023.

[259] Ziyuan Zhang, Christopher Brian Boyer, and Marc Lipsitch. Use of the test-negative design to estimate the protective effect of a scalar immune measure: A simulation analysis. page 2024.11.22.24317757, November 2024.

Chapter 6

Appendix

6.1 Chapter 2 supplementary materials

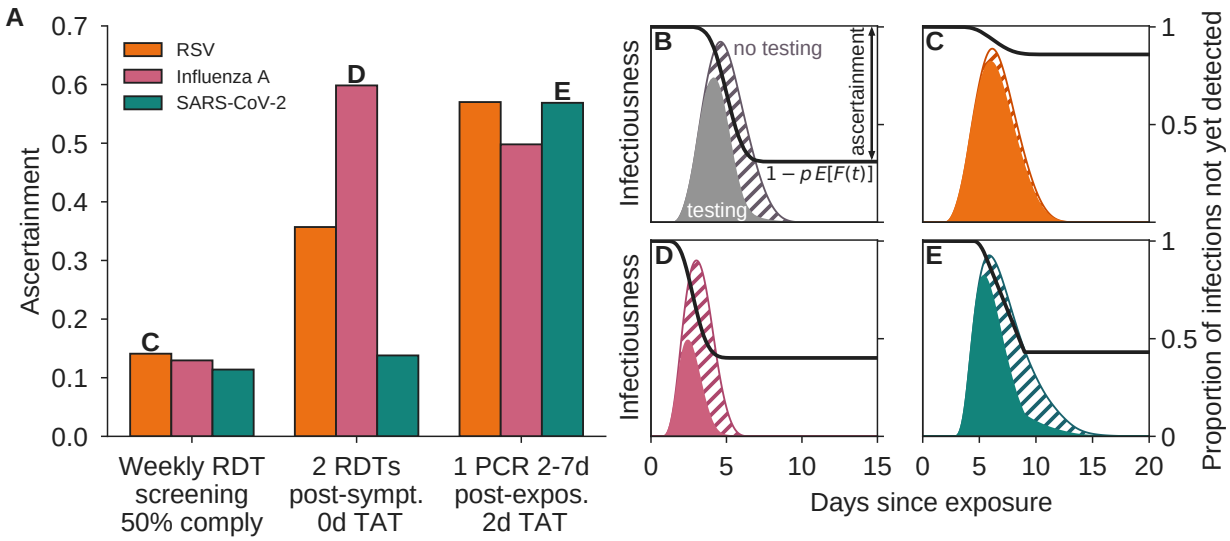

Figure S1: **Ascertainment rates vary considerably by strategy and pathogen.** Ascertainment is shown for RSV (orange), influenza A (pink), and SARS-CoV-2 omicron in experienced hosts (green) under three testing programs: (1) weekly rapid diagnostic test (RDT) screening with 50% compliance, (2) testing with one RDT per day for two days starting at symptom onset, and (3) one RT-qPCR test administered 2-7d after exposure, with 75% participation and 2d test turnaround time (TAT). Panels B-E depict population-level infectiousness curves without (hatched) and with (filled) testing and isolation for the labeled pathogen and testing program. Black curves represent the proportion of infections not yet detected by time t. See Supplemental Figure 2.2 for scenario Testing effectiveness estimates.

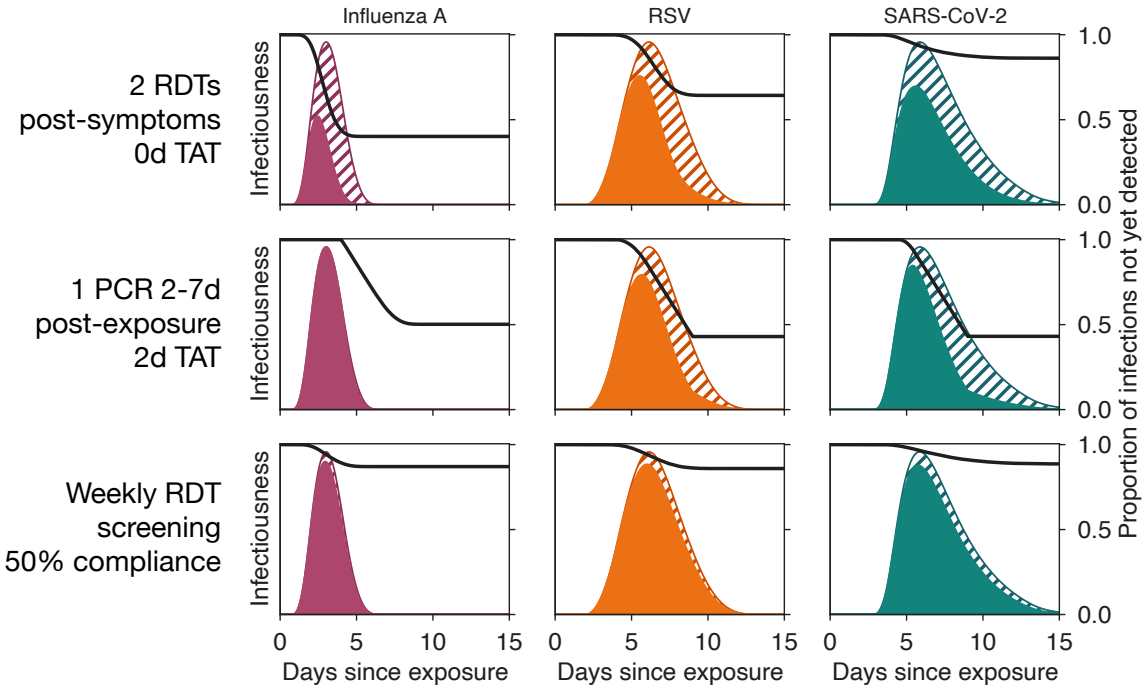

Figure S2: **Population-level infectiousness curves for all Figure 2.2 scenarios.** Scenario results are shown for RSV (orange), influenza A (pink), and SARS-CoV-2 omicron in experienced hosts (green) under three testing programs: (1) weekly rapid diagnostic test (RDT) screening with 50% compliance, (2) testing with one RDT per day for two days starting at symptom onset, and (3) one RT-qPCR test administered 2-7d after exposure, with 75% participation and 2d test turnaround time (TAT). Panels depict population-level infectiousness curves without (hatched) and with (filled) testing and isolation for the labeled pathogen and testing program. Black curves represent the proportion of infections not yet detected by time t.

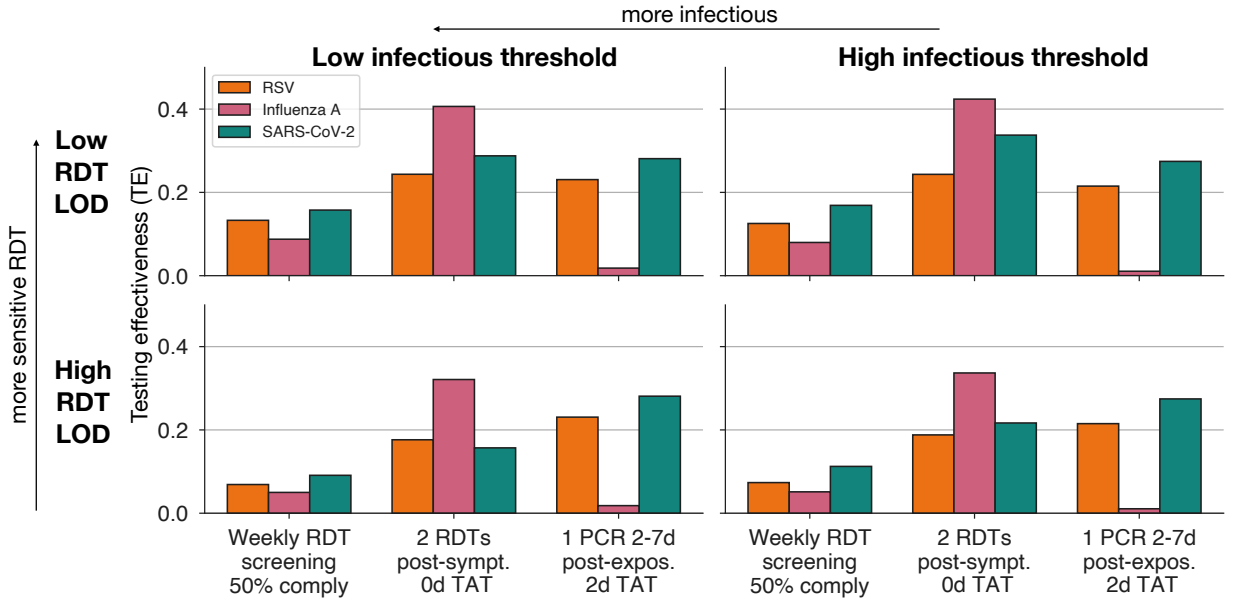

Figure S3: **Sensitivity analysis of testing effectiveness patterns observed in Figure 2.2.** Testing effectiveness is shown for RSV (orange), influenza A (pink), and SARS-CoV-2 omicron in experienced hosts (green) under three testing programs: (1) weekly rapid diagnostic test (RDT) screening with 50% compliance, (2) testing with one RDT per day for two days starting at symptom onset, and (3) one RT-qPCR test administered 2-7d after exposure, with 75% participation and 2d test turnaround time (TAT). Each scenario is considered for a 0.5 log-fold increase or decrease in infectious threshold or RDT limit of detection (LOD), as labeled. In this sensitivity analysis, although precise values change, the relative patterns and orderings discussed in the main text are unaffected.

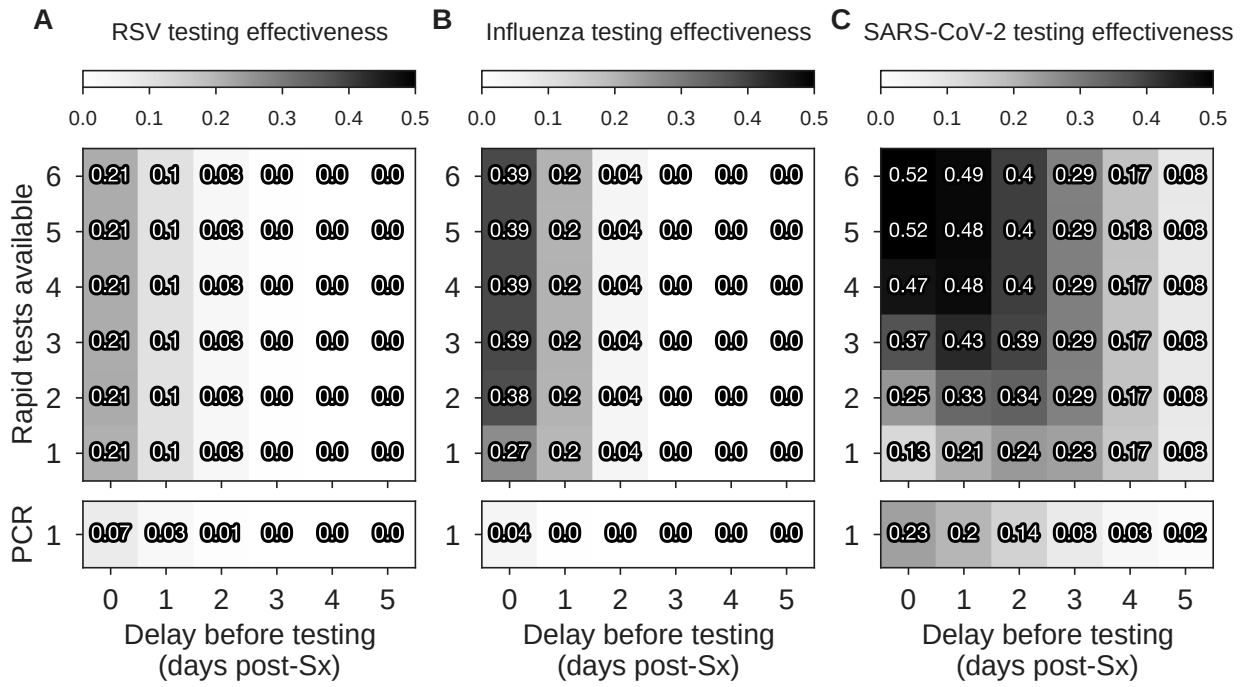

Figure S4: **Testing effectiveness after symptom onset depends on the pathogen, the number and type of tests available, and when they are used.** Testing effectiveness (TE) of rapid test (RDT) and RT-qPCR with 2 day turnaround time, used x days after symptom (Sx) onset using y tests once per day is shown for RSV, influenza type A, and SARS-CoV-2 omicron in experienced hosts. Darker colors represent higher TE as indicated, and the associated TE for each strategy is shown. Turnaround times: rapid tests, TAT $= 0$; RT-qPCR TAT $= 2$. See Supplementary Table S1 for limits of detection and other parameters and Figure 2.4 for colored heatmaps with annotated optima.

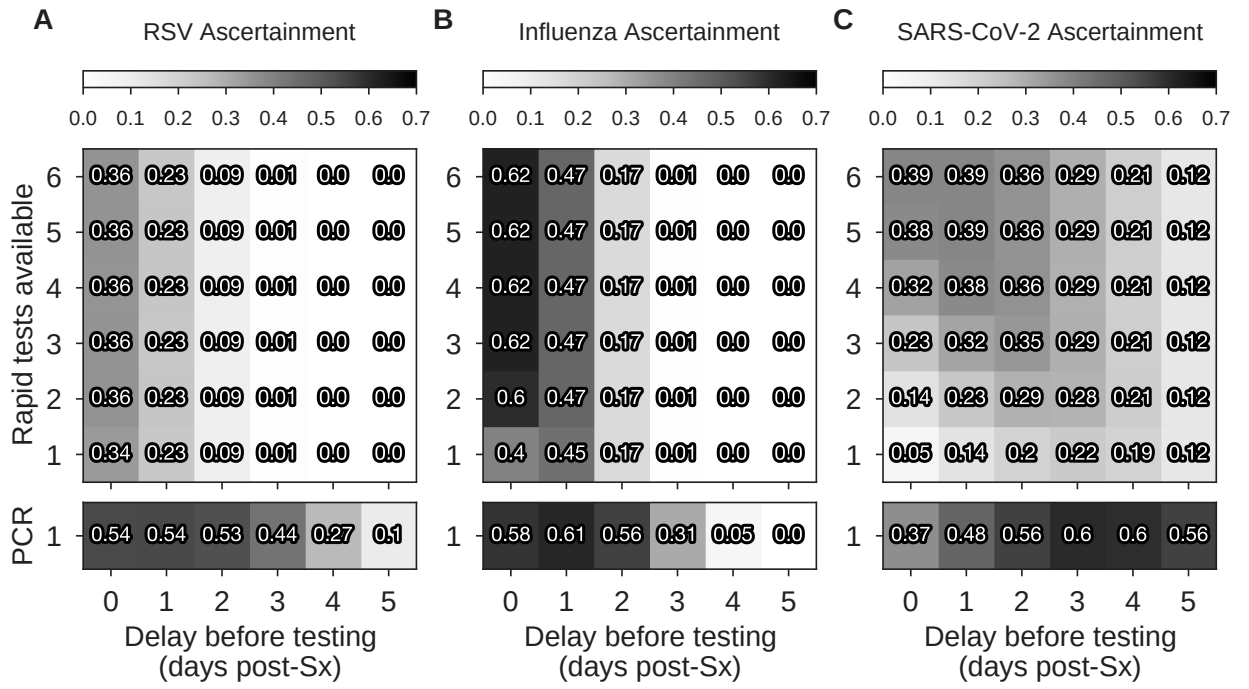

Figure S5: **Ascertainment of testing after symptom onset depends on the pathogen, the number and type of tests available, and when they are used.** Ascertainment—defined as the total proportion of infections diagnosed—of rapid diagnostic test (RDT) and RT-qPCR with 2 day turnaround time, used x days after symptom (Sx) onset using y tests once per day is shown for RSV, influenza A, and SARS-CoV-2 omicron in experienced hosts. Darker colors represent higher ascertainment as indicated, and the ascertainment values are shown. Turnaround times: rapid tests, TAT $= 0$; RT-qPCR TAT $= 2$. See Supplementary Table S1 for limits of detection and other parameters.

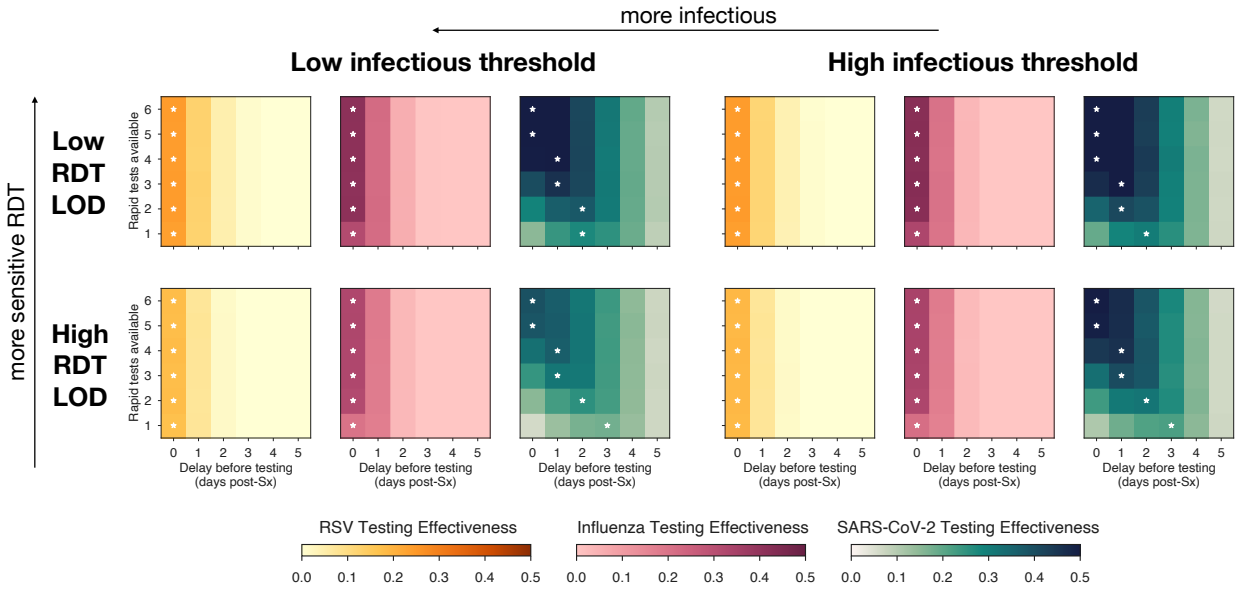

Figure S6: **Sensitivity analysis of optimal timing of RDT usage after symptom onset.** Testing effectiveness (TE) of rapid test (RDT), used x days after symptom (Sx) onset using y tests once per day is shown for RSV (orange), influenza A (pink), and SARS-CoV-2 omicron in experienced hosts (green). Darker colors represent higher TE as indicated. In each row, the testing strategy with highest TE is annotated with a white star. Each scenario is considered for a 0.5 log-fold increase or decrease in infectious threshold or RDT limit of detection (LOD), as labeled. In this sensitivity analysis, optimal test timing recommendations for RSV and influenza A are unaffected, and are shifted by at most 1d for SARS-CoV-2. Turnaround times: rapid tests, TAT $= 0$; RT-qPCR TAT $= 2$.

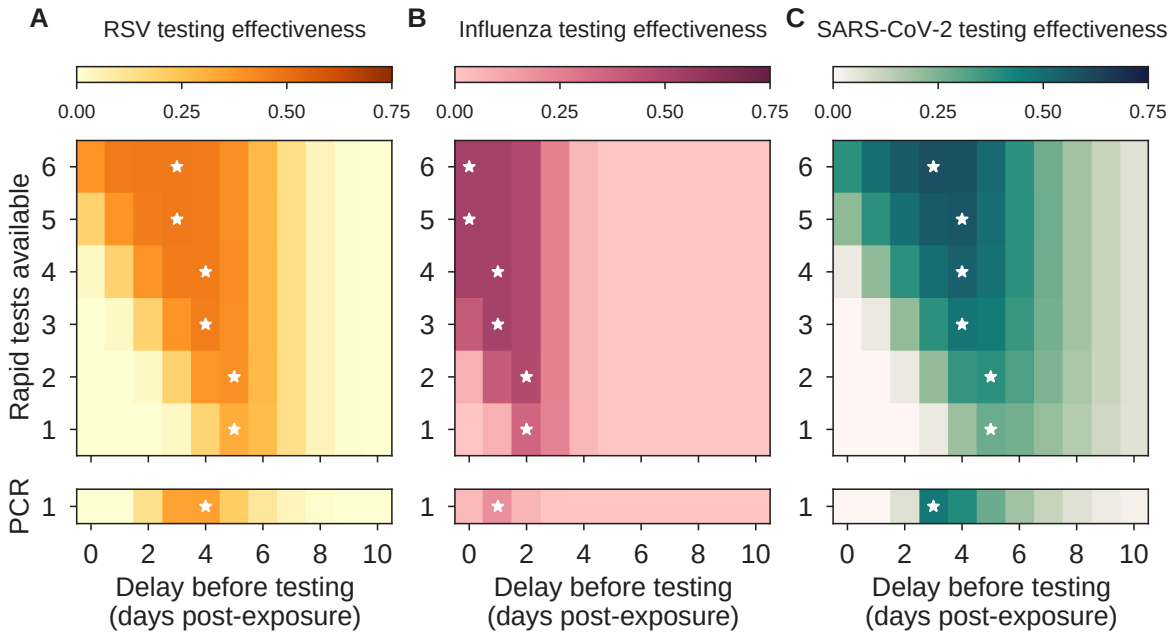

Figure S7: **Optimal timing of testing after known exposure depends on the number of tests available.** Testing effectiveness (TE) of rapid test (RDT) and RT-qPCR with 2 day turnaround time, used x days after exposure using y tests once per day is shown for RSV (orange), influenza A (pink), and SARS-CoV-2 omicron in experienced hosts (green). Darker colors represent higher TE as indicated. In each row, the testing strategy with highest TE is annotated with a white star. Turnaround times: rapid tests, TAT $= 0$; RT-qPCR TAT $= 2$. See Supplementary Table S1 for LODs and Figure 2.4 for TE estimates.

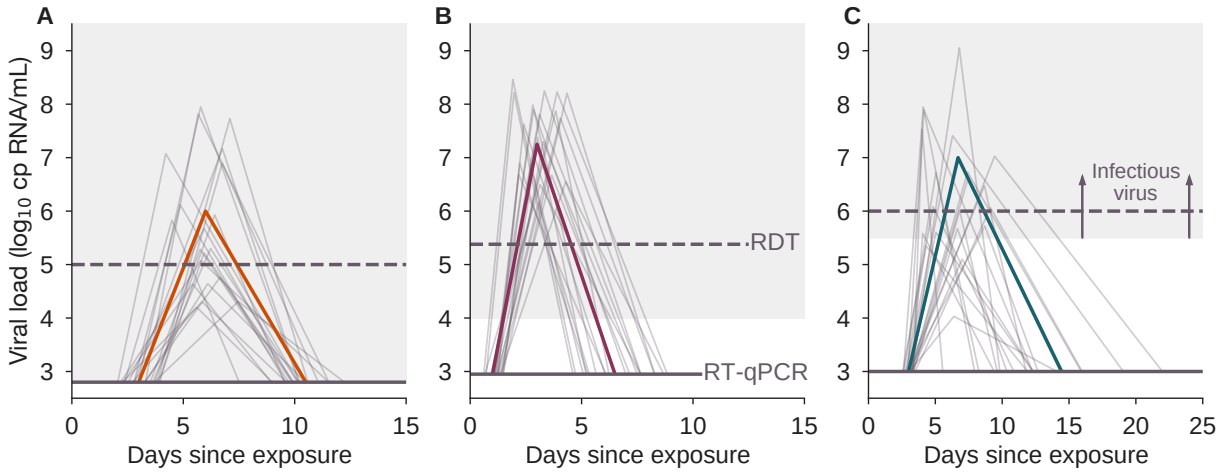

Figure S8: **Examples of modeled viral kinetics.** Stochastic realizations (gray lines; n=15) and a single characteristic realization (colored line) of the piecewise linear model of viral load kinetics for RSV (orange), influenza A (pink), and SARS-CoV-2 omicron/experienced (green). Horizontal lines show the pathogen-specific limit of detection of RT-qPCR (solid line) and rapid diagnostic tests (RDTs; dashed line). Infectious viral load is indicated by the gray shaded region.

Pathogen	Parameter	Value	Units	Source
Influenza A	Latent period	Unif[0.5,1.5]	Days from exposure	[34, 220]
	Peak time	Unif[1,3]	Days from latent	[34, 108, 220]
	Peak VL	Unif[6,8.5]	$\log_{10}$ cp RNA/mL	[108]
	Clearance time	Unif[2,5]	Days from VL peak	[34, 108, 220]
	Infectious threshold	4	$\log_{10}$ cp RNA/mL	[138]
	High sensitivity LOD	2.95	$\log_{10}$ cp RNA/mL	[108]
	Low sensitivity LOD	5.38	$\log_{10}$ cp RNA/mL	[233]
	% symptomatic	64	% of infections	[34, 108, 220]
	Symptom onset time	Unif[-2,0]	Days from VL peak	[138]
	Failure rate	5	% of tests above LOD	See text
RSV	Latent period	Unif[2,4]	Days from exposure	[210, 213]
	Peak time	Unif[2,4]	Days from latent	[213]
	Peak VL	Unif[4,8]	$\log_{10}$ cp RNA/mL	[210, 213]
	Clearance time	Unif[3,6]	Days from VL peak	[210, 213]
	Infectious threshold	2.8	$\log_{10}$ cp RNA/mL	[210]
	High sensitivity LOD	2.8	$\log_{10}$ cp RNA/mL	[213]
	Low sensitivity LOD	5	$\log_{10}$ cp RNA/mL	[197]
	% symptomatic	57	% of infections	[173, 247]
	Symptom onset time	Unif[-1,1]	Days from VL peak	[141]
	Failure rate	5	% of tests above LOD	See text
SARS-CoV-2 omicron strain experienced host	Latent period	Unif[2.5,3.5]	Days from exposure	[121, 136]
	Peak time	Lognorm[1.053,0.688]*	Days from latent	[94]
	Peak VL	Lognorm[1.876,0.181]	40 - Cycle threshold	[94]
	Clearance time	Lognorm[1.704,0.491]†	Days from VL peak	[94]
	Infectious threshold	5.5	$\log_{10}$ cp RNA/mL	[7, 72, 116, 188]
	High sensitivity LOD	3	$\log_{10}$ cp RNA/mL	[94, 121]
	Low sensitivity LOD	6	$\log_{10}$ cp RNA/mL	[14, 15]
	% symptomatic	65	% of infections	[94]
	Symptom onset time	Unif[-5,-1]	Days from VL peak	[86, 94, 232]
	Failure rate	5	% of tests above LOD	[14]
SARS-CoV-2 founder strain naive host	Latent period	Unif[2.5,3.5]	Days from exposure	[121, 136]
	Peak time	Lognorm[0.873,0.788]*	Days from latent	[125]
	Peak VL	Lognorm[1.999,0.199]	$\log_{10}$ cp RNA/mL	[125]
	Clearance time	Lognorm[1.953,0.611]†	Days from VL peak	[125]
	Infectious threshold	5.5	$\log_{10}$ cp RNA/mL	[7, 72, 116, 188]
	High sensitivity LOD	3	$\log_{10}$ cp RNA/mL	[94]
	Low sensitivity LOD	5	$\log_{10}$ cp RNA/mL	[15]
	% symptomatic	65	% of infections	[94, 121]
	Symptom onset time	Unif[0,3]	Days from VL peak	[121, 130, 181]
	Failure rate	5	% of tests above LOD	See text

Table S1: **Summary of viral load, infectiousness, and testing parameters.** For a description of how parameters were extracted from the cited sources, please see Materials and Methods. LOD, limit of detection; VL, viral load; Unif, uniform; * bounded within $[0.5, 10]$; † bounded within $[0.5, 25]$.

6.1.1 Imperfect isolation behaviors

To include imperfect post-diagnosis isolation behaviors, we consider a behavior change function $B(\tau)$, one's relative infectiousness at time since diagnosis τ. For instance, perfect isolation upon diagnosis would be modeled as $B(\tau) = 0$, while a one-week partial isolation might be modeled as $B(\tau) = 0.5$ for $0 \leq \tau \leq 7$, and $B(\tau) = 1$ for $\tau > 7$. The individual reproduction number can thus be written as the sum of the total infectiousness before and after diagnosis,

$$\nu_{\text{testing}}(t_{\text{Dx}}) = \int_0^{t_{\text{Dx}}} \beta(t)\, dt + \int_{t_{\text{Dx}}}^{\infty} B(t - t_{\text{Dx}})\beta(t)\, dt\,. \tag{S1}$$

Simplifying yields

$$\bar{\nu}_{\text{testing}} = \nu_0 - \int_0^{\infty} \int_0^{t} \beta(t)\big[1 - B(t - t_{\text{Dx}})\big] f(t_{\text{Dx}})\, dt_{\text{Dx}}\, dt\,. \tag{S2}$$

This equation offers a helpful term-by-term interpretation: diagnosis decreases total infectiousness from its baseline of ν_0 by an amount that depends on (i) the probability distribution of diagnosis times $f(t_{\text{Dx}})$ and (ii) the quality of isolation after said diagnosis $B(\tau)$, weighted by (iii) the infectiousness $\beta(t)$ at the time of isolation and thereafter. Under a specified isolation behavior $B(\tau)$, TE is computed as

$$TE = p \int_0^{\infty} \mathbb{E}\left[\beta(t) \left(\int_0^{t} \big[1 - B(t - t_{\text{Dx}})\big] f(t_{\text{Dx}})\, dt_{\text{Dx}}\right)\right] dt \Big/ \int_0^{\infty} \mathbb{E}\left[\beta(t)\right]\, dt\,. \tag{S3}$$

Thus, more complex post-diagnosis behaviors may be easily modeled, but such scenarios were not explored numerically in the main text.

6.1.2 Test to exit strategies

Test-to-exit (TTE) is a strategy designed to maximize the effectiveness of post-diagnosis isolation while minimizing the number of days spent in isolation by requiring one or more negative test(s) before exiting isolation. While various formulations of TTE may exist, here we analyze a simple version in which individuals wait w days after receiving a diagnosis and then begin testing at a rate $\bar{A}$ tests per day, with a per-test failure rate of ϕ and a test turnaround time of TAT. We assume that compliance with TTE is $c = 1$ due to individuals' expected desire to leave isolation.

Mirroring Eq. (S1), the expected infectiousness under a test-to-exit program, assuming perfect isolation between the time of diagnosis t_{Dx} and the time of isolation exit t_{exit}, is given by

$$\nu_{\text{testing}}(t_{\text{Dx}}, t_{\text{exit}}) = \int_0^{t_{\text{Dx}}} \beta(t)\, dt \; + \int_{t_{\text{exit}}}^{\infty} \beta(t)\, dt \; . \tag{S4}$$

We define the PDF and CDF of t_{exit} as g and G, respectively, allowing us to rewrite the previous equation as

$$\bar{\nu}_{\text{testing}} = \nu_0 - \int_0^{\infty} \beta(t) F(t)\, dt + \int_0^{\infty} \beta(t) \int_0^{t} G(t, t_{\text{Dx}}) f(t_{\text{Dx}})\, dt_{\text{Dx}}\, dt \; . \tag{S5}$$

This expression takes on the interpretable form of total infectiousness in the absence of testing ν_0, minus post-diagnosis infectiousness prevented due to perfect and indefinite isolation, plus any residual infectiousness realized by an exit from isolation.

To model post-isolation exit testing, we assume that one waits w days before testing at a rate $\bar{A}$ using a test with turnaround time TAT and failure rate ϕ. Under these conditions, $n(t) = \bar{A}(t - t_{\text{Dx}} - \text{TAT} - w)$ represents the expected cumulative number of scheduled tests with the potential to return an exit-inducing result by time t, with $\bar{n}(t) = n(t) \text{mod} 1$. The distribution for t_{exit} is then given by the rather cumbersome

$$G(t, t_{\text{Dx}}) = \begin{cases} 0 & t \leq t_{\text{Dx}} + w + \text{TAT} \\ \psi_1(t) & t_{\text{Dx}} + w + \text{TAT} \leq t \leq t_{max} \\ \psi_2(t) & t \geq t_{max} \end{cases} \tag{S6}$$

where the function

$$\psi_1(t) = 1 - \left[(1 - \bar{n}(t))(1 - \phi)^{n(t) - n\bar{(}t)} + n\bar{(}t)(1 - \phi)^{n(t) - \bar{n}(t) + 1} \right] \tag{S7}$$

represents the cumulative probability that one receives a negative test due to a false negative (i.e., a test failure when above that test's limit of detection), and where

$$\psi_2(t) = \min \left\{ 1, \bar{A} \left[1 - \psi_1(t_{max}) \right] [t - t_{max}] + \psi_1(t_{max})) \right\} \tag{S8}$$

captures the rapid approach of G toward guaranteed exit from isolation after one is no longer detectable. The quantity $t_{max} = \max \left[t_u + \text{TAT}, t_{\text{Dx}} + w + \text{TAT} \right]$ represents the latest possible time at which a person

testing to exit could receive a positive test. The corresponding PDF is

$$g(t, t_{\text{Dx}}) = \begin{cases} 0 & t \leq t_{\text{Dx}} + w + \text{TAT} \\ \bar{A}\phi(1-\phi)^{n(t)-\bar{n}(t)} & t_{\text{Dx}} + w + \text{TAT} \leq t \leq t_u + \text{TAT} \\ \bar{A}\left[1 - \psi_1(t_{max})\right] & t_u + \text{TAT} \leq t \leq t_u + \text{TAT} + 1/\bar{A} \\ 0 & t \geq t_u + \text{TAT} + 1/\bar{A}. \end{cases} \tag{S9}$$

Under the above TTE assumptions, the typical number of days spent in isolation may be computed as the expected difference between the t_{exit} and t_{Dx} distributions. One may also update $\bar{q}_{\text{Dx}}$ in computing test consumption (Materials and Methods) to include the additional tests consumed while testing to exit,

$$\bar{q}_{\text{TTE}} = 1 + \int_0^\infty \int_{t_{\text{Dx}}+w}^\infty \left(\left\lfloor \int_{t_{\text{Dx}}+w}^{t_{\text{exit}}-\text{TAT}} \bar{A}\, dt \right\rfloor + \left\lfloor \int_{t_{\text{exit}}-\text{TAT}}^{t_{\text{exit}}} \bar{A}\, dt \right\rfloor \right) g(t_{\text{exit}}, t_{\text{Dx}}) f(t_{\text{Dx}}) dt_{\text{exit}} dt_{\text{Dx}}\,. \tag{S10}$$

6.2 Chapter 3 supplementary materials

Parameter	Description	Value	Reference
Population parameters			
N	Population size	20,000	—
ϕ	Proportion of population vaccinated	$[0, 1]$ US: 0.58	[236]
ψ	Proportion of population with infection-acquired immunity	$[0, 1]$ US: 0.35	[42]
Infection parameters			
σ^{-1}	Latent period	3 days	[48]
γ^{-1}	Infectious period	6 days	[36]
R_0^{NPI}	Basic reproductive number	$\{4, 6\}$	see Methods
α	Probability of transmission given contact (tuned to achieve the desired R_0^{NPI})	$R_0^{\text{NPI}}\gamma/N$	—
IHR	Infection hospitalization rate for naive unvaccinated	delta: 0.02 omicron: 0.01	[4, 101] [143, 235]
Testing parameters			
θ	Fraction by which screening & isolation reduces typical *unvaccinated* infectious period*		
	no screening	0	—
	weekly screening, 50% compliance	0.242	[136]
	weekly screening, 99% compliance	0.473	[136]
	2× weekly screening, 99% compliance	0.808	[136]

Table S2: **Summary of population, infection and testing parameters used in modeling and simulation.** *Assuming PCR testing with a one day turnaround time for test results.

Parameter	Description	Value	Reference
Immunity parameters			
VE_S	Vaccine effectiveness to decrease susceptibility to infection	**delta** waning = 50% baseline = 65% boosted = 80%	[40] [25, 64] [74]
		omicron 35%	[73]
VE_I	Vaccine effectiveness to decrease infectiousness	**delta** waning = 10% baseline = 35% boosted = 60%	[64] [25, 64] [74]
		omicron 5%	[73]
VE_P	Vaccine effectiveness to decrease disease progression to hospitalization given infection	**delta** waning = 80% baseline = 86% boosted = 90%	[12, 73, 230] [12, 73, 230] [73, 230]
		omicron 77%	[73, 230]
XE_S	Infection-acquired immunity effectiveness to decrease susceptibility to infection	**delta** 63%	[74]
		omicron 35%	[8]
XE_I	Infection-acquired immunity effectiveness to decrease infectiousness	**delta** 13%	[74]
		omicron 5%	[8]
XE_P	Infection-acquired immunity effectiveness to decrease disease progression to hospitalizations given infection	**delta** 54%	[8, 39]
		omicron 74%	[8]
HE_S	Hybrid immunity effectiveness to decrease susceptibility to infection (vaccine- and infection-acquired immunity)	**delta** waning = 81.5% baseline = 87.1% boosted = 92.6%	see Methods
		omicron 50%	—
HE_I	Hybrid immunity effectiveness to decrease infectiousness	**delta** waning = 21.7% baseline = 43.5% boosted = 65.2%	see Methods
		omicron 10%	—
HE_P	Hybrid immunity effectiveness to decrease disease progression to hospitalizations given infection	**delta** waning = 80% baseline = 86% boosted = 90%	see Methods
		omicron 77%	—

Table S3: **Summary of immunity parameters used in modeling and simulation.**

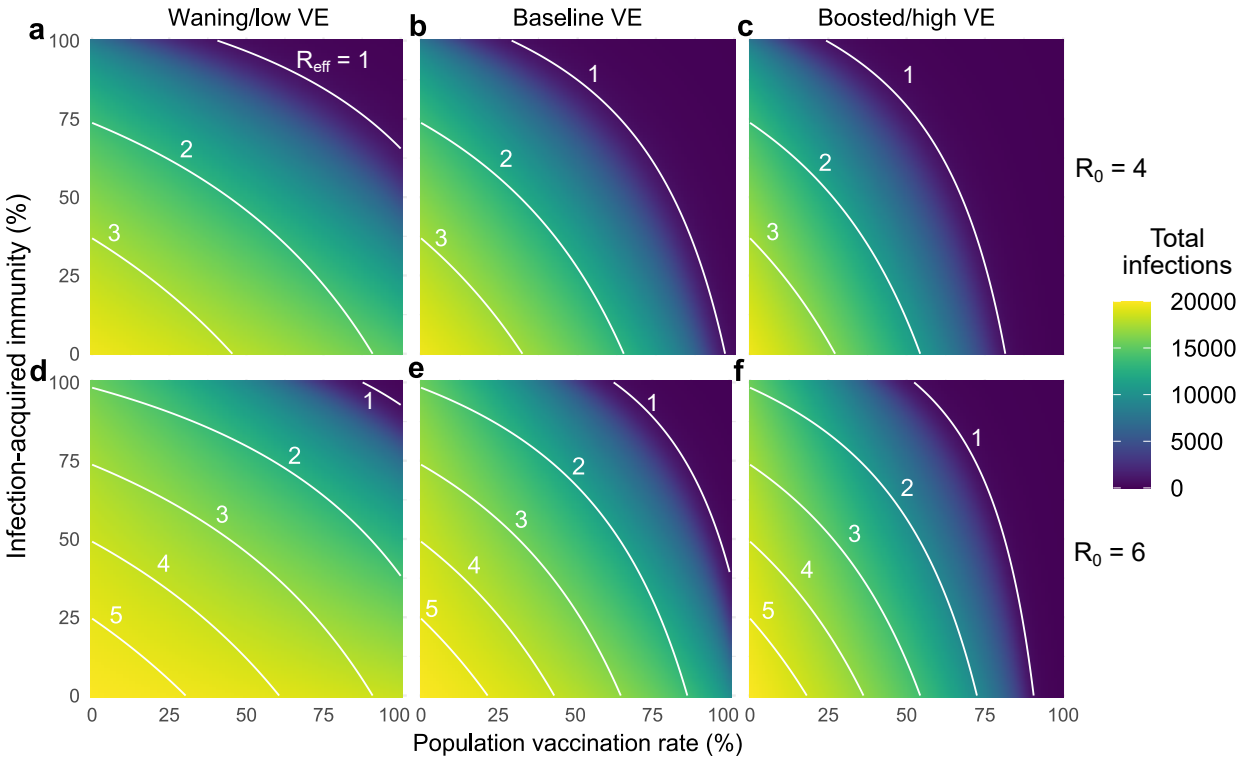

Figure S9: **Vaccination's impact on the total number of infections depends on vaccine effectiveness and R_0^{NPI}.** For (top row) $R_0^{\text{NPI}} = 4$ and (bottom row) $R_0^{\text{NPI}} = 6$, heatmaps show the total number of infections as past infection and vaccination rates vary for vaccines with (a) waning, (b) baseline, and (c) boosted effectiveness vs the delta variant. See Supplementary Tables S2 and S3 for scenario parameter values. Curves denote the effective reproductive number R_{eff} at $t = 0$ as annotated. $N = 20,000$.

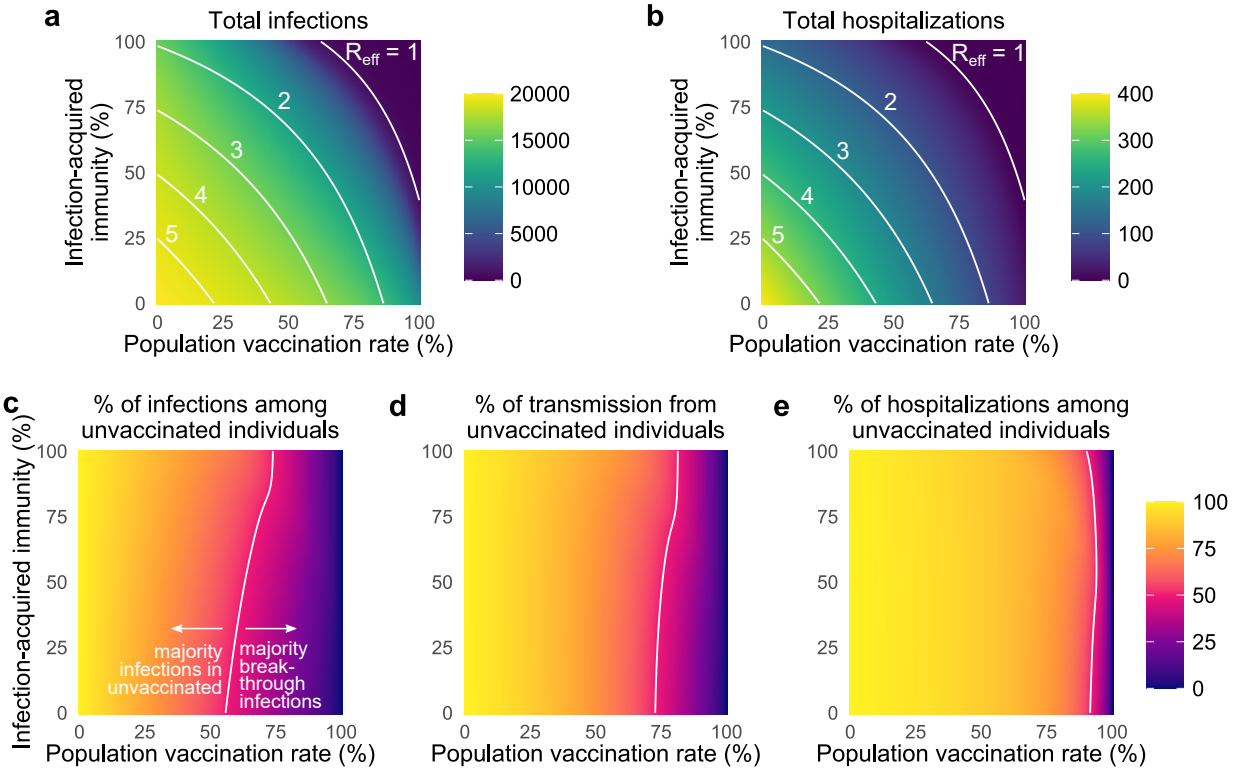

Figure S10: **Vaccination and past infection affect epidemic potential, vaccine breakthroughs, and drivers of transmission**. (a) Curves denote the effective reproductive number R_{eff} at $t = 0$ as annotated, as past infection and vaccination rates vary. Heatmaps show (a) the total number of infections, (b) the percentage of total infections occurring in the unvaccinated population and (c) the percentage of total infections caused by the unvaccinated population. White annotation curves in (b) and (c) indicate the 50% point. $N = 20,000$ and $R_0^{\text{NPI}} = 6$ in all panels, with baseline VE and immunity parameters vs the delta variant; see Figure 3.2 for $R_0^{\text{NPI}} = 4$. See Supplementary Table S3 for values for infection-acquired, vaccine-acquired, and hybrid immunity parameters.

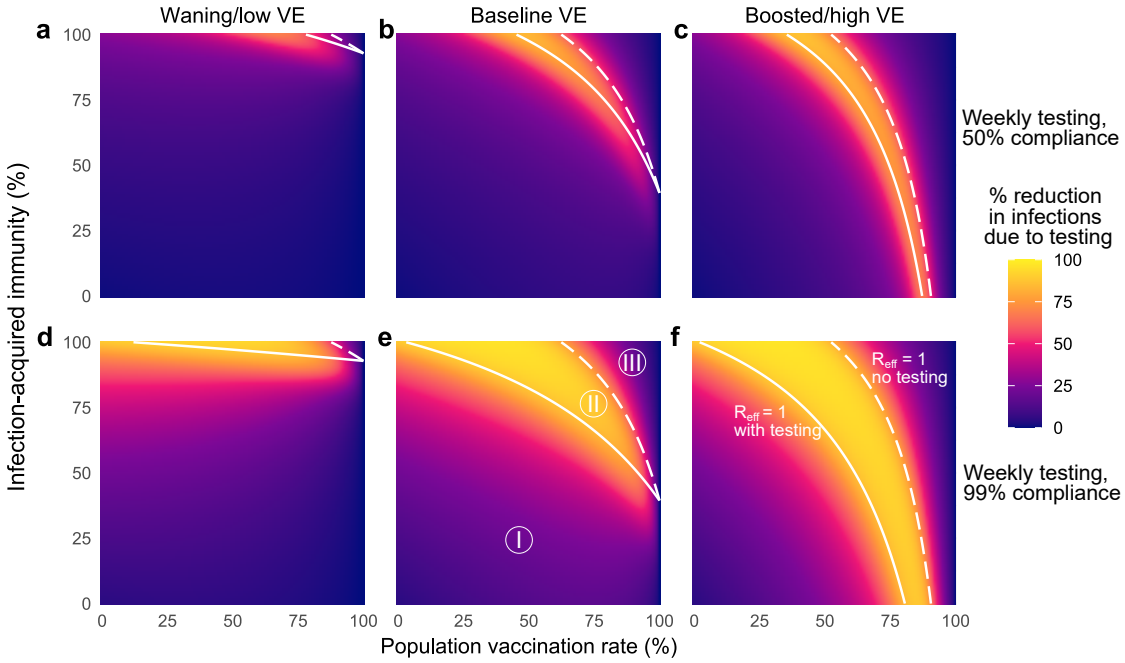

Figure S11: **The impacts of unvaccinated-only screening on total infections depend on population immunity, compliance, and vaccine effectiveness.** Percent reduction in infections due to screening over various population vaccination rates assuming low (a, d), baseline (b, e), and high (c, f) vaccine effectiveness with once-weekly screening at 50% (top row) and 99% (bottom row) compliance. White lines indicate the population immunity rate at which $R_{\text{eff}} = 1$ with screening (solid) and without screening (dashed), which divide the space into three regions, labeled I, II and III. See Supplementary Table S3 for immunity parameter values. $R_0^{\text{NPI}} = 6$ in all panels; see Figure 3.5 for $R_0^{\text{NPI}} = 4$.

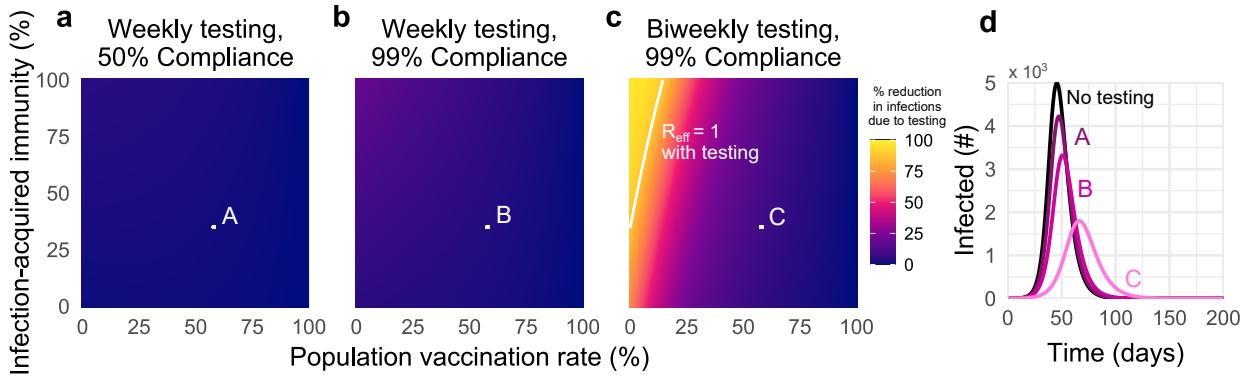

Figure S12: **Unvaccinated-only screening during omicron transmission cannot achieve $R_{\text{eff}} < 1$ except in low-vaccination and high-frequency regimes.** Percent reduction in infections due to screening over various population vaccination rates assuming plausible parameters for immunity associated with prior infection, vaccination, or both, with (a) once-weekly screening at 50% compliance, (b) once-weekly screening at 99% compliance, and (c) twice-weekly screening at 99% compliance. (d) Number of individuals infected over time, under screening scenarios denoted A, B, C, compared with no screening (black) with 58% vaccination rate and 35% rate of prior infection. Solid white line indicates the population immunity combinations for which $R_{\text{eff}} = 1$ with screening; no combinations exist to produce $R_{\text{eff}} = 1$ without screening. See Supplementary Table S3 for immunity parameter values. $R_0^{\text{NPI}} = 6$ in all panels. See Figure 3.6 for $R_0^{\text{NPI}} = 4$.

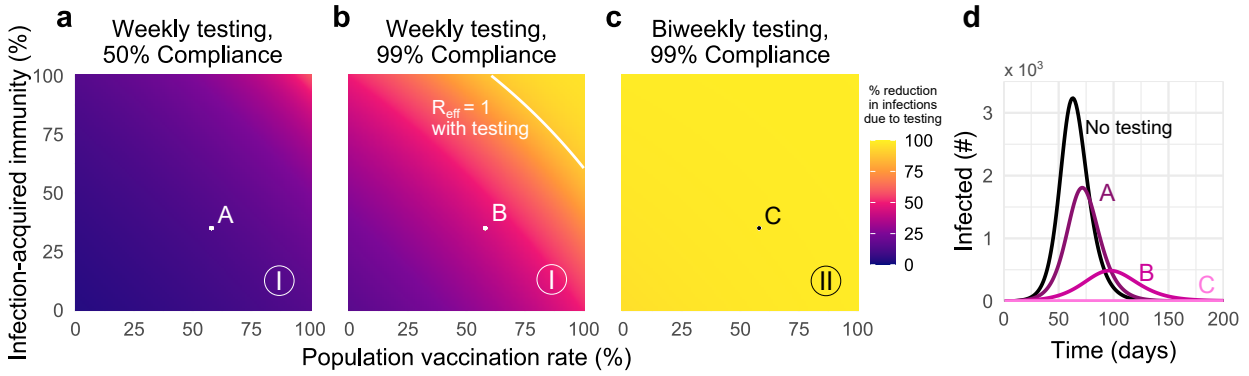

Figure S13: **Universal testing during omicron transmission can achieve $R_{\text{eff}} < 1$ in high-compliance and high-frequency regimes.** Percent reduction in infections due to universal screening over various population vaccination rates assuming plausible parameters for immunity associated with prior infection, vaccination, or both, with (a) once-weekly screening at 50% compliance, (b) once-weekly screening at 99% compliance, and (c) twice-weekly screening at 99% compliance. (d) Number of individuals infected over time, under universal screening scenarios denoted A, B, C, compared with no screening (black) with 58% vaccination rate and 35% rate of prior infection. Solid white line indicates the population immunity combinations for which $R_{\text{eff}} = 1$ with screening; no combinations exist to produce $R_{\text{eff}} = 1$ without screening. See Supplementary Table S3 for immunity parameter values. $R_0^{\text{NPI}} = 4$ in all panels. See Figure 3.6 for unvaccinated-only screening.

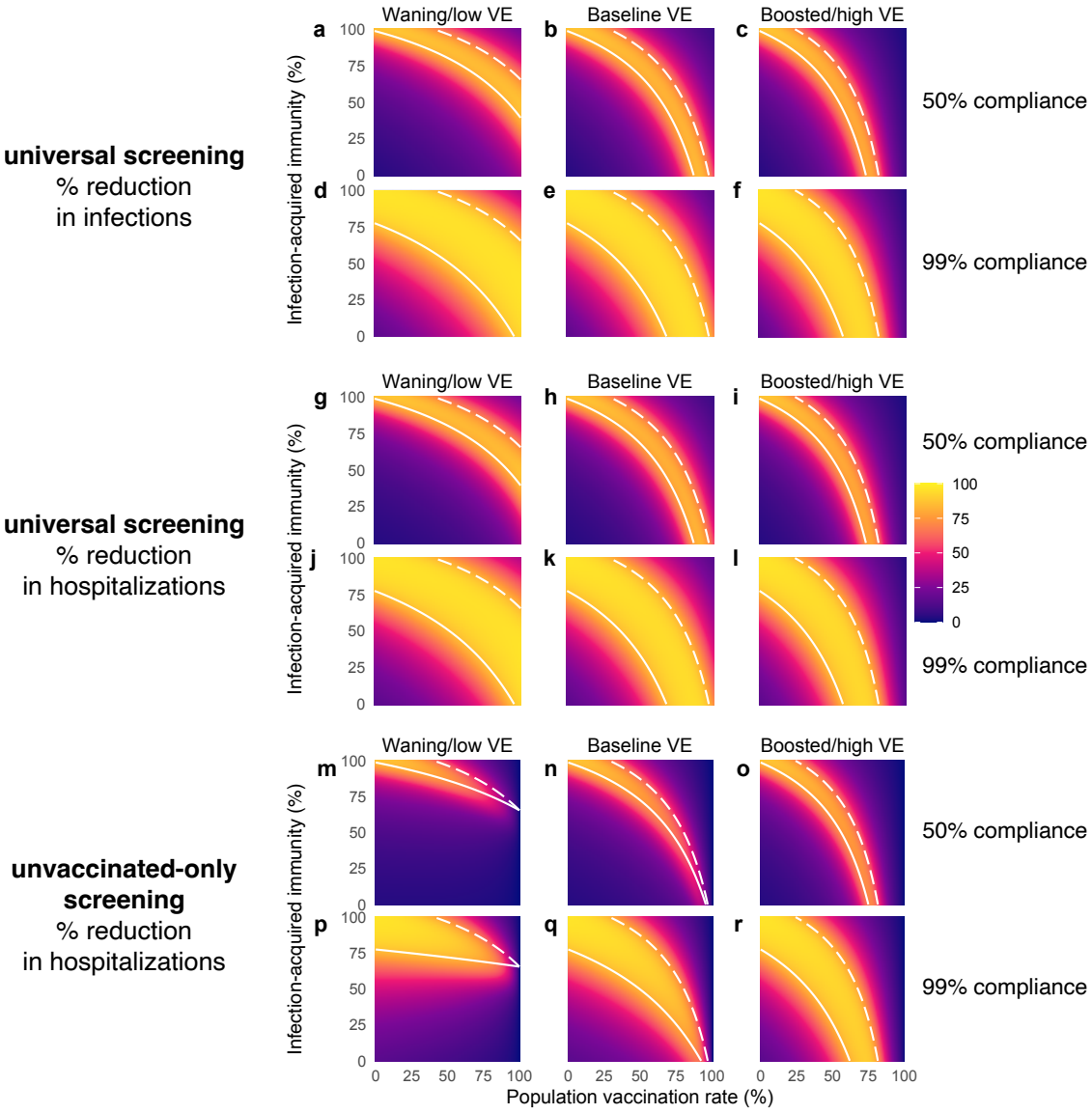

Figure S14: **The impacts of screening on total infections and hospitalizations depend on population immunity, compliance, and vaccine effectiveness.** (Top/middle panel) Percent reduction in infections/hospitalizations due to universal screening over various population vaccination rates assuming low (a, d, g, j), baseline (b, e, h, k), and high (c, f, i, l) VE vs the delta variant with once-weekly screening at 50% (top row) and 99% (bottom row) compliance. (Bottom panel) Percent reduction in hospitalizations due to unvaccinated-only screening over various population vaccination rates assuming low (m, p), baseline (n, q), and high (o, r) VE vs the delta variant with once-weekly screening at 50% (top row) and 99% (bottom row) compliance. White lines indicate the population immunity rate at which $R_{\text{eff}} = 1$ with screening (solid) and without screening (dashed), which divide the space into three regions, labeled I, II and III. See Supplementary Table S3 for immunity parameter values. $R_0^{\text{NPI}} = 4$ in all panels; see Figure 3.5 for percent reduction in infections under unvaccinated-only testing.

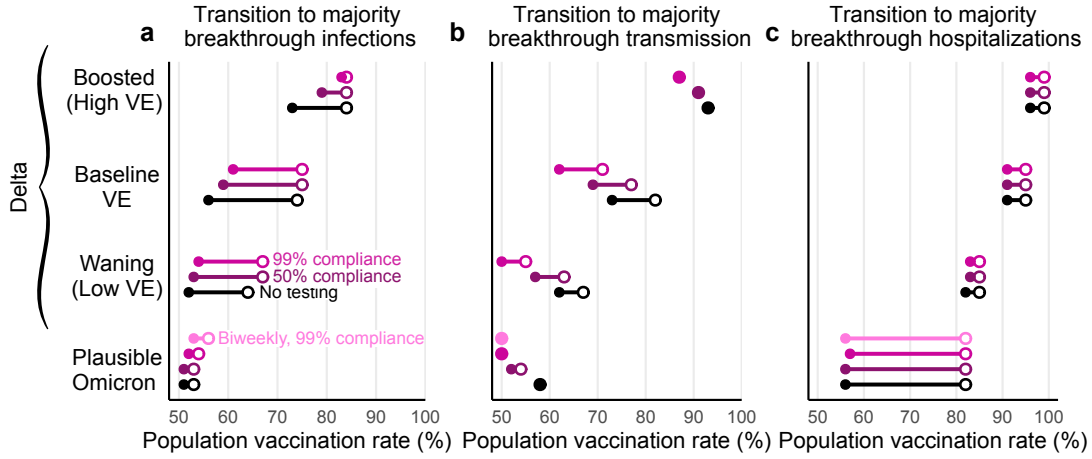

Figure S15: **Screening via testing and vaccine effectiveness affect transition points to majority-breakthrough regimes.** The vaccination rates at which the vaccinated population makes up the majority of (a) infections and (b) transmission for low, moderate, and high vaccine effectiveness scenarios. Minimum (filled circle) and maximum (open circle) endpoints show the variation in transition points over all combinations of vaccination and prior infection rates for no screening (black), 50% compliance (purple), and 99% compliance (pink) over all possible values for past infection rates. $R_0^{\text{NPI}} = 6$ for all plots; see Figure 3.7 for $R_0^{\text{NPI}} = 4$.

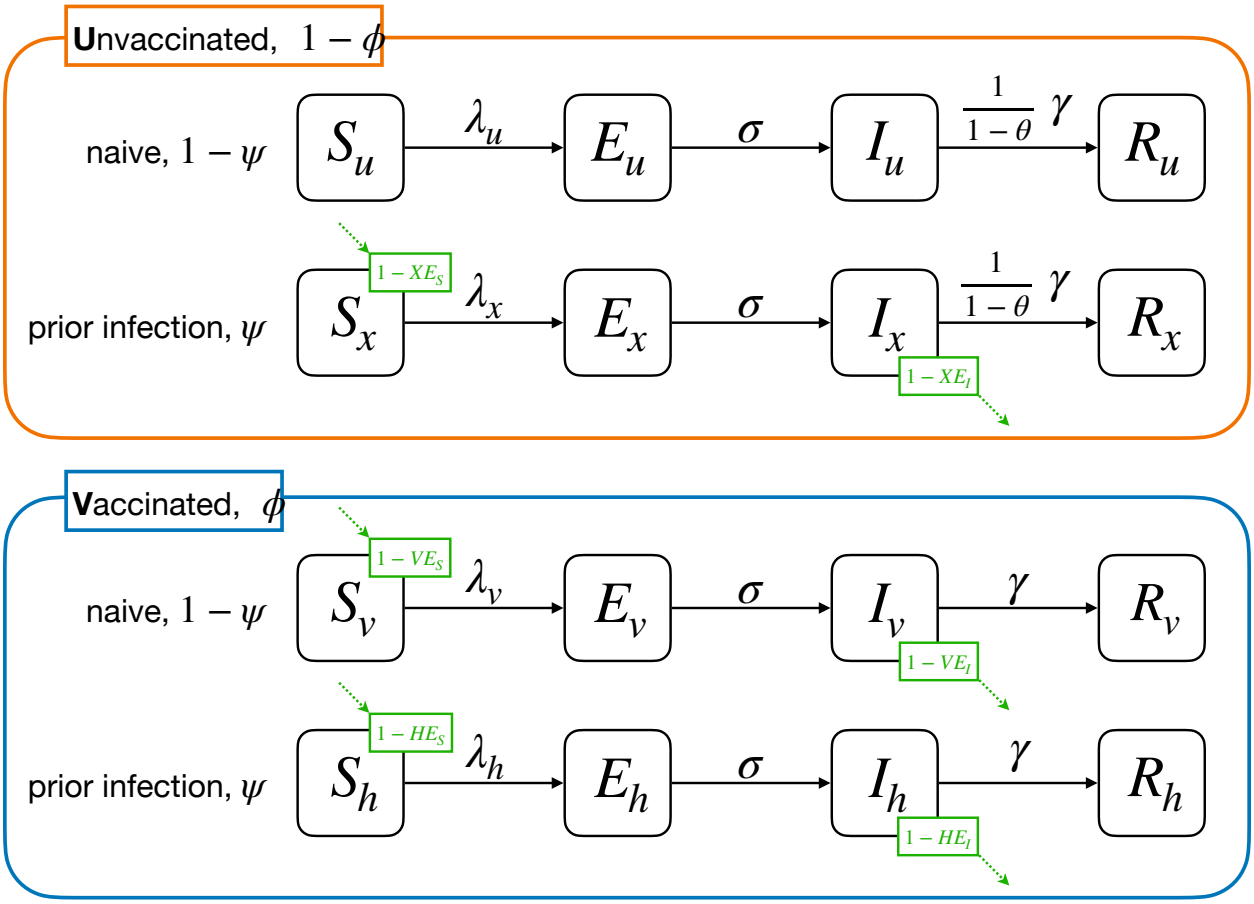

Figure S16: **SEIR Model Flow Diagram.** SEIR model schematic depicting unvaccinated (u subscript), SARS-CoV-2 experienced (x subscript), vaccinated (v subscript), and both experienced and vaccinated ("hybrid"; h subscript) populations. Solid lines denote movement of individuals between classes at the given rate. The time spent infectious, $1/\gamma$, may be shortened by a factor of $1-\theta$ due to screening. Dashed lines denote infectious interactions, scaled by protection against infection ($\text{VE}_S, \text{HE}_S, \text{XE}_S$) and transmission ($\text{VE}_I, \text{HE}_I, \text{XE}_I$).

6.2.1 Derivation of effective reproductive number

With unvaccinated-only screening, this model's next generation matrix M, used to calculate the effective reproductive number R_{eff}, is given by

$$M = \frac{\alpha}{\gamma} \begin{pmatrix} 1 & 0 & 0 & 0 \\ 0 & 1-\text{XE}_S & 0 & 0 \\ 0 & 0 & 1-\text{VE}_S & 0 \\ 0 & 0 & 0 & 1-\text{HE}_S \end{pmatrix} C \begin{pmatrix} 1-\theta & 0 & 0 & 0 \\ 0 & (1-\text{XE}_I)(1-\theta) & 0 & 0 \\ 0 & 0 & 1-\text{VE}_I & 0 \\ 0 & 0 & 0 & 1-\text{HE}_I \end{pmatrix} \tag{S11}$$

where C is the contact matrix

$$C = \begin{pmatrix} c_{u\to u} & c_{x\to u} & c_{v\to u} & c_{h\to u} \\ c_{u\to x} & c_{x\to x} & c_{v\to x} & c_{h\to x} \\ c_{u\to v} & c_{x\to v} & c_{v\to v} & c_{h\to v} \\ c_{u\to h} & c_{x\to h} & c_{v\to h} & c_{h\to h} \end{pmatrix} \tag{S12}$$

with units of average number of contacts per person per day. In a well-mixed population of size N with proportions ϕ vaccinated and SARS-CoV-2 prior infection ψ,

$$C_{\text{well mixed}} = N \begin{pmatrix} \phi(1-\psi) & \phi\psi & (1-\phi)\psi & (1-\phi)(1-\psi) \\ \phi(1-\psi) & \phi\psi & (1-\phi)\psi & (1-\phi)(1-\psi) \\ \phi(1-\psi) & \phi\psi & (1-\phi)\psi & (1-\phi)(1-\psi) \\ \phi(1-\psi) & \phi\psi & (1-\phi)\psi & (1-\phi)(1-\psi) \end{pmatrix} . \tag{S13}$$

The effective reproductive number is the absolute value of the dominant eigenvalue of M. It depends on R_0^{NPI}, ϕ, and ψ, as well as values of VE, HE, XE, and θ,

$$\begin{aligned} R_{\text{eff}} = R_0^{\text{NPI}} \Big[& \phi(1-\psi)(1-\text{VE}_S)(1-\text{VE}_I) + \phi\psi(1-\text{HE}_S)(1-\text{HE}_I) \\ & + (1-\phi)\psi(1-\text{XE}_S)(1-\text{XE}_I)(1-\theta) + (1-\phi)(1-\psi)(1-\theta) \Big] . \end{aligned} \tag{S14}$$

This equation has the more compact form

$$R_{\text{eff}} = R_0^{\text{NPI}} \left[f_u(1-\theta) + f_x r_x (1-\theta) + f_v r_v + f_h r_h \right] , \tag{S15}$$

after substituting $f_u = (1-\psi)(1-\phi)$, $f_x = \psi(1-\phi)$, $f_v = (1-\psi)\phi$, and $f_h = \phi\psi$, the fractions of the population in the unvaccinated, experienced, vaccinated, and hybrid immunity groups, respectively, and

$r_x = (1 - \text{XE}_I)(1 - \text{XE}_S)$, $r_v = (1 - \text{VE}_I)(1 - \text{VE}_S)$, and $r_h = (1 - \text{HE}_I)(1 - \text{HE}_S)$, the cumulative impacts of transmission-related immunity on each group. Note that for universal screening testing, this equation becomes

$$R_{\text{eff}}^{\text{universal}} = R_0^{\text{NPI}}(1 - \theta)\left[f_u + f_x r_x + f_v r_v + f_h r_h\right] . \tag{S16}$$

Setting $R_{\text{eff}} = 1$ in Eq. (S14) leads to the following required vaccination fraction ϕ to achieve a reproductive number below one,

$$\phi_{R=1} = \frac{\xi\left[\psi(1 - \text{XE}_S)(1 - \text{XE}_I) + (1 - \psi)\right] - \frac{1}{R_0^{\text{NPI}}}}{\xi\left[\psi(1 - \text{XE}_S)(1 - \text{XE}_I) + (1 - \psi)\right] - (1 - \psi)(1 - \text{VE}_S)(1 - \text{VE}_I) - \psi(1 - \text{HE}_S)(1 - \text{HE}_I)} , \tag{S17}$$

where $\xi = 1 - \theta$. In the absence of screening, this equation simplifies to

$$\phi_{R=1} = \frac{\psi(1 - \text{XE}_S)(1 - \text{XE}_I) + (1 - \psi) - \frac{1}{R_0^{\text{NPI}}}}{\psi(1 - \text{XE}_S)(1 - \text{XE}_I) + (1 - \psi) - (1 - \psi)(1 - \text{VE}_S)(1 - \text{VE}_I) - \psi(1 - \text{HE}_S)(1 - \text{HE}_I)} . \tag{S18}$$

6.3 Chapter 4 supplementary materials

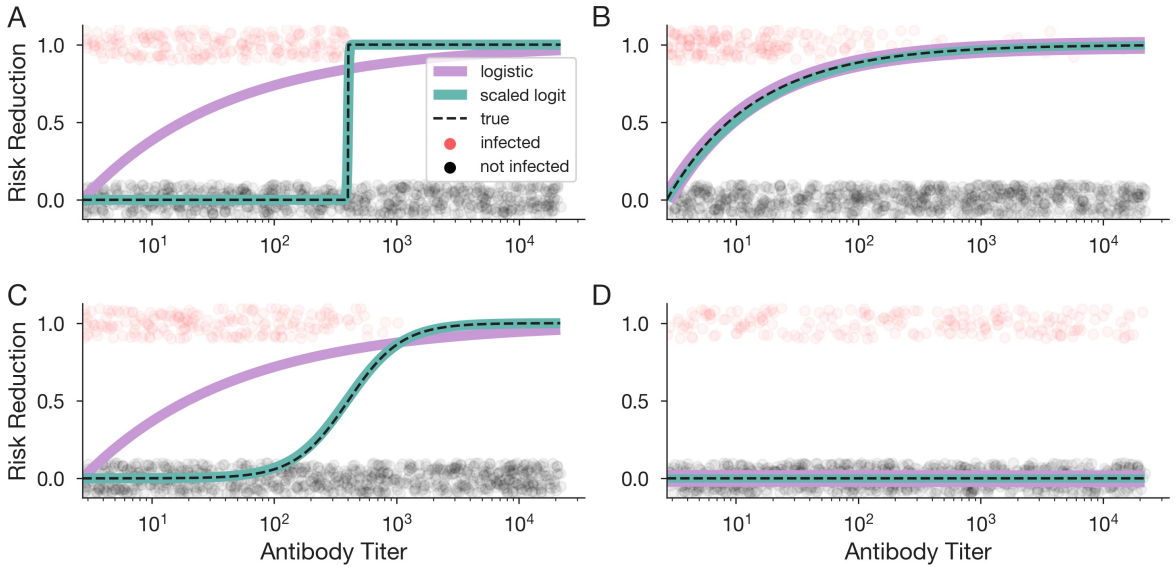

Figure S17: **The scaled logit model can recover complicated antibody protection functions, while logistic regression is limited in its scope.** Estimated protection function using the scaled logit model (green curve) trained on data generated using a threshold (A), exponential (B), sigmoidal (C), and flat (D) protection functions (dashed black curve). Circles show a subset of infected (red) and uninfected (gray) simulated individuals at various antibody titers used to train the model.

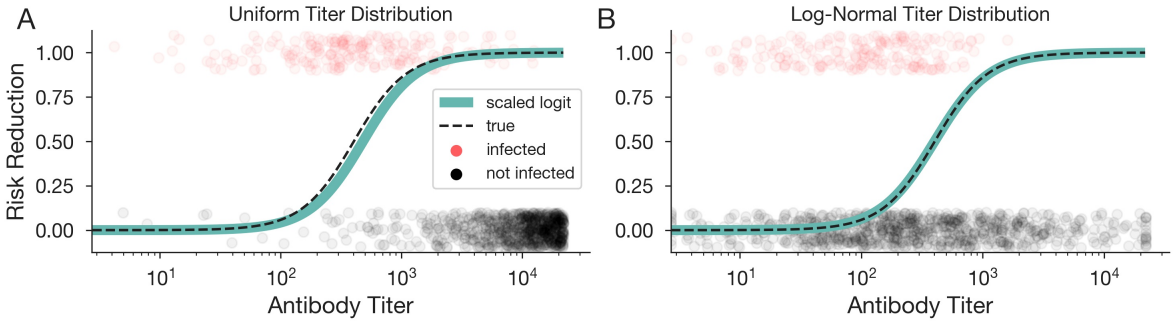

Figure S18: **The scaled logit model can recover complicated antibody protection functions, even under different titer distributions.** Estimated protection function using the scaled logit model (green curve) trained on data generated using exponential (A) and sigmoidal (B) protection functions (dashed black curve) for uniformly (A) and normally (B) distributed titers. Circles show a subset of infected (red) and uninfected (gray) simulated individuals at various antibody titers used to train the model.

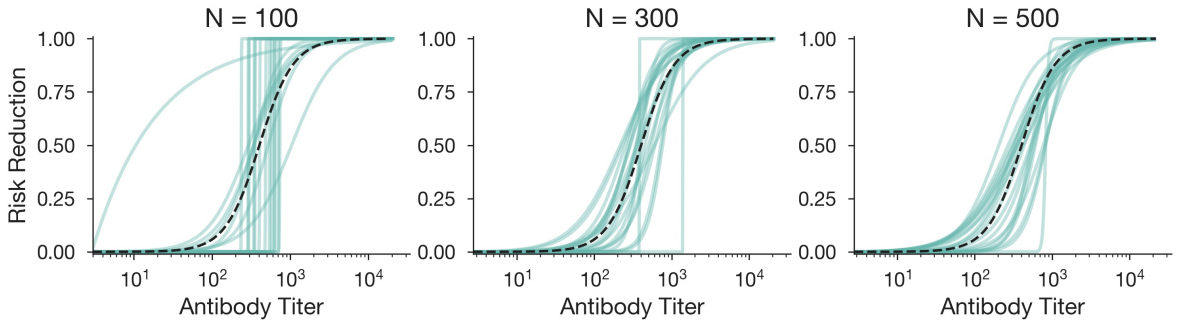

Figure S19: **Scaled logit model fit with low sample sizes.** Estimated protection function using the scaled logit model (green curves) for 20 stochastic simulations at the specified sample size (N) using a sigmoidal true protection (dashed black curve).

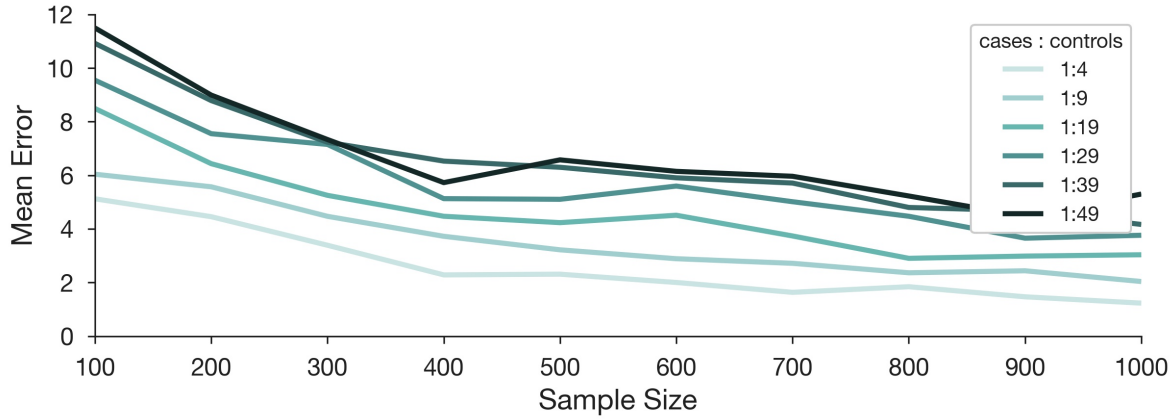

Figure S20: **The scaled logit model has low accuracy at small sample sizes.** Average error over 50 simulations per scenario for various sample sizes and case-to-control ratios using the scaled logit model. Error was defined as the discrete ℓ_2 norm (Euclidean distance) between the modeled and true protection functions. Darker-colored lines represent scenarios with more controls per case.

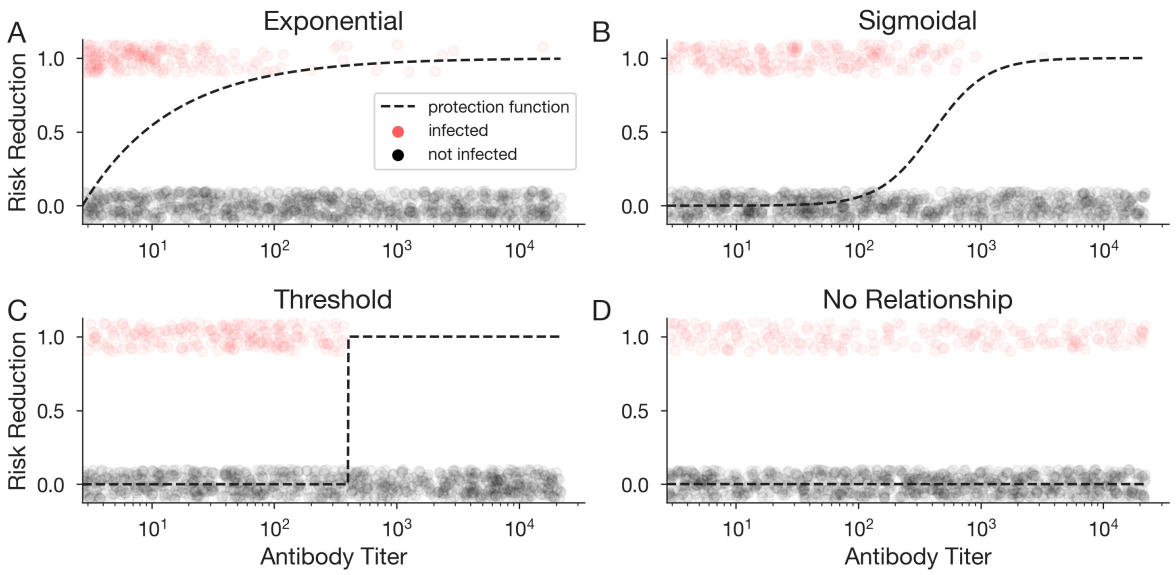

Figure S21: **Protection functions used for data simulation.** Risk reduction as a function of antibody titer for exponential (A), sigmoidal (B), threshold (C), and no relationship (D) protection functions.

6.3.1 Fitting the scaled logit model to TND data

Under the scaled logit model, the likelihood of observing a given data set is given by

$$\mathcal{L}(\lambda, \beta_0, \beta_1; \{y_i, A_i\}) = \prod_i \left(\frac{\lambda}{1 + e^{(\beta_0 + \beta_1 A_i)}} \right)^{y_i} \left(1 - \frac{\lambda}{1 + e^{(\beta_0 + \beta_1 A_i)}} \right)^{(1-y_i)}, \tag{S19}$$

where A_i denotes individual antibody titers and $y_i = 1/0$ denotes an observed infection or non-infection, respectively. We wish to find the parameters $(\lambda, \beta_0, \beta_1)$ which maximize this likelihood function, or equivalently the parameters that minimize the negative log-likelihood:

$$\mathcal{NLL}(\lambda, \beta_0, \beta_1; \{y_i, A_i\}) = \sum_i \left[-y_i \log \left(\frac{\lambda}{1 + e^{(\beta_0 + \beta_1 A_i)}} \right) - (1 - y_i) \log \left(1 - \frac{\lambda}{1 + e^{(\beta_0 + \beta_1 A_i)}} \right) \right]. \tag{S20}$$

The latter form is preferable for computational methods, given limitations of machine epsilon when computing extremely small values.

We use the built in `scipy.minimize` function in python, implemented with the Nelder-Mead minimization algorithm and options to increase the number of iterations before convergence. Sample code is provided for MLE in both python and R in the Appendix. In python, this process uses the following code, where λ has been replaced with k to avoid conflict with built-in functions:

```
# Import required packages
import numpy as np
from scipy.optimize import minimize

# Define the scaled logit function
def scaled_logit(x, k, beta_0, beta_1):
    """
    Scaled logit function
    Parameters:
        x (array-like): Input values.
        k (float): Maximum value (scale).
        beta_0 (float): Intercept parameter for linear regression.
        beta_1 (float): Slope parameter.

    Returns:
    array-like: Scaled logistic function values.
    """
    return k / (1 + np.exp(beta_0 + beta_1*x))

def neg_log_likelihood_scaled_logit(params, data):
```

```
    '''
    Defines negative log-likelihood function for scaled logit model
    Parameters:
        params: list of model params [k, beta_0, beta_1]
        data: list of lists containing [Ab_titers, infected_status] for all oberved samples

    Returns:
        Scalar negative log-likelihood value
    '''
    k, beta_0, beta_1 = params
    Abs = np.array(data[0]); infected = np.array(data[1])

    # Get likelihood
    prob_pos = infected * np.log(scaled_logit(Abs, k, beta_0, beta_1))
    prob_neg = (1-infected) * np.log(1-scaled_logit(Abs, k, beta_0, beta_1))
    return -1*np.sum(prob_pos + prob_neg)

def fit_scaled_logit(x_data, y_data, initial_guess=(0.5, 1, -1)):
    """
    Fit the scaled logit model to data.
    Parameters:
        x_data (array-like): Independent variable values.
        y_data (array-like): Dependent variable values.
        initial_guess (tuple): Initial guesses for k, beta_0, and beta_1.

    Returns:
        tuple: Fitted parameters (k, beta_0, beta_1)
    """
    data = [x_data,y_data]
    result = minimize(neg_log_likelihood_scaled_logit, initial_guess, method='Nelder-Mead', args=(data), options={'xatol': 1e-10,
    ↪  'fatol': 1e-8, 'maxiter': 10000, 'maxfev': 20000})
    return result.x

# Example of fitting the model to data

# Generate anibody titers for 1000 cases and controls
Ab_titers_cases = np.random.uniform(np.log(1), np.log(1000), 1000)
Ab_titers_controls = np.random.uniform(np.log(1), np.log(8000), 1000)
Ab_titers = np.concatenate([Ab_titers_cases, Ab_titers_controls])

# Generate infected status array
infected = np.concatenate([np.ones(1000),np.zeros(1000)])

# Fit sccaled logit model to data
fitted_params = fit_scaled_logit(Ab_titers,infected)
fitted_k, fitted_beta_0, fitted_beta_1 = fitted_params
print(fitted_params)

# Create vector of model predictions for increasing titers
potential_Abs = np.arange(np.log(1),np.log(8000))
prob_infection = scaled_logit(potential_Abs, fitted_k, fitted_beta_0, fitted_beta_1)
```

If the researcher prefers to work in R, the equivalent script is:

```r
# Load necessary library
library(stats)

# Define the scaled logit function
scaled_logit <- function(x, k, beta_0, beta_1) {
  return(k / (1 + exp(-(beta_0 + beta_1 * x))))
}

# Define the negative log-likelihood function for the scaled logit model
neg_log_likelihood_scaled_logit <- function(params, data) {
  k <- params[1]
  beta_0 <- params[2]
  beta_1 <- params[3]

  Abs <- data[[1]]
  infected <- data[[2]]

  # Compute likelihood
  prob_pos <- infected * log(scaled_logit(Abs, k, beta_0, beta_1))
  prob_neg <- (1 - infected) * log(1 - scaled_logit(Abs, k, beta_0, beta_1))

  return(-sum(prob_pos + prob_neg))
}

# Function to fit the scaled logit model
fit_scaled_logit <- function(x_data, y_data, initial_guess = c(0.5, 1, -1)) {
  data <- list(x_data, y_data)

  result <- optim(
    par = initial_guess,
    fn = neg_log_likelihood_scaled_logit,
    data = data,
    method = "Nelder-Mead",
    control = list(reltol = 1e-6, maxit = 4000)
  )

  return(result$par)
}

# Example of fitting the model to data

# Generate antibody titers for 1000 cases and controls
Ab_titers_cases <- runif(1000, log(1), log(1000))
Ab_titers_controls <- runif(1000, log(1), log(8000))
Ab_titers <- c(Ab_titers_cases, Ab_titers_controls)

# Generate infected status array
```

```
infected <- c(rep(1, 1000), rep(0, 1000))

# Fit scaled logit model to data
fitted_params <- fit_scaled_logit(Ab_titers, infected)
fitted_k <- fitted_params[1]
fitted_beta_0 <- fitted_params[2]
fitted_beta_1 <- fitted_params[3]
print(fitted_params)

# Create vector of model predictions for increasing titers
potential_Abs <- seq(log(1), log(8000), length.out = 100)
prob_infection <- scaled_logit(potential_Abs, fitted_k, fitted_beta_0, fitted_beta_1)
```